

QUARTERLY REPORT of

RTRI

Aug. 2024 Vol. 65 No. 3
CONTENTS

PAPERS

Study on Interlocking Devices in a Cloud Computing Environment **I O**

Design Method for Corrosion of Reinforcing Bars in Concrete Structures by Water Penetration and Carbonation Progress **I**

Development of Automatic Generation of Maintenance Worker Schedule Using Tabu Search **O R**

Development of Safety Check Support Device for Drivers Using Side Cameras on Rolling Stock **O**

Rolling Stock Scheduling Algorithm for Temporary Timetable After Natural Disaster **O**

Cage Wear Prediction for Traction Motor Bearings of Railway Vehicles Based on Measurement of Contact Force between Rolling Element and Cage **R**

REVIEWS

Outline of Design Standard and Commentary for Railway Structures (Concrete Structures) **I N**

Introduction Manual for Natural Frequency Identification System of Bridge Piers by Constant Microtremor Measurement **I**

SUMMARIES

Summaries of RTRI REPORT (in Japanese)

- H** Human factors
- I** Infrastructure
- N** Natural hazards
- O** Operations
- R** Rolling stock
- T** Technical system integration and interaction



CONTENTS

PAPERS

-
- 155 Study on Interlocking Devices in a Cloud Computing Environment [I] [O]
.....N.TERADA, S.SHIOMI, T.TOYAMA
- 162 Design Method for Corrosion of Reinforcing Bars in Concrete Structures by Water Penetration and Carbonation Progress [I]
.....S.TODOROKI, T.ISHIDA, H.UEDA, T.TADOKORO
- 170 Development of Automatic Generation of Maintenance Worker Schedule Using Tabu Search [O] [R]
.....T.KOKUBO, S.KATO, T.NAKAHIGASHI
- 176 Development of Safety Check Support Device for Drivers Using Side Cameras on Rolling Stock [O]
.....W.GODA, H.MUKOJIMA, N.NAGAMINE
- 182 Rolling Stock Scheduling Algorithm for Temporary Timetable After Natural Disaster [O]
.....S.KATO, T.NAKAHIGASHI, T.KOKUBO, J.IMAIZUMI
- 188 Cage Wear Prediction for Traction Motor Bearings of Railway Vehicles Based on Measurement of Contact Force between Rolling Element and Cage [R]
.....D.SUZUKI, K.TAKAHASHI, Y.OKAMURA, F.ITOIGAWA, S.MAEGAWA

REVIEWS

-
- 195 Outline of Design Standard and Commentary for Railway Structures (Concrete Structures) [I] [N]
.....K.WATANABE, T.TADOKORO, M.IKEDA, M.OKAMOTO
- 201 Introduction Manual for Natural Frequency Identification System of Bridge Piers by Constant Microtremor Measurement [I]
.....S.WATANABE, H.IRI, S.FUJIWARA

SUMMARIES

-
- 207 Summaries of RTRI REPORT (in Japanese)

- | |
|--|
| [H] Human factors |
| [I] Infrastructure |
| [N] Natural hazards |
| [O] Operations |
| [R] Rolling stock |
| [T] Technical system integration and interaction |

Study on Interlocking Devices in a Cloud Computing Environment

Natsuki TERADA Shunsuke SHIOMI Takashi TOYAMA
 Signalling Systems Laboratory, Signalling and Operation Systems Technology Division

We report on our study and proposal for interlocking devices in a cloud computing environment. This proposal realizes resilience, reduces time and cost of replacement, and provides interlocking processes as a service. The proposed system has the feature of processing interlocking logics of different stations independently. Furthermore, the proposed system has three layers: terminal devices to interface track circuits, signals, and switches, etc., logic units to process interlocking logics, and controllers to assign the interlocking table to logic units. We defined the specifications for terminal devices, logic units and controllers, and verified them.

Key words: interlocking device, cloud computing, interlocking as a service, segment, asynchronous logic

1. Introduction

Interlocking devices control physical devices such as signals and switches with safety integrity, based on the command of train movements and train locations. Interlocking functions are achieved with relays and/or computers. Conventional relay interlocking devices are installed at individual stations or parts of a station. Over the past few years, however, computer-based interlocking devices have become more widespread. Although computer-based interlocking devices were initially installed at individual stations, centralized computer-based interlocking devices controlling several stations along sections of a line have recently been developed and brought into service. This centralization of interlocking devices is an effective way to reduce the burden of maintenance, especially on low density lines.

By extending the concept of centralized interlocking devices and introducing the concept of cloud computing, the authors are developing an interlocking device system which can operate in a cloud computing environment. This enables the interlocking function to be supplied to many stations across different lines [1]. This report describes the concept of the cloud-based interlocking system environment and issues which remain to be solved. We then propose a comprehensive cloud-based interlocking device system structure and describe the function of its sub components. Finally, we describe the possibilities of realization based on simulations.

2. Concept of cloud-based interlocking devices

2.1 Current situation regarding interlocking devices in Japan

Interlocking devices are classified as mechanical interlocking devices, relay based interlocking devices and electronic (or solid state) interlocking devices. Currently, 40% of interlocking devices used by JR companies are electronic. Since interlocking devices were installed in Japan for the first time in 1985, older devices on the network will soon need to be replaced. 80% of older relay-type interlocking devices are on smaller train operator networks, and most of these are estimated to be over 50 years old. However, replacement of interlocking devices, which involves system design, installation, changing connections and device verification, is labor intensive. Therefore, there is a strong need to reduce the burden of work involved for their replacement.

In general, interlocking devices are installed at individual sta-

tions. However, recently, centralized interlocking devices have been developed and introduced to control several stations along a certain line [2-4]. While the centralized interlocking device with logic unit are installed in one place, terminals are installed at each station instead of a logic unit to interface with physical devices such as signals and switches. The logic units and terminals are connected with communication lines. The interlocking tables at each station are assembled into one interlocking table and processed with the logic unit. These kinds of interlocking devices have been introduced on low density lines [2, 3] and some high speed lines [4].

In addition, network based interlocking devices have been developed and introduced [5], in which physical devices are connected with object controllers over the network, not peer to peer.

2.2 Problem of interlocking devices and cloud computing e

Electronic interlocking devices are generally installed at stations or along the wayside to control. When a large disaster and/or ground fault occurs, whole system is severely damaged and system repair is time consuming. In addition, replacement of interlocking devices is labor intensive. Installation of an electronic interlocking device, requires preparation of the new device, installation and checking of the interlocking logic, installation of the device at the side of the existing device, and then wiring of the device to existing connectors. For a small company, not only is the cost of replacement unaffordable, but also they often lack the capacity to plan and carry out the replacement.

In the case of cloud computing services however, which provide large scale computational resources remotely, customers can access servers regardless of their actual location or computational situation. These kinds of services provide robust systems against disaster and the need for replacement, which is also favorable in the light of the safety integrity required of interlocking devices. Therefore, we will explore how a cloud-based interlocking device service changes railway operations, and how the technology is provided.

2.3 Schematic presentation of “Interlockings as a Service”

Figure 1 illustrates the concept of interlockings as a service. Logical parts of interlocking functions, currently distributed at each station, are concentrated in an “Interlocking Center.” The interlocking center is relocatable and can be located where the risk of disasters is low. Interlocking centers can also be distributed depending on available networking conditions, optimizing robustness against di-

sasters.

Large railway operating companies which own their own interlocking devices can benefit from ease of replacement and robustness against disasters. On the other hand, small railway operating companies, who do not have their own devices, can receive “Interlocking as a Service” from large railway operating companies or service providers including signal device suppliers. Small companies would thus pay a fee for this service to the larger railway operating companies, enabling the larger companies to improve the financial return on their own equipment. The impact of the system is expected to be as follows:

(1) Resilience against disasters

If logical controllers for interlocking functions are located in disaster-free areas, when disasters and/or accidents do happen, it will be easier to repair interlocking functions in stations, since the logical components will be safe. Even if a signal house is severely damaged, it will be enough to repair the terminals and connections. In addition, repairs to remedy degraded conditions will be available using radio when cables between terminals and devices are damaged.

(2) Reduction of replacement cost

Replacement of interlocking devices is resources and labor intensive. In the case of electronic interlocking device replacement in particular, a new device must be prepared and its programs, and connection with field devices must be checked. If an old device is obsolete, compatibility must be ensured between the old device and the new device. On the other hand, when interlocking function processing can switch from one server to another, seamless replacement is possible. Server-based interlocking functions can thus reduce the replacement cost and in turn problems related to concerns about serviceable life of interlocking devices.

(3) Interlocking as a Service

This technology enables a new business model of “Interlocking as a Service,” in which function of interlocking logic process is made accessible over the network for a subscription. Especially for small railway operating companies, this removes the burden of maintenance and replacement of signalling devices, results in reduction of demand for human resources.

2.4 Overseas versions of the concept

There are also some proposals for “Interlocking as a Service” outside of Japan. In Europe, the systems are developed in which existing electronic and centralized interlocking devices are com-

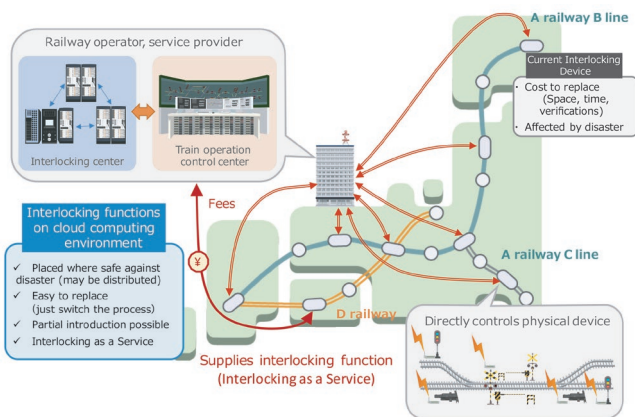


Fig. 1 Projected image for realization of “Interlocking as a Service”

bined with physical devices over an IP-network. DSTW (Digitales Stellwerk, or digital interlocking) by Deutsch Bahn [6] and SIMIS IaaS by Siemens [7] are examples. DSTW carries out centralized maintenance work and remote control by arranging several electronic interlocking devices in one place.

3. Proposal on basic structure of interlocking devices on cloud computing environments

This section examines the current process associated with electronic interlocking devices, and identifies issues for consideration in the development of cloud-based interlocking devices systems.

3.1 Procedure of current interlocking devices

Usually, logical units for electronic interlocking devices comprise a program and interlocking table which are stored in ROM or flash memory. The program and interlocking table are loaded into RAM, and processed according to the stored program. Objects of interlocking tables are fixed to specific stations, which cannot be changed dynamically.

Input from / output to field devices and processing of logic are cyclically executed in the designed cycle. Even with many objects, all input/outputs and logic processing is executed once in the cycle. Therefore, suspension of just one station requires suspension of all other stations controlled by that interlocking device. When a small change needs to be made to logic at one station, not only is suspension of the whole station required, but also the influence of the change on the other stations has to be checked.

Current electronic interlocking devices have 2 or 3 logic units which compare processing output, enabling a transition to a safe state when an incompatibility is detected. This fail-safe architecture includes special devices to achieve safety. In addition, when different logic units are to be compared over the network, network delays must be considered.

For this reason, when communication over the network is used, current electronic interlocking devices restrict the delay to within specified limits.

Based on the above considerations, technology described below has to be developed to enable a cloud-based interlocking device system for realizing “Interlocking as a Service”:

- (1) A method to independently process logic from different stations
- (2) A structure which enables cooperation of many logic units, and processing under the structure
- (3) A method to accept delay over the network

In addition, when we realize a large scale system, technology to achieve a fail-safe outcome by using Commercial Off the Shelf (COTS) CPUs is required. In our proposal, the architecture is based on a logic unit with fail-safe CPUs, because achieving fail-safe with general COTS CPUs [8] is not current practice.

3.2 Method to process each station’s logic independently

As mentioned, each station’s logic is required to be processed independently. As a result of our study, we propose to divide the cycles of the processor into segments, as shown in Fig. 2. A segment represents a certain processing capability. The number of segments that one processing unit can handle differs depending on the capacity of the processor. In Fig. 2, segment #2 is used to process interlocking function of Station A, while two segments #3 and #4 are used for Station B. The common procedure in segment #1 and #8

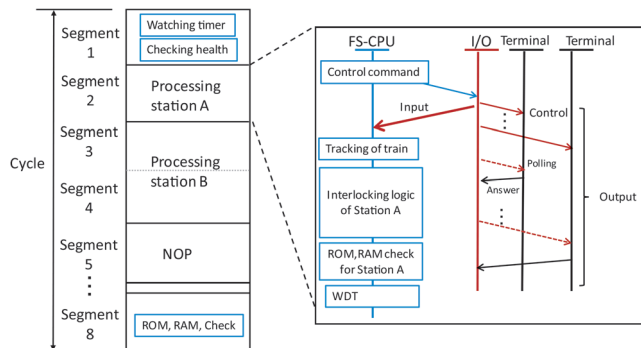


Fig. 2 Concept of segment, or divided resource of logic units

includes checking the cycle, input/output and memories.

3.3 Structure enabling cooperation of multiple logic units and processing under the structure

Interlocking devices in a cloud computing environment provide interlocking functionality for multiple stations by a combination of many logic units. This system requires a function to allocate processing resources to each station. An additional function is required to reallocate processing to alternative available resources in case of a logic unit failure. We propose controllers, which aim to execute the above functions. The controllers allocate logic unit processing resources, monitor the health of logic units, keep interlocking tables and upload the tables to the logic units. If there is more than one controller, the controllers share the status of logic units, allocation table and interlocking tables. They work cooperatively.

The proposed controllers enable scalability of the system. We can increase the number of logic units according to the required resources. The controllers also enable partial suspension of work on logic units, and logic units can be replaced without halting the whole system.

The proposed structure of interlocking devices is shown in Fig. 3. The system is composed of three layers: terminals to interface with physical devices, logic units, and controllers. There are two networks: controller network and interlocking network. Cur-

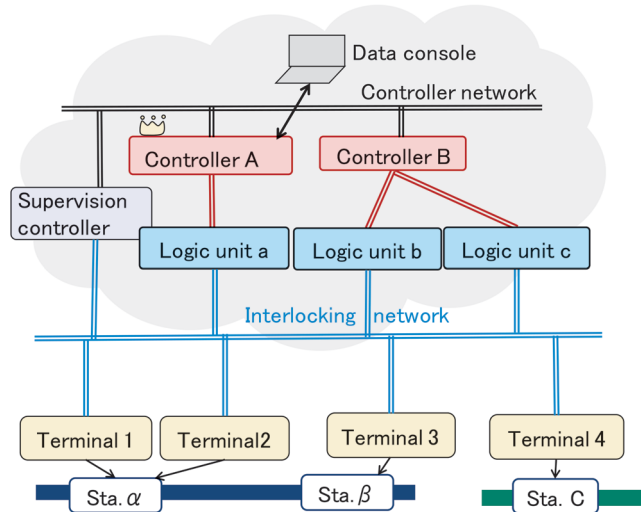


Fig. 3 Three layered structure of cloud-based interlocking system

rently, all the network requires is sufficient bandwidth for communications. Radio connections are also possible. For security, appropriate technical security mitigations are required in accordance with the type of network used.

3.4 Development of interlocking logic less affected by communication delay

Current electronic interlocking devices assume that the state of physical devices is collected within a certain time period, i.e., synchronously, and logic is processed cyclically. Any delay or packet loss of the state of objects causes processing to halt. Therefore, communication and terminal delays need to be allowed within specified time limits, to enable reasonable performance and reliability.

Imposing a zero-delay precondition in this system would be difficult for networks to implement. In addition, considering cost and maintainability of the system, other available communication methods can be envisaged, including radio communication. Therefore, to take into account the need to work with real communication networks, we should assume that logic units and physical devices are asynchronous. The logic needs to be configured such that delay or lack of status information has less impact on interlocking logic.

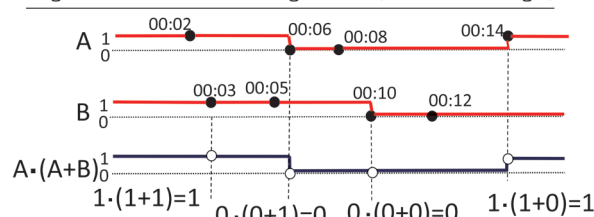
The main concept which we propose is based on three-value logic in which an extra “undetermined” state is considered. Some outputs of logical calculations are deterministic even if some inputs are undetermined. We can expect that the influence of delay is reduced introducing three-value logic. In addition, it is not required to change formulas used in the interlocking logic, which means current interlocking table data can be used as it is.

Figure 4 shows an example of asynchronous interlocking in contrast with current logic. Current logic determines the output at 00:10 when each value of A and B is determined, while asynchronous logic determines the output at 00:08 when only the value of A is determined.

4. Specification of components

We defined the specification of components mentioned above.

Logic of current interlocking device (Two-valued logic)



Asynchronous logic based on three-valued logic

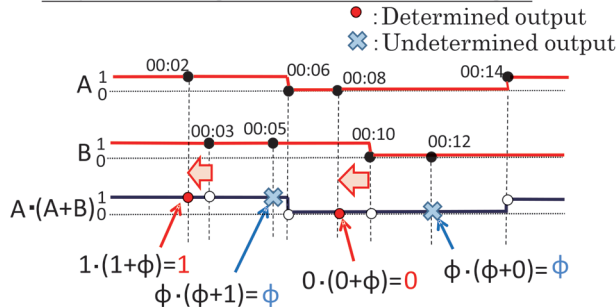


Fig. 4 An example of asynchronous logic

In this chapter we consider the specifications of controllers, logic units and terminals associated issues.

4.1 Specifications of Controllers

Controllers have following functions: sharing interlocking tables and list of logic units as databases, making allocation tables of how the logic units and its segments are allocated to the interlocking table, and monitoring the health of logic units and other controllers as well their own health. Relationships between controllers and logic units can be arbitrary, but we suppose that for each logic unit, only one controller is connected to the unit, i.e., the relationship is one controller to 'n' logic units.

4.1.1 Monitoring health of controllers and sharing of data

Each controller monitors the health of the other controllers, and shares a list of controllers and logic units with their status, interlocking tables and allocation tables. The procedure of monitoring health and data sharing is executed simultaneously, and it is based on the polling from the primary controller to the secondary controllers as shown in Fig. 5.

One controller is elected and acts as the primary and the other controllers act as the secondary. However, any of the controllers can be the primary. The primary controller sends secondary controllers a list of controllers and logic units with their status, list of interlocking tables, and allocation tables. Each secondary controller checks the list, updates the status of logic units in responsibility, and returns the list of new data when it has newer data. When there is data that the secondary needs, the secondary controller requests the primary controller to send the data. On the other hand, when the primary controller receives information about new data, it requests the secondary controller to send the data.

When there is no response from one of the secondary controllers for a specified time, the primary controller determines that the secondary controller has failed. On the other hand, when a secondary controller does not receive any information from the primary controller, the secondary controller determines that the primary controller has failed. When the primary controller fails, a new primary controller is elected from among the secondary controllers.

4.1.2 Election of primary controller

Determining rules to elect the primary controller. In principle,

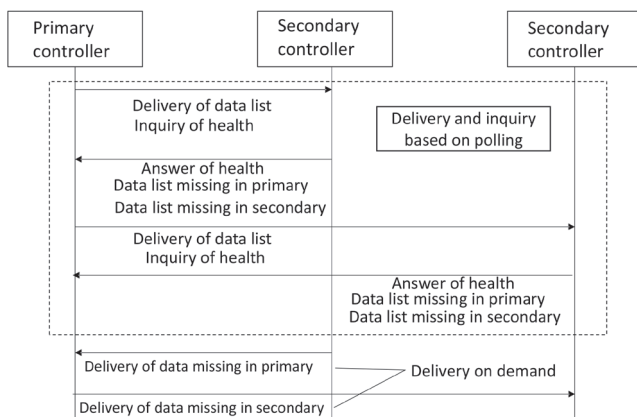


Fig. 5 Procedure of checking health of controllers and sharing data

one of the servers stands as a candidate for the primary controller, and the rest approves. However, if some of the servers are not active or are disconnected, the candidate cannot receive an answer from all of the other servers, therefore the approval of all other servers is not mandatory. From the point of view of non-active servers, the role of the primary controller may turn to another controller during non-active time. In this case the secondary controller receives an answer from the unexpected server. In addition, if there is no inquiry from the expected server, the secondary controller changes recognition of primary to the new primary controller.

It is noted that if the 'health' of the server is determined by the existence of messages, then a server failure cannot be distinguished from a connection failure. If controllers are split into two or more clusters due to the trouble in the network, another secondary controller is elected in the cluster without the primary controller, even if the original primary controller is active. In this case when the network is resumed, the primary controllers arbitrate, and one of the primary controllers remains as the primary. In order to activate the arbitration, the inquiry of the primary controller is continued to the controllers recognized as nonactive, and the servers answer the inquiry. When the network is resumed after the split, the primary controllers send messages of inquiry to each other, which makes them aware of existence of the other primary controller and need for arbitration.

If there is an inquiry from the other primary controller to activate the arbitration procedure and one of the primary controllers remains as the primary controller. The primary controllers exchange the information on the arbitration procedure, and inform the secondary controllers which one remains as the primary controller.

4.1.3 Monitoring health of logic units

Another important function of controllers is to monitor logic units. The controllers communicate with the logic units under their responsibility. The communication is based on the polling from the controller and to the logic units. The controller sends the allocation table. The logic unit responds to the inquiry by sending the status of itself and the segment. The version of interlocking table is specified in the allocation table and the data is requested by the logic unit during the processing of the segment.

4.1.4 Supervision controller to back up monitoring function of controllers

If a controller fails, the health monitoring function for logic units also fails. In order to cover the failure of the health monitoring function, supervision controllers are arranged in the controller network. A supervision controller is a controller which monitors the health of logic units. Supervision controllers are connected not only to the controller network, but also to the logic unit network. Supervision controllers monitor messages in the logic unit network and determine the health of logic units by analyzing messages. Each supervision controller monitors a part of a logic unit because monitoring whole logic units is not feasible.

Even if a controller fails, logic units under the controller continue to work. However, it is not possible to allocate a new segment or to release segment related to logic units under the failed controller. In this case, if another failure happens in one of the logic units, the supervision controller finds the failure, and the primary controller can allocate a new segment to another working logic unit.

4.2 Specification of logic units

Logic units receive the state of the physical device via terminals and the network, process the interlocking logic and send the command to the device. The main function of logic units consists of a segment function and processing interlocking logic. Figure 6 shows the state diagram of logic units. When interlocking table changes, current interlocking devices are reset. On the other hand, interlocking devices in the cloud computing environment do not reset themselves and are partially initialized for each station.

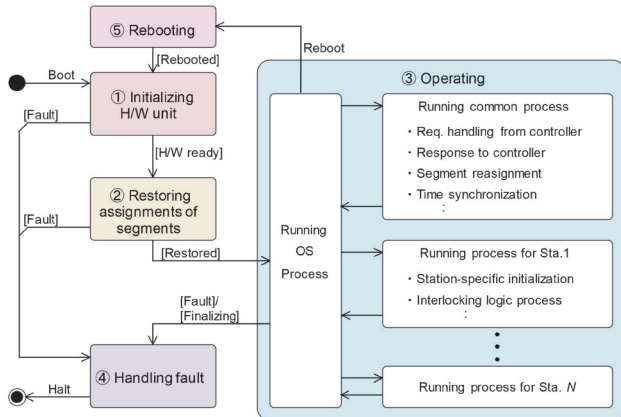


Fig. 6 State diagram of logic units

4.2.1 Process and protection of segment

We studied the partition and protection of computational resources of logic units from the point of view of minimizing the interaction between segments.

The processing of large-scale logic requires more than one segment. Therefore, the group of segments for processing the logic for a certain station are defined as a “task.” The task is identified by context ID, which is given by a controller.

The logic unit with segments is a kind of multi-task system. However, within the segments the single thread process is adopted to ensure safety, which is often used in interlocking devices. The basic function of logic units is to switch to the processing of segments in a certain period. The processing of segments is supposed to finish within the specified period. Even if a problem occurs, the basic function of the logic unit forces task switching, or pre-emption.

Memory is allocated independently to each segment, and the allocated memory of one segment is not accessed by the other segments. The allocation is based on segment, but not on task, which does not require the continuity of segment, i.e., fragmentation of segment is accepted. The internal state of a segment is loaded into the allocated memory before each processing of segment switches.

Figure 7 shows the state diagram of segment. The life cycle of a segment shown in Fig.7 is described as follows. First, the segment is initialized. If the interlocking table is not found in the logic unit, the table is requested from the controller. If the interlocking table is loaded in the logic unit, the logic is initialized and ready to process until the segment is released by the order of the controller.

4.2.2 Asynchronous process of interlocking logic

We define more concretely asynchronous logic mentioned in Section 3.4, especially on the concept of time. In the logic, time-stamped state is exchanged between logic units and terminals. Logic

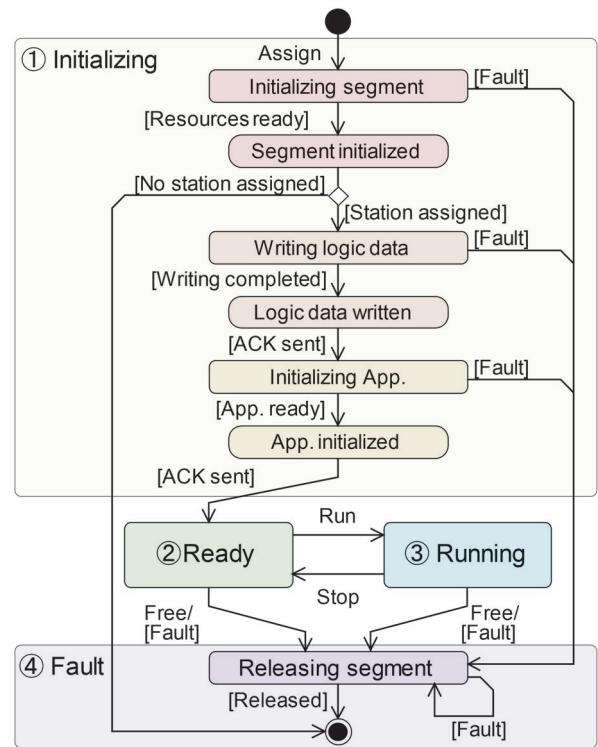


Fig. 7 State diagram of segment

units determine the result of the part in which required input is collected. Even if a part of the status has not arrived, the irrelevant part is not affected. Logics with a time-stamped value are advantageous in that there is less inconsistency due to time difference.

Four kinds of time stamp are used in the proposed logic: real time, internal front time, internal rear time, and referenced time. Internal rear time means the newest time at which all of input/output values are determined, i.e., the values are determined earlier than the internal rear time. Internal front time is the time at which the logic units received the newest value, i.e., calculation of the values at a later time than the internal front time is not required because status is not expected to be determined due to the lack of information. The referenced time is the time at which the calculation of the logic is targeted at. Figure 8 shows an example of the four times. Three of the four times without a real time are based on the time-stamp. As shown in Fig.8, the calculation is executed with referenced time between internal front and rear time. When some input/outputs are determined at some time, or new values are received, internal front and rear times are updated. In addition, timeout is applied to determine the lack of information.

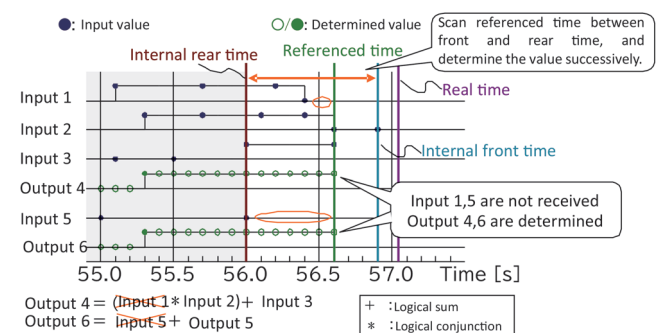


Fig. 8 Four internal times of a logic unit

4.3 Specification of terminals

The terminals interface with physical devices such as track circuits, signals and point machines. They control physical devices and receive the status of physical devices. The main functions are as follows: (a) receiving control from logic units, (b) processing control according to the priority, (c) checking consistency between controls from logic units, (d) controlling physical devices, and (e) obtaining status of physical devices.

Terminals are arranged in two ways to cope with multiple cases. The first is centralized control in which one terminal is arranged in the signal house or signal box and many physical devices are controlled by the terminal. The second is distributed control in which the terminal is integrated into the physical device or installed alongside it.

When inconsistency is detected between the controls of different logic units, an abnormality is detected. This detection function is built into the supervision controller introduced in section 4.1.

4.3.1 Receiving and processing control from logic units

Commands from logic units are received by the terminals regardless of the object of the control. The terminal process is cyclical. In the first step of the cycle, the terminal checks the object of the command. If the object is the device under the management, the terminal controls the device. If not, the command is neglected.

4.3.2 Checking command and controlling physical device

Usually, the logic is processed by more than one logic unit, controls are also sent from more than one logic unit. The terminal selects a control taking into account the priority added in the control. Controls are time-stamped, and if the control with same time stamp from different terminals are different, the terminal detects the abnormality and informs the supervision controller.

The terminals check the status of the physical device and send it to the logic units. If a mismatch is detected between inputs from the different segments, the mismatch is notified to the supervision controller. It has been noticed that the information may be delayed and asynchronous, therefore mismatches based on to the time-stamp of the control as shown in Fig. 9. In Fig. 9, the logic units related with mismatches are determined to have failed.

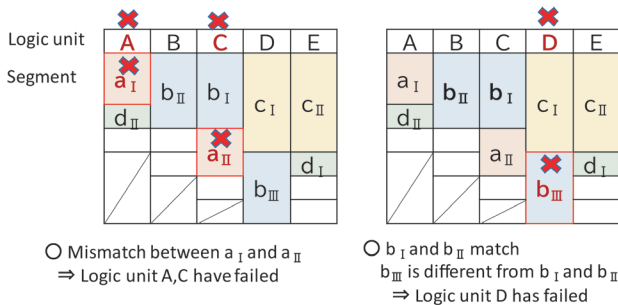


Fig. 9 Failure detection by supervision controller

4.3.3 Specification of supervision controller on the interlocking network

In addition to the other controllers, the supervision controller monitors the health of logic units. The supervision controller also checks the health of logic units and the network health based on an

analysis of communication between logic units and terminals. Supervision controllers also receive information about lack or inconsistency of control detected by terminals.

These abnormalities are delivered to other controllers via the controller network.

5. Verification of specification by simulation

5.1 Verification of controller

The behavior of controllers is verified using model checking. We used SPIN [9], which is a traditional model checking tool originally developed as a verification tool for communication protocols. We checked the functions of monitoring health and election of a new primary controller when the primary controller stops or the network splits.

5.2 Verification of synchronous logic

We made a simulator of asynchronous logic, and confirmed feasibility of our proposal by the simulator. In the simulator, scenarios including delays were set and simulation was carried out in real conditions.

This section introduces a case study of train movement tracking. The tracking logic of train movement expresses the status of track circuits in five states. A logic is incorporated that when the interval between the breaking of the preceding track circuit and that of the track circuit itself, the state of track circuit is determined to be erroneous, i.e., it is not a normal train movement. We confirmed that this logic works well when an interval of 0.5 seconds with a delay of 1 second delay occurs against an error detection threshold of 0.9 seconds. In this way, the asynchronous logic is applicable to the logics including time judgement.

5.3 Verification of whole system

We constructed a simulator on a PC, which focuses mainly on communication between components, and simulates the controllers, the logic units and the terminals, as well as communications between them.

For the function of controllers, the simulator simulates controller or logic unit failures as well as network separation and re-unification. When failure of controller or separation of networks happens, a new master controller is elected. When unification of network occurs, the primary controllers are unified. The reallocation of segment also works for both a controller and a logic unit under the controller.

For control and status information, communications are simulated, such as control from the logic units to the terminal, and status of physical device via terminal to logic units. When a failure of one logic unit happens, the supervision controller detects the failure and informs the controller.

Precise logical process is not simulated, but control based on the asynchronous logical calculation is simulated. The simulator also has the function of analyzing the influence of a communication delay.

For example, when a controller fails, reallocation of segments is executed as follows. The controller detects its own failure and another segment is allocated by the primary controller. The logic controller starts working with the newly allocated segment and the new allocation table is shared by other controllers.

6. Conclusion

We proposed a cloud-based interlocking device, in which interlocking logics for multiple stations are independently processed, and partially stopped for maintenance or upgrade purposes. The proposed system is structured in three layers: controllers to allocate computational resources to interlocking logics, logic units to process interlocking logics, and terminals (i.e., object controllers) to interface with physical devices.

The cycles of logic units are divided into segments, and the logic units process the segments independently. The allocation is scheduled by controllers, and the allocation tables and interlocking tables are shared by controllers. Controllers also monitor the health of logic units. Supervision controllers are provided to back up the failure of controllers. The number of the logic units can be increased as required, i.e., our proposal is scalable.

We also proposed asynchronous interlocking logics to reduce the requirements of delay based on the three-value logics considering an “undetermined” state.

Our verification is currently limited to a simulation. However, our concept is not only applicable to interlocking devices, but also to a wide range of railway signalling systems. Our plan is to realize the interlocking function of a new train control system in the way we proposed in this paper.

The final form of our concept will be realized using COTS CPU, which is not practical for now. In this case, the logic units will be virtualized on cloud computing environments enabling more flexibility. Currently, our focus will be studying how to achieve fail-safe mode using COTS CPU.

References

- [1] Terada, N., Shunsuke, S., Hiroyuki, F., Yuto, O., Takashi, T., “Towards cloud type interlocking systems,” *Proceedings of the J-RAIL 2017*, S2-5-2, Dec. 2017 (in Japanese).
- [2] Okutani, T., Shimazoe, T., “Development of Centralized Interlocking System for Railway Signalling and its Evaluation,” *Transactions of IEE Japan*, Vol. 119-D, pp. 1307-1314, Nov 1999 (in Japanese. Extend Summary in English available).
- [3] Nakano, H., 「加古川線CTC化（線区集中連動方式）」, *鉄道と電気技術*, Vol. 15, No. 11, 2004 (in Japanese).
- [4] Ono, S., 「九州新幹線（博多・新八代間）集中連動方式の開発と実用化」, *鉄道と電気技術*, Vol. 24, No. 8, pp. 11-16, 2013 (in Japanese).
- [5] Nishiyama, J., Kunifuji, T., 「ネットワーク信号制御システム—システム概要とモニターラン試験について—」, *鉄道と電気技術*, Vol. 17, No. 4, 2006 (in Japanese).
- [6] Kaldenbach, A., “Die Digitale LST bei der DB Netz AG Eine Einführung in die Digitale Stellwerkstechnik,” *Fachvortrag BF Bahnen*, 2019 (in German).
- [7] Siemens, Trackguard® Simis Interlocking as a Service (SlaaS), <https://www.mobility.siemens.com/ch/en/portfolio/rail/automation/interlocking-systems.html>, 2018 (visited on 17/8/2020).
- [8] Takashi, T., Fukumoto, S., “A Fundamental FMEA of Railway Signaling Systems Using Majority Voting over Networks,” *IEICE Technical Report*, Vol. 120, No. 288, DC2020-67, pp. 43-48, 2020 (in Japanese).
- [9] Holzman, G. J., *The SPIN Model Checker*, Addison-Wesley, 2004.

Authors



Natsuki TERADA, Dr.Eng.
Senior Chief Researcher, Signalling Systems Laboratory, Signalling and Operation Systems Technology Division
Research Areas: Signalling Systems, Track Circuits, Automatic Train Control System



Takashi TOYAMA
Assistant Senior Researcher, Signalling Systems Laboratory, Signalling and Operation Systems Technology Division
Research Areas: Signalling Systems, Track Circuits, Automatic Train Control System



Shunsuke SHIOMI
Senior Chief Researcher, Head of Signalling Systems Laboratory, Signalling and Operation Systems Technology Division
Research Areas: Signalling Systems, Point Machine

Design Method for Corrosion of Reinforcing Bars in Concrete Structures by Water Penetration and Carbonation Progress

Shuntaro TODOROKI

Concrete Structures Laboratory, Structures Technology Division

Tetsuya ISHIDA

Department of Civil Engineering, The University of Tokyo

Hiroshi UEDA

Materials Technology Division

Toshiya TADOKORO

Concrete Structures Laboratory, Structures Technology Division

The effect of water and carbonation on the corrosion of reinforcing bars in concrete was investigated by field surveys on members with different levels of supplied water. In addition, a design method to suppress corrosion of reinforcing bars due to water penetration was verified by comparing the cover depth where spalling of concrete occurred and the design cover depth determined by taking carbonation into account. Even if the un-carbonation depth (= cover depth—carbonation depth) is less than 10 mm, when water is not supplied, the probability of spalling is lower and the corrosion rate of reinforcing bars is slower, so it is important to consider the effect of supplied water on corrosion of reinforcing bars. It was also confirmed that the design method based on corrosion of reinforcing bars due to water penetration is applicable.

Key words: railway concrete structures, corrosion of reinforcing bars, supplied water, carbonation of concrete

1. Introduction

As the corrosion of reinforcing bars in concrete structures progresses, it may cause a spalling of the concrete due to corrosion expansion or a decrease in the load bearing capacity due to a lack of the cross section of reinforcing bars, and so on. Therefore, suppressing the progression of corrosion is important to ensure the durability of concrete structures.

Immediately after construction, reinforcing bars in concrete, that remains alkaline, are less likely to corrode. However, as the concrete around the reinforcing bars becomes neutralized by carbon dioxide penetrating through the concrete surface, corrosion becomes more likely. For this reason, carbonation of concrete has traditionally been used as an indicator to prevent corrosion of reinforcing bars. For example, in design, the cover depth (distance from the concrete surface to the reinforcing bar surface) has been set to prevent the area around the reinforcing bars from becoming neutralized during the design lifetime. On the other hand, oxygen and water are also essential for reinforcing bars to corrode.

In the design method that uses carbonation as an index (referred to as “study on carbonation” in [1] (see Appendix)), when the concrete surface is dry without water supply from rain, etc., the carbonation depth is calculated to be large (Fig. 1), and therefore it is judged that corrosion and spalling are likely to occur. On the other hand, in real field situations, it has been pointed out that, although carbonation is certainly less likely to progress in areas that are exposed to water and get wet, contrary to the design, more spalling due to corrosion occurs [2] (Fig. 2). In other words, using carbonation as an indicator may result in a response that contradicts what actually occurs.

Consequently, to clarify the effect of water on corrosion, which is known about so far mainly based on experience, data related to

corrosion, such as the rate of corrosion, was obtained and estimated from a field survey on members with different levels of water supply (Chapter 2), and the effects of water and carbonation on corrosion were analyzed (Chapter 3). In addition, as a design method that is consistent with the real situation, rather than carbonation, we aim to introduce a “study on the corrosion of reinforcing bars due to water penetration” that directly evaluates the corrosion of reinforcing bars and takes into account the effect of water. The applicability of the “study on the corrosion of bars due to water penetration” was verified by comparing the cover depth of areas where spalling occurred and the design cover depth determined from the “study on carbonation” and the “study on the corrosion of reinforcing bars due to water penetration” (Chapter 4).

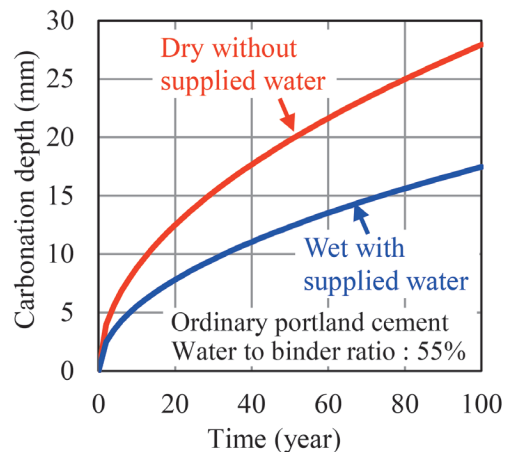


Fig. 1 Supplied water and calculated value of carbonation depth

2. Survey overview

2.1 Target of survey

Table 1 shows an overview of the members targeted for surveys. The target members are outdoor structures, exposed to the outside air and made of reinforced concrete. These are the outside of columns and handrail walls of rigid frame viaducts, which are generally exposed to rainwater (referred to in this paper as “presence of supplied water”), and the bottom of the intermediate slabs of a rigid frame viaduct and the bottom of the main beams of T shaped girders, which are comparatively less likely to be exposed to water (referred to in this paper as “absence of supplied water”). In addition, water leakage marks due to poor drainage were found on the outside of the columns within a range of 0.5 m to 1.5 m from the bottom of the horizontal beam and on the bottom of the intermediate slab within a range of 4.4 m to 5.0 m from the side of the longitudinal beam (Fig. 3). Details of shapes and reinforcing bar arrangements of the members are given in [4]. Viaducts A to D in [4] and A to D in this paper are the same.

Furthermore, the target structures are located in areas that are not affected by freezing and thawing or airborne salt, and no deterioration in concrete quality due to poor construction such as cold joints or rock pockets was observed. The chloride ion concentration in the concrete which derived from materials such as the use of sea sand was less than 0.4 kg/m³, and the effect of chloride ions on corrosion is small.

2.2 Method of survey

2.2.1 How to obtain data

As shown in Fig. 4, a mesh is created directly above the outermost reinforcing bar (the hoop reinforcing bars in Fig. 4). Regarding each mesh unit as one exposed test specimen, data were obtained and analyzed from several exposed test specimens with different cover depths, carbonation depths, and presence or absence of spalling. Cover depths were the measured values for the meshes on the survey line and the interpolated values for other meshes from the measured values based on previous research [5]. Carbonation depths were the measured values obtained in the vicinities of the



Fig. 2 Supplied water and spalling of concrete [3]

meshes.

Cover depths were measured using an electromagnetic induction method. The carbonation depth was the average value of distances from the concrete surface to the coloring point at four locations (top, bottom, left and right) in the holes, after spraying a 1% phenolphthalein solution into drill holes with a diameter of approximately 24 mm.

2.2.2 Method for estimating the corrosion rate of reinforcing bars

Figure 5 shows the method for estimating the corrosion rate of reinforcing bars. Visual inspection (Fig. 5(i)) and spalling prediction (Fig. 5(iii)) were carried out for each mesh shown in Fig. 4. Then, the corrosion rate is calculated (Fig. 5(v)) so that the patterns formed by the spalling areas and sound areas (Fig. 5(ii) and 5(iv)) match. If the age of each mesh at the time of spalling can be determined, the corrosion rate can be calculated for each mesh using a spalling prediction model. However, since the age at the time of spalling is unknown, we decided to estimate the corrosion rate based on the surface pattern formed by spalling areas and sound areas.

The spalling prediction model requires settings for the corrosion rate, and the corrosion depth when spalling occurs. The corrosion rate was assumed to be constant, similar to the corrosion rate

Table 1 Outline of members targeted for surveys

Name of viaduct	A	B	C	D
Structural type	Rigid frame viaduct			T shaped girder
Targeted members	Outside of column	Outside* of handrail wall	Bottom of intermediate slab	Bottom of main beam
Presence/Absence of supplied water due to visual inspection	Presence**	Presence	Absence**	Absence
Age at the time of surveys, Completion year	36, 1973	36, 1979	87, 1927	48, 1962
Cover depth (mm)	4 - 68	0 - 43	10 - 49	2 - 41
Carbonation depth (mm)	8 - 30	0 - 15	31 - 99	10 - 34
Un-carbonation depth (mm)	-26 - 45	-13 - 37	-66 - 9	-29 - 29
Estimated water to binder ratio W/B*** (%)	54 - 95	40 - 67	63 - 113	50 - 74
Initial chloride ion concentration (kg/m ³)	0.16 - 0.30	0.23 or less	-	0.19 - 0.40
Compressive strength (N/mm ²)	32, 38	-	24	30 - 41

* North side and South side

** There are water leakage marks due to poor drainage in some areas

*** Estimation equation based on "study on carbonation" [1] (see Appendix) $W/B = 1/9 \cdot \{y_g / (\beta_c \cdot \gamma_c \cdot \sqrt{t}) + 3.57\}$, y_g : carbonation depth (mm), β_c : when presence of supplied water 1.0 if viaduct A and B, when absence of supplied water 1.6 if viaduct C and D, γ_c : 1.0, t : age at the time of surveys (year)

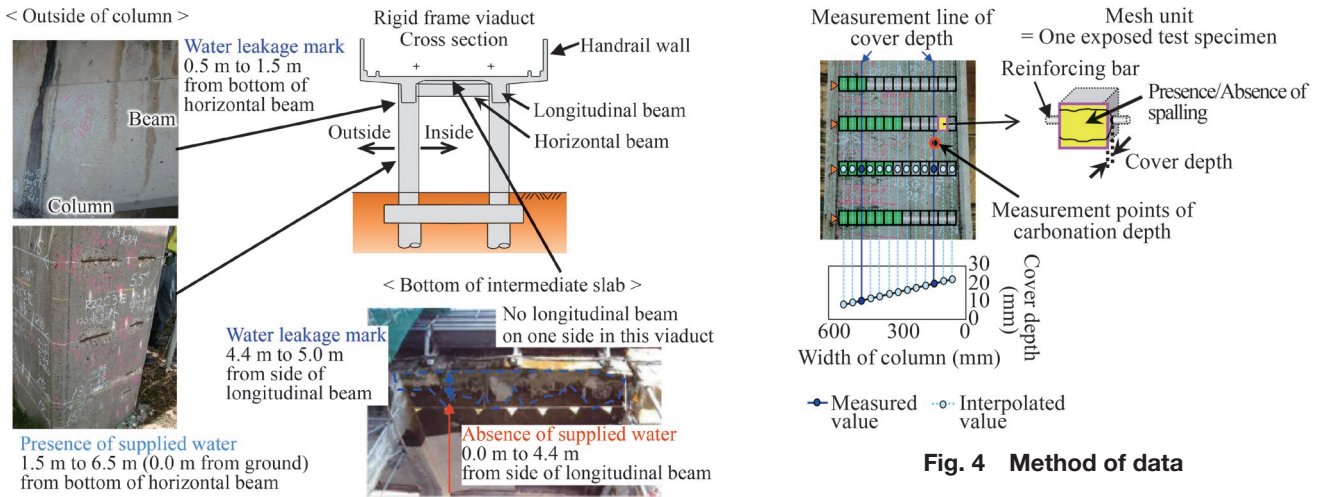


Fig. 3 Appearance of outer of columns and acquisition bottom of intermediate slabs

Fig. 4 Method of data

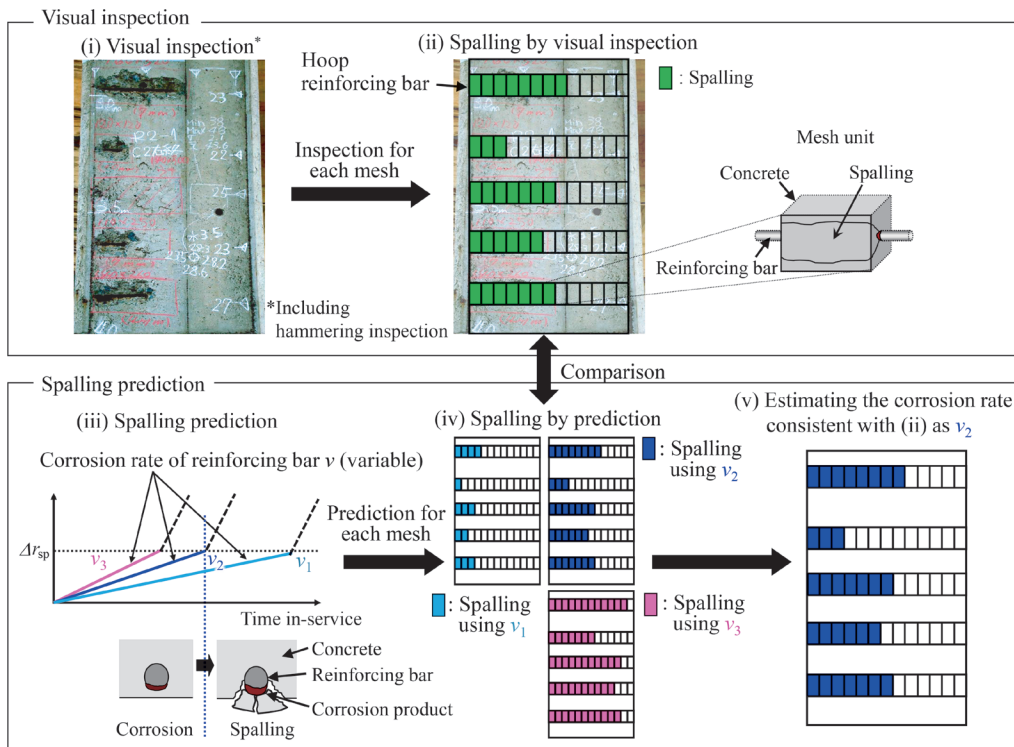


Fig. 5 Method for estimating the corrosion rate of reinforcing bars

equation used in the “study on corrosion of reinforcing bars due to water penetration” verified in Chapter 4. For the equation of the corrosion depth Δr_{sp} when spalling occurs, an equation was used that targets a cover of 30 mm or less, which is similar to the spalling locations in this survey [6].

3. Effect of water and carbonation on corrosion

3.1 Cover depth, un-carbonation depth, and supplied water in presence/absence of spalling

Figure 6 shows the relationship between the cover depth at

spalling areas or sound areas and the un-carbonation depth (the value obtained by subtracting the carbonation depth from the cover depth). At the bottom of the main beam (d), areas where repairs were thought to have been carried out for deterioration caused by corrosion of reinforcing bars, such as cross-sectional repairs, are shown separately from spalling.

Spalling occurred on all members with an un-carbonation depth of less than 10 mm. The maximum un-carbonation depth at which spalling occurred was 1 to 10 mm on the outside of columns, the outside of handrail walls, and the bottom of intermediate slabs in the presence of supplied water. Whereas it was less at the bottom of intermediate slabs and the bottom of main beams in the absence of supplied water, at -5 mm and 3mm respectively. Even if the cover

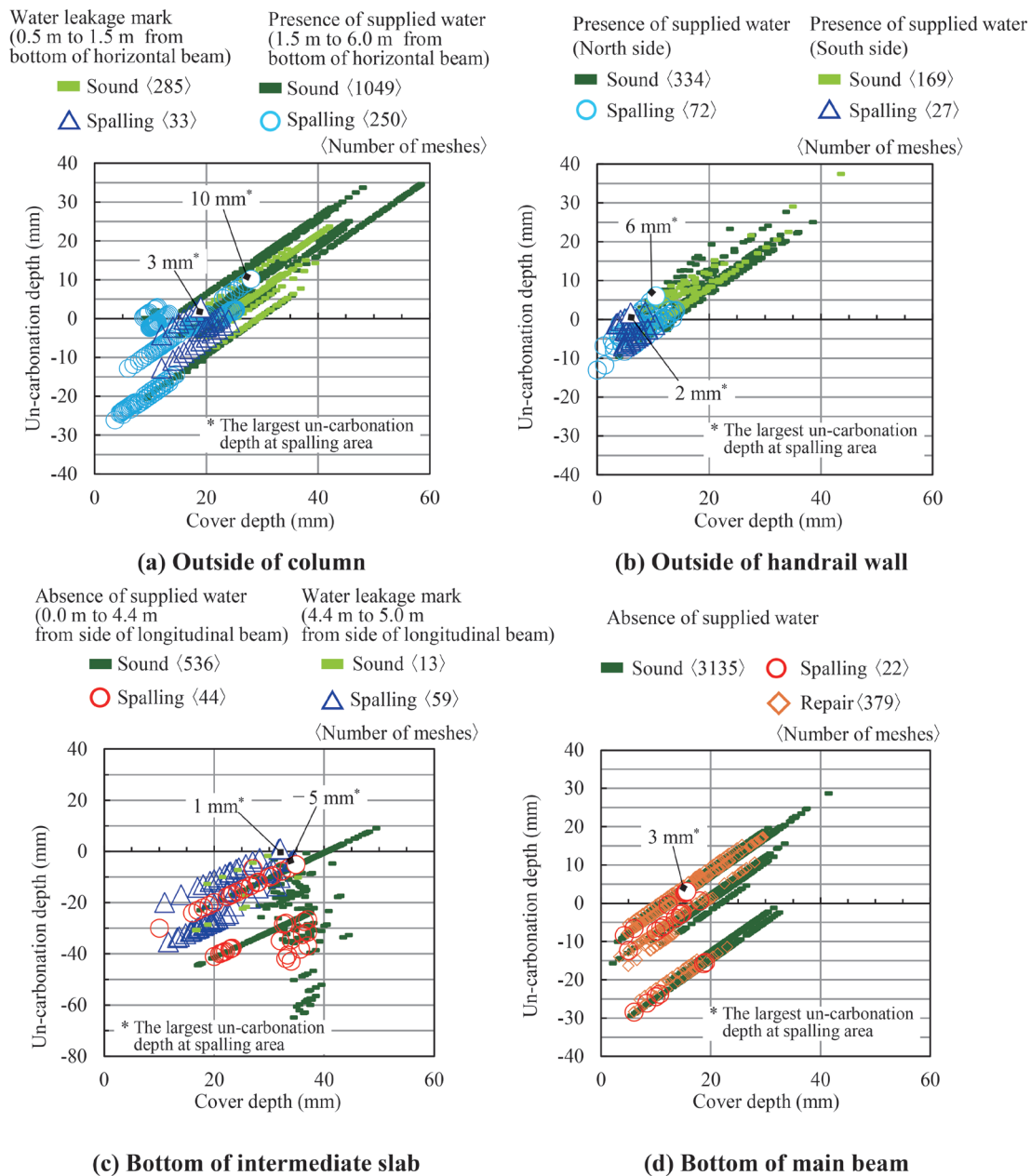


Fig. 6 Cover depth and un-carbonation depth in presence/absence of spalling

depth and un-carbonation depth were small, there were many sound areas on the bottom of intermediate slabs and main beams in the absence of supplied water compared to the outside of columns and handrail walls in the presence of supplied water.

3.2 Probability of spalling at different levels of supplied water

Figure 7 shows the relationship between cover depth or un-carbonation depth and the probability of spalling. The probability of spalling was calculated by dividing the number of meshes in the spalling area within each 5 mm classification (0 mm to 5mm, 5 mm to 10 mm, follows in the same way) by the total number of meshes in the sound and spalling areas. The repaired areas on the bottom of the main beam were categorized as spalling areas. Focusing on the cover depth, the shallower the cover depth, the higher the probability of spalling. Spalling tended to occur when the cover was less

than 30 mm at the time of the surveys, regardless of whether water was supplied or not.

Focusing on the un-carbonation depth, the probability of spalling increases when the un-carbonation depth is less than 10 mm on the outside of columns and handrail walls in the presence of supplied water. On the bottom of the intermediate slab and on the bottom of the main beam in the absence of supplied water, when the un-carbonation depth is less than 10 mm, the probability of spalling increases as with the presence of supplied water. A characteristic feature is that the probability of spalling in the absence of supplied water is lower than in the presence of supplied water, even when the un-carbonation depth is less than 10 mm. These results were obtained at different parts of different structures, and the qualities of materials and environments are not the same, so they cannot be easily compared. However, the same results were obtained in real surveys of members with and without supplied water in the same

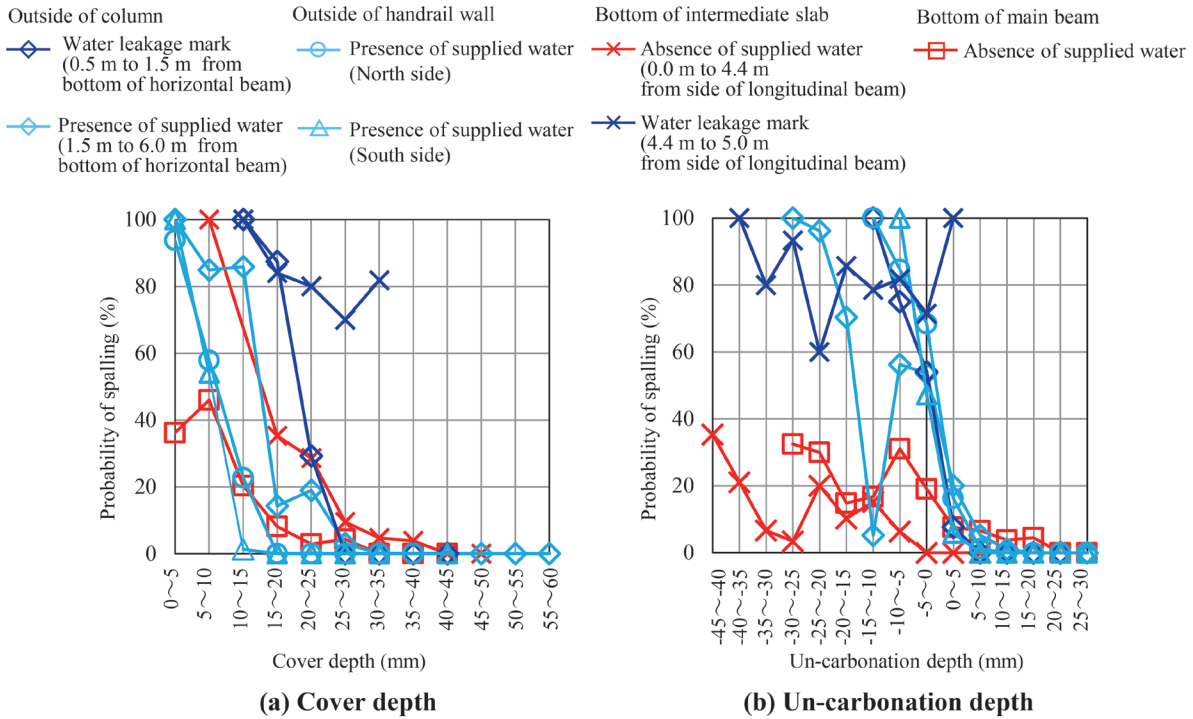


Fig. 7 Cover depth, un-carbonation depth and probability of spalling

structure [7].

Comparing the probability of spalling on the bottom of the intermediate slab at the same cover depth with and without water leakage marks, it is found that the probability of spalling is higher in areas where water leakage marks were observed.

3.3 Relationship between presence/absence of supplied water, un-carbonation depth, and corrosion rate

Figure 8 shows the relationship between the presence and absence of supplied water, the un-carbonation depth, and the corrosion rate. The average corrosion rate of the outside of handrail walls and columns in the presence of supplied water is 0.9×10^{-3} mm/year (0.4×10^{-3} to 1.4×10^{-3} mm/year), and the average corrosion rate of the bottom of main beams and intermediate slabs in the absence of supplied water was 0.7×10^{-3} mm/year (0.3×10^{-3} to 1.0×10^{-3} mm/year). The members surveyed in this paper were those where spalling had occurred and cover depth was less than 30 mm. Therefore, even members which, on visual inspection, appeared to have no supplied water, may in fact have been in conditions where water could be easily supplied by rain blow-in or the effect of moisture absorption and condensation. Nevertheless, the corrosion rate in the absence of supplied water was on average 0.8 times slower than that in the presence of supplied water. Since there is a possibility that water may be supplied from these sources even in those members where it is thought that there will be no supplied water, it is considered a safe design judgement to set the corrosion rate of the members in the absence of supplied water to be the same as that in the presence of supplied water.

The corrosion rate of reinforcing bars on the outside of the columns and the intermediate slabs where water leakage marks were observed due to poor drainage, was faster than average corrosion rates of members in the presence and absence of supplied water, at 0.8 to 1.8×10^{-3} mm/year. In general, carbonation does not proceed easily in members that are easily exposed to water. But in members

showing water leakage marks due to poor drainage, carbonation progress before poor drainage occurs, and water is supplied due to poor drainage. As a result of this, the corrosion rate may have increased.

From Sections 3.1 to 3.3, even when the un-carbonation depth is less than 10 mm, the probability of spalling is lower and the corrosion rate is slower in the absence of supplied water than those in the presence of supplied water. So, it is important to consider the effect of water on corrosion of reinforcing bars.

4. Applicability of “study on the corrosion of reinforcing bars due to water penetration”

4.1 Cover depth in spalling areas and design cover depth determined by the “study on corrosion of reinforcing bars due to water penetration”

Figure 9 shows the cover depth of the spalling areas, excluding areas displaying marks of water leakage due to poor drainage. Since it is unknown how many years a building had been in service when the spalling occurred, the age at the time of the surveys was plotted. In addition, based on the “study on the corrosion of reinforcing bars due to water penetration” (“verification of the corrosion depth of steel materials” shown in the Japan Society of Civil Engineers’ Standard Specifications for Concrete Structures (Design Edition) [8]), the corrosion depth obtained by multiplying the corrosion rate s_{dy} by the design life t is taken as the design value (1), the limit value (2) is determined, and the design cover depth when s_d/s_{lim} is 1.0 is shown in the figure. This equation is formulated on the assumption that water supplied by rainfall is the main cause of corrosion, and takes into account corrosion progress due to repeated dry and wet cycles.

$$s_d = \gamma_w \times s_{dy} \times t \quad (1)$$

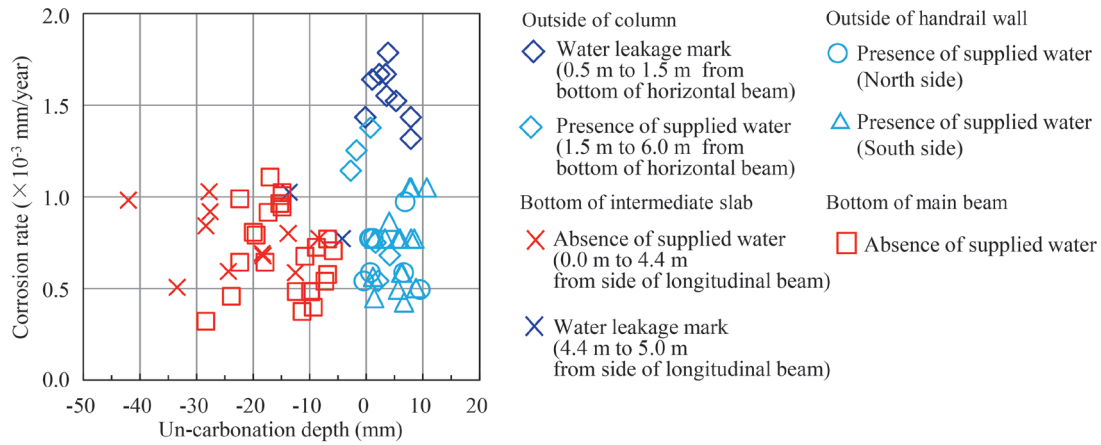


Fig. 8 Un-carbonation depth and corrosion rate in presence/absence of supplied water

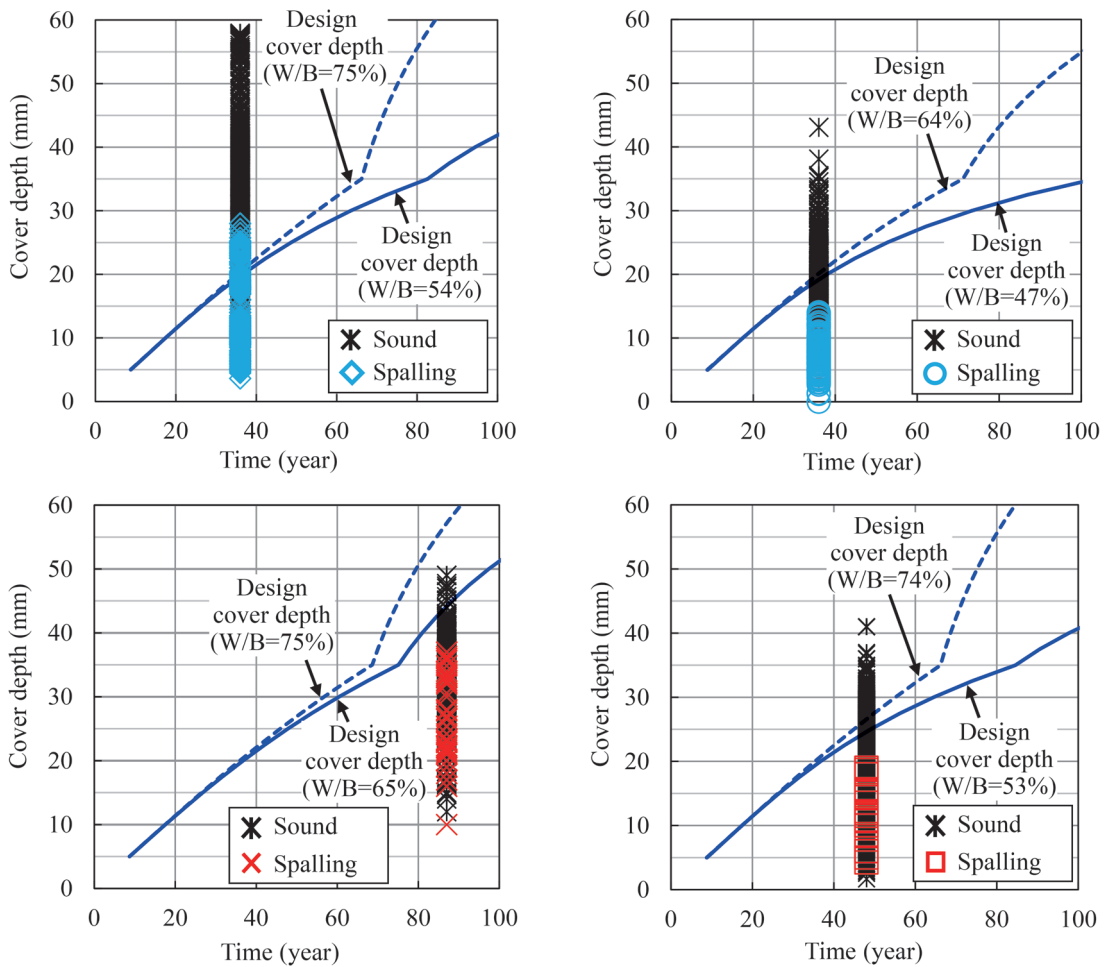


Fig. 9 Cover depth in spalling areas and design cover depth determined by “study on the corrosion of reinforcing bars due to water penetration”

$$s_{lim} = 3.81 \times 10^{-4} \times c \quad (2)$$

if $c > 35$ mm, $s_{lim} = 1.33 \times 10^{-2}$

Here,

- s_d : design value of corrosion depth of reinforcing bars (mm)
- s_{lim} : limit value of corrosion depth of reinforcing bars (mm)
- γ_w : safety factor considering variation in design value s_d , general-

ly 1.15.

- s_{dy} : design value of corrosion depth per year (referred to as corrosion rate in this paper) (mm/year)
- $s_{dy} = 1.9 \times 10^{-4} \times \exp(-0.068 \times (c - \Delta c_c)^2 / q_d^2)$
- c : design cover depth (mm)
- Δc_c : construction error of cover depth (mm). 5 mm for intermediate slab, 10 mm for others

- q_d : design value of water penetration rate coefficient of concrete (mm/ $\sqrt{\text{hour}}$)
 $q_d = \gamma_c \times q_k$
- γ_c : safety coefficient for concrete, generally 1.3.
- q_k : characteristic value of water penetration rate coefficient of concrete (mm/ $\sqrt{\text{hour}}$)
 $q_k = 31.25 \times (W/B)^2$
- W/B : water to binder ratio. The minimum and maximum value of the estimated value from the carbonation depth of the spalling area (calculated by *** in Table 1), with an upper limit of 75%.
- t : design life (year). In Fig. 9, time in-service.

As can be seen from the figure, the cover in the spalling areas is generally smaller than the design cover determined by the “study on the corrosion of reinforcing bars due to water penetration.” On the outside of the columns, spalling occurred in some areas with a cover depth of 20 mm to 30 mm, which was larger than the design cover depth determined by the “study on the corrosion of reinforcing bars due to water penetration.” The estimated W/B of the outside of this column is large. So, it is possible that a lower quality concrete was used, which differs from the current type found in new structures. Despite this, the rate of spalling at a cover depth of 20 mm to 30 mm is small, less than 5%.

4.2 Design cover depth determined by “study on carbonation” and “study on the corrosion of reinforcing bars due to water penetration”

Figure 10 shows a comparison of the design cover determined by the “study on carbonation” [1] (see Appendix) and the “study on the corrosion of reinforcing bars due to water penetration” (see Section 4.1). The design cover determined by a study on corrosion of steel due to water penetration is 30 mm or more ($W/B = 40\%$ to 60%). This is larger than that determined by the “study on carbonation” in the presence of supplied water ($\beta_c = 1.0$). The design cover determined by the “study on the corrosion of reinforcing bars due to water penetration” is 30 mm or more ($W/B = 40\%$ to 60%). This is larger than that determined by the “study on carbonation” in the presence of supplied water. On the other hand, the design cover by the “study on carbonation” is determined so that the un-carbonation depth would be more than 10 mm during the design life. So, if the

design cover determined by the “study on the corrosion of reinforcing bars due to water penetration” is ensured, the un-carbonation depth during the design life remains more than 10 mm.

If the un-carbonation depth is more than 10 mm, the pH around the reinforcing bars has not decreased, and it is thought that the corrosion rate will not increase due to a decrease in pH around the reinforcing bars [9]. Therefore, when determining a design cover based on the “study on the corrosion of reinforcing bars due to water penetration,” it is thought that the design cover can be determined in consideration of the effect of carbonation.

The design cover determined by the “study on carbonation” in the absence of supplied water is larger at $W/B = 45\%$ or more than the design cover determined by the “study on the corrosion of reinforcing bars due to water penetration.” According to Chapter 3, in the absence of supplied water, the probability of spalling is lower and the corrosion rate is slower than in the presence of supplied water. Therefore, it makes sense that the design cover depth in the absence of supplied water is smaller than that in the presence of supplied water. In the design, even for members that are not supposed to be exposed to rain, the design cover depth must be determined in consideration of the fact that water may be supplied due to, for example, water from facilities under rigid frame viaducts, rain blowing in, water penetration from other parts, moisture absorption, dew condensation, and so on.

5. Conclusion

The effect of water and carbonation on the corrosion of reinforcing bars in concrete was investigated by field surveys on members under different levels of supplied water. In addition, the applicability of the “study on the corrosion of reinforcing bars due to water penetration” was verified by comparing the cover depth where spalling of concrete occurred and the design cover depth determined by the “study on carbonation.”

- (1) It is important to consider the effect of supplied water on corrosion of reinforcing bars, because even when the remaining un-carbonation depth is less than 10 mm, if there is no water exposure, the probability of spalling is lower and the corrosion rate of reinforcing bars is slower than that in the presence of supplied water.
- (2) It was confirmed that the cover depth in the areas where spalling

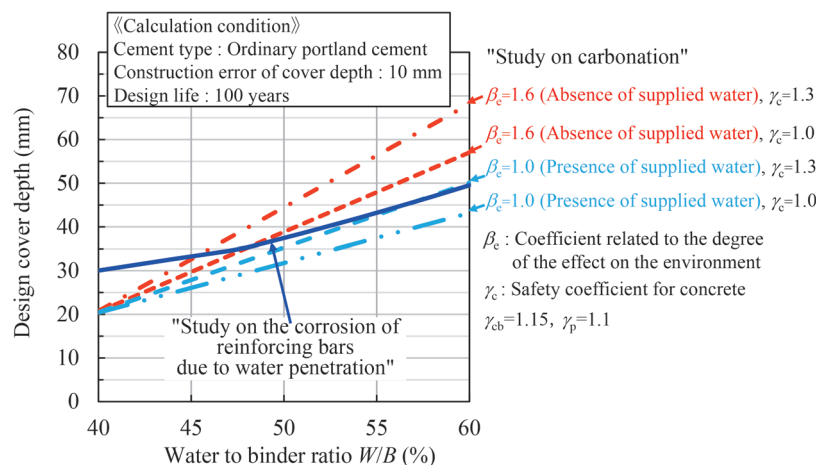


Fig. 10 Design cover depth determined by “study on carbonation” and “study on the corrosion of reinforcing bars due to water penetration”

had occurred was generally smaller than the design cover depth determined by the “study on the corrosion of reinforcing bars due to water penetration.” It was also confirmed that if the design cover depth determined by the “study on the corrosion of reinforcing bars due to water penetration” with a design life of 100 years is ensured, the “study on carbonation” will also be satisfied. Therefore, as a design method for corrosion of reinforcing bars due to water penetration and concrete carbonation, it is considered that it is possible to determine the design cover depth using the “study on the corrosion of reinforcing bars due to water penetration” instead of the “study on carbonation.”

Appendix “study on carbonation”

In the “study on carbonation” [1], the design cover depth is set so that the remaining un-carbonation depth is at least 10mm ($y_g \leq y_{lim}$). Figure 10 shows the design cover depth when y_g / y_{lim} is 1.0.

$$y_g = \gamma_{cb} \times \alpha_d \times \sqrt{t} \quad (A1)$$

$$y_{lim} = c - \Delta c_c - c_k \quad (A2)$$

Here,

y_g : estimated value of carbonation depth of concrete (mm)

y_{lim} : limited value of carbonation depth of concrete (mm)

γ_{cb} : safety factor considering variation in estimated value y_d , generally 1.15.

α_d : estimated value of carbonation rate coefficient (mm/ $\sqrt{\text{year}}$)

$$\alpha_d = \alpha_k \times \beta_c \times \gamma_c$$

α_k : characteristic value of carbonation rate coefficient (mm/ $\sqrt{\text{year}}$)

$$\alpha_k = \gamma_p \times \alpha_p$$

γ_p : coefficient related to the accuracy of α_p . In general, 1.1 when using the estimation equation α_p listed below.

α_p : predicted value of carbonation rate coefficient (mm/ $\sqrt{\text{year}}$)

$$\alpha_p = -3.57 + 9.0 \times W/B$$

W/B : water to binder ratio

β_c : coefficient related to the degree of the effect on the environment when members tend to be wet, 1.0 and dry, 1.6.

γ_c : safety coefficient for concrete. In general, 1.0. In members where quality of concrete may deteriorate due to bleeding, 1.3.

t : design life (year)

c : design cover depth (mm)

Δc_c : construction error of cover depth (mm)

c_k : un-carbonation depth (mm). In general, 10mm

References

- [1] Railway Technical Research Institute, *Design Standards for Railway Structures and Commentary (Concrete Structure)*, Maruzen co., Ltd, Tokyo, pp. 222-233, 2004 (in Japanese).
- [2] Ishibashi, T., Furuya, T., Hamazaki, N., and Suzuki, H., “Investigation of falling on concrete fragments from RC structures,” *Journal of Materials, Concrete Structures and Pavements*, No. 711/V-56, pp. 125-134, 2002.8 (in Japanese).
- [3] Ueda, H., Iijima, T., and Suzuki, H., “Investigating the effect of water penetration into concrete structures,” *RRR*, No. 71, No. 6, pp. 20-23, 2014 (in Japanese).
- [4] Todoroki, S., Ishida, T., Tadokoro, T., and Ueda, H., “Effect of water migration and carbonation progress on rebar corrosion rate in concrete,” *Journal of Japan Society of Civil Engineers, Ser. E2 (Materials and Concrete Structures)*, Vol. 75, No. 4, pp. 226-238, 2019 (in Japanese).
- [5] Matsushita, M., Todoroki, S., Tadokoro, T., and Ishida, T., “Estimation method of cover depth for vertical members of RC structures,” *Proceedings of the Japan Concrete Institute*, Vol. 40, No. 2, pp. 1303-1308, 2018 (in Japanese).
- [6] Kadono, T., Todoroki, S., Watanabe, K., and Tadokoro, T., “Analytical study on rebar corrosion depth threshold initiating cracks and spalling of cover concrete affected by rebar placement of RC members,” *Concrete Structure Scenarios, JSMS*, Vol. 18, pp. 161-166, 2018 (in Japanese).
- [7] Tabata, K., Ishibashi, N., Todoroki, S., and Tadokoro, T., “Effects of rain exposure and concrete quality on spalling of cover concrete based on investigation of railway RC viaducts,” *Proceedings of the Annual Meeting of Japan Society of Civil Engineers*, Vol. 75, V-168, 2020 (in Japanese).
- [8] Japan Society of Civil Engineers, *Standard Specifications for Concrete Structures (Design Edition) established in 2017*, 2018 (in Japanese).
- [9] Todoroki, S., Ueda, H., Ishida, T., and Tadokoro, T., “Effects of supplied water and PH around reinforcing bars on the spalling occurring due to corrosion,” *Proceedings of the Japan Concrete Institute*, Vol. 43, No. 1, pp. 467-472, 2021 (in Japanese).

Authors



Shuntaro TODOROKI, Dr.Eng.
Senior Researcher, Concrete Structures
Laboratory, Structures Technology Division
Research Areas: Design Methods for Railway
Concrete Structures



Hiroshi UEDA, Dr.Eng.
Director, Head of Materials Technology
Division
Research Areas: Durability of Concrete and
Related Materials.



Tetsuya ISHIDA, Ph.D.
Professor, Department of Civil Engineering,
The University of Tokyo
Research Areas: Multi-scale Modeling of
Cementitious Materials and Structures



Toshiya TADOKORO, Dr.Eng.
Senior Chief Researcher, Head of Concrete
Structures Laboratory, Structure Technology
Division
Research Areas: Design Methods for Railway
Concrete Structures

Development of Automatic Generation of Maintenance Worker Schedule Using Tabu Search

Tatsuya KOKUBO Satoshi KATO Taichi NAKAHIGASHI
 Transport Operation Systems Laboratory, Signalling and Operation Systems Technology Division

Maintenance worker schedules are daily schedules for teams performing inspection and maintenance work such as cleaning of rolling stock during turnaround operations at terminal stations. Since these schedules vary from day to day according to changes in rolling stock operations, they have to be created for each day. We have therefore proposed a method for automatically generating maintenance worker schedules using tabu search. In this paper, to confirm the effectiveness of the proposed method, we compared an actual schedule with schedules generated using proposed method. The results indicated that the proposed method could generate a practical solution within 3 minutes.

Key words: maintenance worker scheduling, rolling stock scheduling, metaheuristics, tabu search, mixed integer programming

1. Introduction

When trains providing high-end services turnaround at a terminal station, maintenance such as cleaning and inspection of rolling stock is required. Maintenance is carried out by teams of workers (referred to as “a set”), and the daily maintenance work plan for each set is shown in a maintenance worker schedule. The maintenance worker schedule is prepared each day in accordance with train schedules and rolling stock schedules that vary from day to day. Currently, maintenance worker schedules are prepared manually by skilled planners. However, because of multiple constraints on the workload of maintenance workers, it takes several hours to prepare one day’s schedule, which is labor intensive. This has created a need for automatic generation of the maintenance worker schedule for improving labor-saving.

There has not been reported existing studies on the automatic generation of the maintenance worker schedule. The maintenance worker scheduling problem is similar to a shift scheduling problem [1], a flow-shop scheduling problem, a job-shop scheduling problem [2], and a crew scheduling problem [3]. The shift scheduling problem and the crew scheduling problem basically minimize the number of staff. The flow-shop scheduling problem and the job-shop scheduling problem generally minimize the time required for all work, since the order in which each job is processed is predetermined. However, it is considered difficult to apply the existing studies to the problem of maintenance worker scheduling, because this problem has a given number of sets but no predetermined order of maintenance tasks. Moreover, it is necessary to consider specific conditions such as differences in the number of maintenance tasks carried out by each set, and different time intervals required for teams moving track to track between maintenance interventions.

For practical purposes, it is important for the automatic generation of maintenance worker schedules to take less than 3 minutes to calculate, have a small number of parameters, and output the same results for the same input data. In addition, depending on the input data, there may not be a feasible solution that satisfies all the constraints. After analyzing actual maintenance worker schedules (referred to as “actual schedules”) we identified two types of constraints: high priority non-relaxable constraints and low priority relaxable constraints.

Based on these requirements, we developed a generation method using tabu search (referred to as “TS”), a metaheuristics method that can automatically generate maintenance worker schedules in 3

minutes (referred to as “proposed method”) [4, 5, 6]. To confirm the effectiveness of the proposed method, we compared it with actual schedules and maintenance worker schedules generated by mixed integer programming (referred to as “MIP”) [6].

2. Overview of maintenance worker scheduling

This chapter provides an overview of maintenance worker scheduling and definitions of terms. The train that needs maintenance is given, and a start time of each maintenance intervention is determined by an arrival time of the train. The number of sets per day is predetermined, and each set is classified (referred to as “group”) according to the time of day (AM/PM).

Figure 1 shows an example of the input data for generating the maintenance worker schedule. 14 trains are shown in Fig. 1, with 2 groups, 4 sets, and maintenance from 2M to 28M. Figure 1 shows the maintenance schedule for one day for each “track No.”. “2M” etc. is a train number, the light blue time zone indicates maintenance of the corresponding train, and the track number and work time are given. The bottom of Fig. 1 shows the available and unavailable time for each set indicated by “group No.” and each set indicated by “set No.”. “B” and “M” are breaks and meetings time (referred to as “fixed time”), and the start and end times are given. Fixed time is defined only between maintenance interventions, and one or more fixed times are defined for each set. “S” is the preparation time after start time, “F” is the preparation time before finish time, “I” is the preparation time before fixed time, and “R” is the preparation time after fixed time, and each required time is given. Excluding these preparation time and fixed time, maintenance are performed for all trains.

Figure 2 shows an example of the maintenance worker schedule based on the input data in Fig. 1. The planner assigns each maintenance intervention to one of the sets in Fig. 1, excluding the preparation time and fixed time. “t” is an interval required for moving from one track to the next between maintenance interventions (referred to as “track interval”). In addition, when a certain amount of time cannot be ensured between the end time of the maintenance work or the end time of track interval and the start time of the next maintenance work (referred to as “continuous work”), the additional time described in “a” must be ensured. The additional time is added after the track interval to the next maintenance work, and corresponds to a restroom break, etc.

Maintenance per target train per track

Track No.	07:00	10:00	13:00	16:00	19:00
1		8M			26M
2		4M	6M 12M 16M	22M	
3			14M	20M	24M
4	2M	10M	18M		28M

2M : Train No.
 : Maintenance required for each train

Available intervals of each worker set at each group

Group No.	Set No.	07:00	10:00	13:00	16:00	19:00
1	1	S		I B R	E	
	2	S		I M R	E	
2	3		S		I B R	E
	4		S		I M R	E

: Start time and finish time
 : Break and meeting time(fixed time)
 : Preparation time after start time and before finish time
 : Preparation time before and after break and meeting time
 : Available intervals of each worker set
 : Unavailable intervals of each worker set

Fig. 1 An example of input data for generating maintenance worker schedule

Group No.	Set No.	07:00	10:00	13:00	16:00	19:00
1	1	S	2M t	6M 12M I B R	22M E	
	2	S	4M t	8M I M R	24M E	
2	3		S 10M t	16M t a	I B R	26M E
	4		S	14M 18M	I M R	28M E

: Interval required for moving to next track between maintenance interventions
 : Interval required for restroom break after continuous work

Fig. 2 An example of a maintenance worker schedule based on input data in Fig. 1

Node

- : Start or finish for set No.1
- : Fixed time for set No.1
- 1M : Train No.
- : Maintenance work

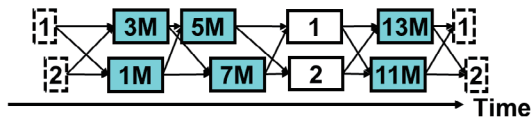


Fig. 3 An example of a graph with candidate nodes and arcs expressing a maintenance worker schedule

3. Modeling of a maintenance worker scheduling problem

3.1 Data Structure

In this paper, the maintenance worker schedule is represented by applying a graph with nodes and arcs. Figure 3 shows an example of the graph expressing the maintenance worker schedule. There are four types of nodes: “maintenance work node” corresponding to each maintenance intervention, “start node” corresponding to each set and indicating the start of work, “finish node” indicating the finish of work, and “fixed work node” corresponding to each fixed work in each set. In addition, “start time” and “end time” are defined for each node. The maintenance work node and fixed work node are

defined by the start time and end time of the corresponding maintenance work and fixed work. The start time of the start node is defined as the corresponding start time of each set. The end time of the end node is defined as corresponding end time of each set. In addition, the start and end times of the start and end nodes are defined as the same time.

With the exceptions noted below, for any two nodes, if the start time of one is equal to or later than the end time of the other, the latter node is extended to the former. The exceptions are: arcs from any node to the start node, arcs from the finish node to any node, arcs between finish nodes, arcs between different sets of fixed work nodes, arcs between the start node and fixed work nodes, and arcs between the finish node and fixed work nodes. Each arc has time information calculated as the start time of the destination node minus the end time of the source node. In this paper, the arcs are defined even in the case where the track interval time, each preparation time, or the additional time are insufficient, so that the graph can violate the low priority for relaxable constraints in order to satisfy the high priority for non-relaxable constraints.

3.2 Constraints

Constraints can be divided into three major types: “constraints related to assignment,” “constraints related to number of maintenance interventions,” and “constraints related to time.” The constraints are shown below.

- (1) Constraints related to assignment
 - Constraint 1: Maintenance work assignment

Only one set is assigned to each maintenance work.

Constraint 2: Maintenance intervention order of assignment

The first maintenance intervention is assigned to the set with the earliest start time and fixed work end time. The last maintenance intervention is assigned to the set with the last start time and fixed work end time.

(2) Constraint related to the number of maintenance interventions

Constraint 3: Upper limit of the number of maintenance works

The number of maintenance interventions assigned to one set in a day is within the predefined threshold.

Constraint 4: Upper limit on the difference in the number of maintenance interventions per set within the group

The difference in the number of maintenance interventions per set within the group is within the predefined threshold.

Constraint 5: Upper limit on the difference in the number of maintenance interventions between groups

The difference in the number of maintenance interventions for each set between groups is within the predefined threshold.

(3) Constraints related to time

Constraint 6: Track interval time

If movement between tracks is required between maintenance interventions, the required track interval time to allow for movement is ensured.

Constraint 7: Preparation time after start time and before finish time

After start time of each set and before finish time of each set, the required preparation time is ensured.

Constraint 8: Preparation time for interruption and resumption

Before fixed work of each set and after fixed work of each set, the required preparation time is ensured.

Constraint 9: Additional time

Additional time is ensured after track interval time for moving between tracks from one continuous maintenance intervention to the next. Specifically, if the interval between the end time of the track interval time and the start time of the next maintenance intervention is less than C_x minutes and C_y consecutive maintenance interventions are performed, additional time C_z minutes are ensured after the next maintenance intervention. There are also multiple combinations of C_x , C_y , and C_z .

Among these constraints, constraints 1 to 5 are high priority for non-relaxable constraints, constraints 6 to 9 are low priority for relaxable constraints. We analyzed actual schedules and found that satisfying high priority constraints is important from a practical point of view.

3.3 Objective function

In this problem, it is necessary to assign maintenance considering the equalization and reduction of the workload of maintenance workers. In addition, the number of sets and the start time and finish time of each set (available working time period) are given. Therefore, in this paper, evaluation value terms of an objective function are the variance of the number of maintenance interventions in each set for the purpose of workload equalization, the total track interval time and additional time in all sets for the purpose of workload reduction. Furthermore, the objective function value is the sum of each term of the objective function multiplied by a weighting coefficient, and minimized.

As discussed in Chapter 1, depending on the input data, there is

a possibility that a feasible solution that satisfies all the constraints may not exist. For practical purposes, even in such cases, it is desirable to return a maintenance worker schedule such that high priority constraints are satisfied, and low priority constraints are violated, rather than judging it to be infeasible. Therefore, in order to output maintenance worker schedule in practice, a penalty is defined based on the amount of violation calculated from the predefined threshold of each constraint and other factors. The penalty that is multiplied by the weighting coefficient is added as a penalty term to the objective function. The penalty for constraint 1 is the number of unassigned maintenance works. The penalty for constraint 2 is the number of combinations that violate the maintenance work order. The penalty for constraints 3 to 5 and 7 to 9 is the sum of the squares of violations from predefined thresholds for each constraint, in order to prevent the large violations from predefined thresholds for each constraint. The penalty for constraint 6 is the sum of the fourth power of the violation from the predefined threshold. Moreover, each penalty is multiplied by the weighting coefficient to consider the priority of constraints. Specifically, the weighting coefficient of high priority constraint 1 to 5 are determined to be large values. The objective function is shown below:

$$\min \left\{ w_1 t_1 + w_2 t_2 + w_3 t_3 + \sum_{n=1}^9 p_n e_n \right\} \quad (1)$$

t_1 : Variance of the number of maintenance in each set

t_2 : Total track interval time

t_3 : Total additional time

w_1, w_2, w_3 : Weighting coefficient for each term
($w_1 + w_2 + w_3 = 1$)

e_n : Penalty for constraint n ($n = 1, \dots, 9$)

p_n : Weighting coefficient for each penalty term

4. Maintenance worker scheduling problem using tabu search

4.1 Tabu search

Tabu search (TS) is a metaheuristics technique proposed by Fred Glover, a general method for solving combinatorial optimization problems [7]. TS performs the search using a tabu list (TL) that saves the most recently searched solutions. In a TL, the number of solutions to be saved is determined by the pre-defined TL length (TLL), and no transitions to solutions contained in the TL are allowed. TS generalizes a local search method and improves solutions by generating neighborhood solutions from the current solution and moving to the best neighborhood solution, which is not tabu. Although the local search method must stop searching if all the neighborhood solutions are not superior to the current solution, TS can continue searching by moving to the best neighborhood solution, which is not tabu even if the best solution is not superior to the current solution. In addition, there is no guarantee that TS will always generate an optimal solution due to the nature of the metaheuristics. In general, TS is a widely used method in many problems because it is known to be able to generate good quality solutions to large-scale problems in a short computation time.

The aspiration level, which is known to enable efficient searches in general, is applied to the proposed method [7]. The aspiration level is that the point with the better total objective function value among the candidates for the neighborhood solutions at the next point is adopted even if it is tabu.

The procedure for TS in the proposed method is shown below.

- Step. 1 Generate an initial solution (see Section 4.2). The initial solution is used as a tentative solution. The number of searches $iter = 1$.
- Step. 2 Generate neighborhood solutions from the tentative solution (see Section 4.3). However, if maintenance to be exchanged by generating the neighborhood solutions is included in the TL, or if the objective function value is higher than a best solution, it is not generated as a neighborhood solution.
- Step. 3 Among the neighborhood solutions, the solution with the best objective function value is selected and used as the tentative solution in the next iteration. Maintenance that has been exchanged by the generating neighborhood solution are put in the TL.
- Step. 4 If $iter$ reaches the preset $iter_{max}$, the best solution is outputted, and the process is terminated. Otherwise, set $iter = iter + 1$ and go back to Step. 2.

4.2 Generation of an initial solution

In generation of the initial solution process, a “current node” is updated for each set. The current node is defined the node with the slowest end time among the nodes assigned to each set. The algorithm for generating an initial solution is shown below:

- Step. 1.1 Assign the corresponding start node to every set. Update the current node as the start node of every set.
- Step. 1.2 Select the set among all sets with the earliest end time of the current node. However, the set whose current node is the end node is not selected. Among the maintenance work nodes connected to the arc from the current node, the maintenance node that is not assigned to any set and has the shortest time between the current node and the maintenance node is selected. If it cannot be extracted, go to Step. 1.5.
- Step. 1.3 If the end time of the extracted maintenance work node exceeds the start time of one of the unassigned fixed work nodes corresponding to the set selected in Step 1.2, go to Step 1.4. If it exceeds the start time of the end node corresponding to the set selected in Step 1.2, go to Step 1.5. Otherwise, assign the extracted maintenance work node, update the current node, and go to Step 1.6.
- Step. 1.4 Assign the fixed work node, update the current node, and go to Step 1.6.
- Step. 1.5 Assign the end node and update the current node.
- Step. 1.6 When all sets of current nodes have become end nodes, output the initial solution, calculate the total objective function value based on (1), and terminate the process. Otherwise, go back to Step. 1.2.

4.3 Generation of neighborhood solutions

This paper proposes three generating neighborhood solutions to improve all evaluation values and to resolve all constraint penalties except constraint 1. The generating neighborhood solution 1 contributes to the improvement of each evaluation value of the objective function related to time and the penalty related to time. On the other hand, it does not contribute to the improvement of each evaluation value and penalties related to distribute the number of maintenance works, since the number of maintenance to be improved is not exchanged. The generating neighborhood solution 2 and 3 contribute to the improvement of all evaluation values and penalty except constraint 1. These three generating neighborhood solutions allow for extensive searches and increase the likelihood of

obtaining the best solution. Figure 4 shows an example of a tentative solution.

Generating neighborhood solution 1: 1-1 exchange

Figure 5 shows an example of a neighborhood solution generated by the “1-1 exchange.” One maintenance work node of the set is exchanged with the interchangeable maintenance node of another set at the same time zone.

Generating neighborhood solution 2: 2-1 exchange

Figure 6 shows an example of a neighborhood solution generated by the “2-1 exchange.” Two maintenance work nodes of the set are exchanged with the interchangeable maintenance node of another set at the same zone.

Generating neighborhood solution 3: 1-0 insertion

Figure 7 shows an example of a neighborhood solution generated by the “1-0 insertion.” One maintenance work node of the set is inserted between two other maintenance work nodes of another set at the same time zone.

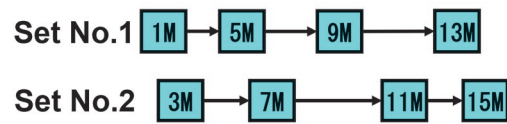


Fig. 4 An example of an original solution.

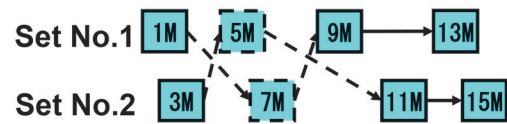


Fig. 5 An example of a neighborhood solution generated by the “1-1 exchange.”

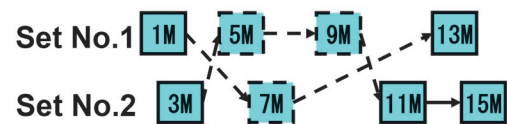


Fig. 6 An example of a neighborhood solution generated by the “2-1 exchange.”

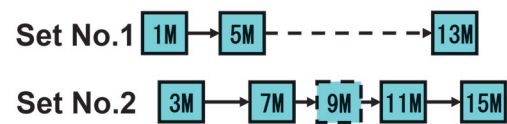


Fig. 7 An example of a neighborhood solution generated by the “1-0 insertion.”

5. Case study

5.1 Case study condition

To confirm the effectiveness of the proposed method, a case study is conducted using actual train schedules and rolling stock schedules for three days. Specifically, the maintenance worker schedule [I] generated by the proposed method is compared with the actual schedule [II] and the maintenance work schedule [III] generated by MIP. For details of MIP formulation, see to Reference 7.

Input data used for case study is 99 trains and 7 sets (small scale) for Case 1; 120 trains, 8 sets (medium scale) for Case 2; and

147 trains, 9 sets (large scale) for Case 3. In addition, following conditions are determined in common for each case.

- Upper limit of the number of maintenance works: 18
- Upper limit on the difference in the number of maintenance work within the group: 2
- Upper limit on the difference in the number of maintenance work between groups: 2
- Preparation time: 10 to 20 minutes
- Track interval time: 0 to 3 minutes
- Additional time 1: $C_x = 4, C_y = 2, C_z = 5$
- Additional time 2: $C_x = 7, C_y = 5, C_z = 10$

Table 1 shows weighting coefficients for the objective function for case study. Weight coefficients for each penalty in the objective function are set with the aim of generating the maintenance worker schedule that satisfies high priority constraints 1 to 5 more than low priority constraints 6 to 9. Parameters of TS are set to the TLL of 50 and the iteration of 5,000. It is important for practical purposes that automatic generation of the maintenance worker schedule takes less than 3 minutes to calculate, all cases' upper limit of computation time is set 3 minutes. The case study software has been developed using C language (Microsoft Visual Studio 2019) on a PC (Intel Core i7-8700 (3.20 GHz) CPU and 64 GB memory) and used the mathematical optimization solver Gurobi (Optimizer 9.5.110) [8] to solve MIP.

5.2 Case study results

Table 2 shows the objective function value, each evaluation value, and each penalty by the actual schedule (I), the proposed method (II), and MIP (III) in each case. In Table 2, each evaluation value and each penalty with high priority constraints of the proposed method are listed in red bold face.

In Case 1, the proposed method reduces the track interval time by 31 minutes and increases the additional time by 5 minutes compared with the actual schedule. In Case 2, the proposed method increases the track interval time by 3 minutes and reduces the additional time by 15 minutes compared with the actual schedule. In Case 3, the proposed method reduces the track interval time by 36 minutes and the additional time by 70 minutes compared with the

actual schedule. Therefore, the proposed method reduces both the track interval time and the additional time by the actual schedule, so that it is confirmed that the proposed method can generate a maintenance worker schedule that reduces the workload on maintenance workers.

The proposed method can generate the best solution in the practical computation time of about 1 minute for all cases. In addition, the proposed method can generate practical solutions in all cases, because the penalty terms corresponding to high priority constraints 1 to 5 are all zero. Since the most important practical aspects of this problem are that computation time is less than 3 minutes and that high priority constraints 1 to 5 are satisfied, results indicate that the proposed method can generate the practical maintenance worker schedule in practical time.

In Cases 1 and 2, maintenance worker scheduling by MIP generate solutions with the objective function value lower than those of the actual schedule and the proposed method. But in all cases, the optimal solution by MIP cannot be generated in computation time of 3 minutes. In Case 3, the total objective function value is clearly inferior, but at the 3 minutes stage, the dual gap representing the accuracy of the solution is extremely large, confirming that the computation time is clearly insufficient. In addition, high priority constraints 1 to 5 are violated, and no practical solution are created. Therefore, MIP cannot generate practical solutions on days with many trains within a practical computation time, because it cannot satisfy high priority constraints.

In conclusion, the proposed method can generate maintenance worker schedules that satisfy high priority constraints 1 to 5 and reduce the track interval time and the additional time, within 3 minutes computation time in each case. This indicates that the proposed method will be effective in practice.

6. Conclusions

Maintenance worker schedules are the daily schedules produced for each worker set, allowing them to carry out inspection and maintenance work such as cleaning of rolling stock during turn-around operations at terminal stations. The maintenance worker

Table 1 Weighting coefficients for the objective function for case study.

w_1	w_2	w_3	p_1	p_2	p_3	p_4	p_5	p_6	p_7	p_8	p_9
0.9	0.05	0.05	100,000	100,000	100,000	100,000	100,000	100	100	100	100

Table 2 The value of each evaluation value term of the objective function and amount of deviation from the predefined threshold for each constraint.

Case.	Object function value	t_1	t_2 [min.]	t_3 [min.]	e_1	e_2	e_3	e_4	e_5	e_6	e_7	e_8	e_9
1-I	708.67	0.69	131	30	0	0	0	0	0	0	1	0	6
1-II	506.86	0.12	100	35	0	0	0	0	0	0	1	0	4
1-III	506.66	0.12	96	35	0	0	0	0	0	0	1	0	4
2-I	5613.65	1.00	165	90	0	0	0	0	0	2	1	19	34
2-II	17313.05	1.00	168	75	0	0	0	0	0	5	104	0	64
2-III	3711.43	0.75	135	80	0	0	0	0	0	3	5	0	29
3-I	14917.35	0.67	200	135	0	0	0	0	0	0	1	92	56
3-II	13912.05	0.67	164	65	0	0	0	0	0	5	20	29	85
3-III	916517.35	0.67	200	135	1	2	1	2	3	7	1	76	81

schedule is prepared every day in accordance with train and rolling stock schedules that vary day to day. Currently, maintenance worker schedules are prepared manually by skilled planners, but because of multiple constraints on the workload of maintenance workers, it takes several hours to prepare one day's schedule, which is labor intensive. This calls for automatic generation of maintenance worker schedules to save labor.

This paper describes the development of automatic generation of maintenance worker schedules by TS. To confirm the effectiveness of the proposed method, we compared schedules it produced with the actual schedules and maintenance worker schedules generated by MIP. Results indicate that the proposed method can generate practical maintenance worker schedules that satisfy high priority constraints and reduce track interval times and the additional time, within 3 minutes computation time. This therefore indicates that the proposed method is effective in practice.

References

- [1] Korte, B. and Vygen, J., “*Combinatorial Optimization*,” Springer-Verlag Berlin Heidelberg, 2006.
- [2] Baker, K. R., “*Introduction to Sequencing and Scheduling*,” Jhon Wiley, 1974.
- [3] Abbink, E., Fischetti, M., Kroon, L., Kroon, T., and Vromans, M., “Reinventing crew scheduling at Netherlands railways,” *Interface*, Vol. 35, No. 5, pp. 393-401, 2005.
- [4] Kokubo, T., Kato, S., Nakahigashi, T., Takeuchi, Y., and Tanaka, S., “Application of Tabu Search to an Automatic Creation Method for Maintenance Worker Diagram,” in *Proceedings of the IEEJ TER*, 22-063, 2022 (in Japanese).
- [5] Kokubo, T., Kato, S., Nakahigashi, T., Takeuchi, Y., and Tanaka, S., “Automatic Creation Method for Maintenance Worker Schedules by Tabu Search that Allows Constraint Violations,” in *Proceedings of the IEEJ IASC*, R5-12, 2022 (in Japanese).
- [6] Kokubo, T., Kato, S., Nakahigashi, T., Takeuchi, Y., and Tanaka, S., “Automatic Creation Method for Maintenance Worker Schedules by Tabu Search that Allows Constraint Violations,” *J-RAIL*, S5-1-2, 2022 (in Japanese).
- [7] Glover, F. and Laguna, M., “*Tabu Search*,” Kluwer Academic Publishers, 1997.
- [8] Gurobi Optimizer: <https://www.octoberky.jp/products/gurobi> (Reference date : April 24, 2024) (in Japanese).

Authors



Tatsuya Kokubo
 Researcher, Transport Operation Systems
 Laboratory, Signaling and Operation Systems
 Technology Division
 Research Areas: Transportation Planning,
 Maintenance Worker Scheduling



Taichi NAKAHIGASHI
 Researcher, Transport Operation Systems
 Laboratory, Signaling and Operation Systems
 Technology Division
 Research Areas: Transportation Planning,
 Train Rescheduling



Satoshi KATO
 Senior Chief Researcher, Transport Operation
 Systems Laboratory, Signaling and Operation
 Systems Technology Division
 Research Areas: Transportation Planning,
 Mathematical Optimization

Development of Safety Check Support Device for Drivers Using Side Cameras on Rolling Stock

Wataru GODA

Hiroki MUKOJIMA

Nozomi NAGAMINE

Image Analysis Laboratory, Information and Communication Technology Division

This paper presents the development of a safety check support device aimed at further enhancing platform safety checks using side cameras installed on rolling stock. The device employs deep learning-based image processing techniques to detect passenger approach on platforms in real-time from camera footage, notifying the driver to assist with safety checks. Additionally, the device is equipped with automatic passenger counting functionality at each station. An overview of the developed device and the results of evaluation experiments are provided.

Key words: side cameras on rolling stock, one-man operation, object detection, image processing, deep learning

1. Introduction

On driver-only operated trains, passenger safety checks are currently carried out visually by the driver using platform mirrors or monitors etc. The recent introduction of side cameras has begun in some driver-only operated sections as a new visualization method for the drivers. In these sections, footage from side cameras is displayed in the driver's cab. This allows the driver to check the safety of the platform before the train departs.

To further improve safety through the use of side cameras, we have developed a device that detects passengers on platforms who may be approaching the train in real-time using image processing technology, and notifies the driver to assist with safety checks.

Using the device can reduce the burden on the driver to check the safety during door operations, as well as enable the monitoring of passengers approaching too close to a moving train on the platform, which was previously undetectable, thereby enhancing overall safety. Figure 1 presents an overview of the entire system.

As well as assisting with safety checks, this device can also provide an automatic passenger counting function. It automatically counts the number of passengers boarding and alighting at each station, and can save the data in CSV format or similar. This detailed data can be used as a decision-making basis for operational matters such as timetable management, fleet size settings, and the further extension of driver-only operated sections.

In this paper, we describe an overview of the side cameras in Chapter 2, explain the proposed algorithm in Chapters 3 and 4, present the implementation of the algorithm in the device in Chapter 5, and show the results of performance evaluation of the device in Chapter 6. Finally, in Chapter 7, we summarize the conclusions.

2. Side Cameras

Each vehicle is equipped with four side cameras: one on each corner. Figure 2 shows a top view of the vehicle. The circular symbols represent the side cameras, and the arrows indicate the direction of the cameras. Each camera is installed at approximately the height of the top of doors and is positioned at an angle that allows the entire platform to be monitored from an elevated perspective.

The monitor in the driver's cab displays footage from the cameras facing towards the rear of the train, in relation to the direction of travel. When the train stops at a station and the doors open, the camera footage is automatically displayed, and after departure the display is turned off when the vehicle exceeds a certain speed. The

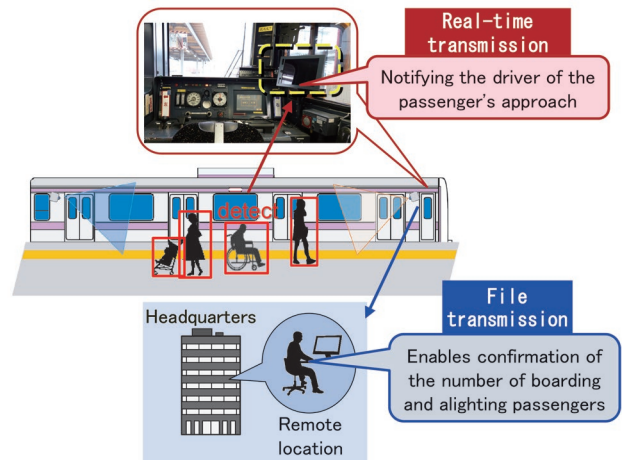


Fig. 1 The entire system

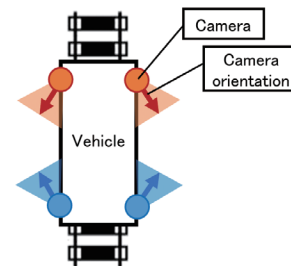


Fig. 2 Placement of side cameras on vehicle

footage from the cameras on the platform side is also displayed.

3. Safety check support algorithm

3.1 Overall processing flow

The safety monitoring algorithm using the image from side cameras on the platform side consists of the following four main processes (Fig. 3). First, passengers appearing in the footage from cameras on the platform side are detected using image processing using deep learning. Secondly, to estimate the approach status of the passengers, the coordinates of each detected person inside the image are converted to real-world coordinates, and the distance to the ve-

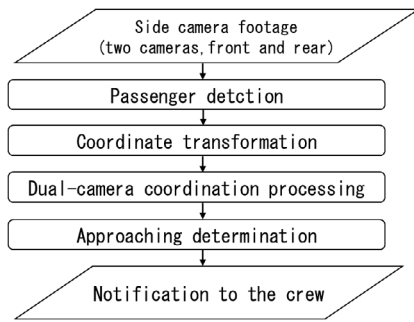


Fig. 3 Safety check support method processing flow

hicle is calculated. Finally, based on the calculated distances of the passengers and a predetermined threshold, the driver receives a notification such as “caution” or “danger.”

The specific contents of the processes are described in the following sections.

3.2 Passenger detection

Passenger detection is carried out on the acquired camera footage using a model created by deep learning. The model was developed to detect passengers as targets for detection, including people (full body and head), wheelchairs, baby strollers, and white canes, which were learned through deep learning. A total of 60,734 image data were used for training, including 36,000 images from a proprietary dataset captured by the Railway Technical Research Institute, as shown in the example in Fig. 4, and an additional 24,734 image data from open data such as the COCO dataset [1] containing images of people.

Figure 5 shows the detection process in the experimental environment at the Railway Technical Research Institute. From Fig. 5, it



Fig. 4 Examples of the created training data

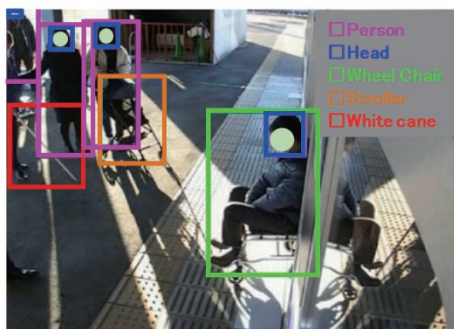


Fig. 5 Examples of the detected passengers

can be observed that the detected passengers are outlined with bounding boxes.

3.3 Coordinate transformation

The center of the bottom edge of the bounding boxes for each detected passenger is defined as the foot coordinate. Using projective transformation [2], the platform overhead coordinates corresponding to the real distance are calculated for these foot coordinates. Any point $X_{cam} \in \mathbb{R}^2$ on the plane captured in the camera coordinate system is considered as a corresponding point $X_{real} \in \mathbb{R}^2$ in the real-world coordinate system. At this point, the mapping between two points is represented by a homography matrix $H \in \mathbb{R}^{3 \times 3}$ (where one of the elements is 1), as shown below.

$$\begin{bmatrix} X'_{real} \\ W' \end{bmatrix} = H \begin{bmatrix} X_{cam} \\ 1 \end{bmatrix} \quad (1)$$

$$X_{real} = \frac{X'_{real}}{W'} \quad (2)$$

Here, \mathbb{R} is the set of real numbers, and $W' \in \mathbb{R}$ satisfies $W' \neq 0$. From the above equation, since there are eight unknown variables, H is uniquely determined if there are four points corresponding to X_{cam} and X_{real} .

The formula for conversion to real-world coordinates, thereby, can be obtained using the four vertices of boxes covering several braille blocks (hereinafter referred to as braille blocks) with known real sizes and the corresponding four points of the braille blocks on the image.

The conversion formula is calculated once for each camera, and as long as the camera installation position is fixed and the height of the station platform surface meets the standard criteria, the conversion formula can be considered the same for each station.

Furthermore, the conversion formula can also be automatically calculated using AR markers [3]. By actually performing projective transformation, the coordinates can be converted to correspond to real-world distances, as shown in Fig. 6.

3.4 Coordinate transformation

To check the safety over a vehicle length of approximately 20 meters, coordination processing of the two cameras is carried out. The detection area of the two cameras is set to cover a range longer than half the vehicle length, as shown in Fig. 7. The reason for set-

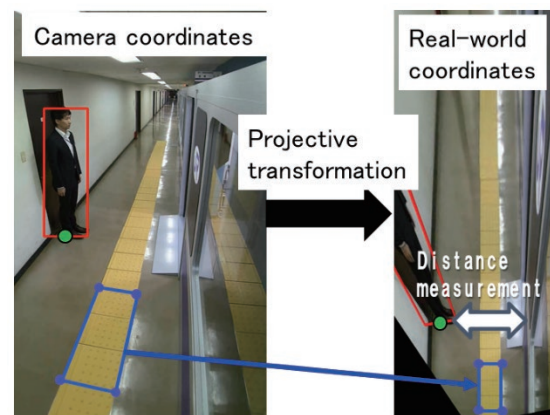


Fig. 6 Passenger detection and calculation of real-world coordinates

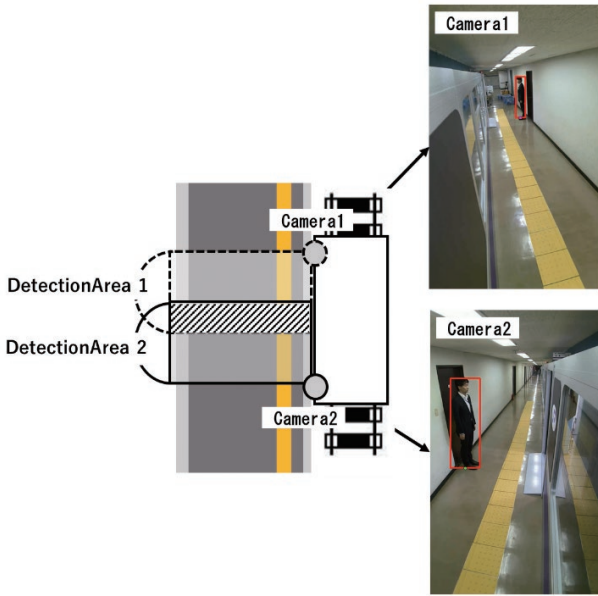


Fig. 7 Dual-camera coordination processing

ting the detection area in this way is that the position calculation accuracy decreases as the person is farther away from the camera, so the detection area is set on the side closer to the respective camera.

Moreover, the hatched area in Fig. 7, which is the overlapping detection area of both cameras, exists near the center of the vehicle. This is to prevent detection omissions near the boundary. Although there is a possibility of detecting the same person twice in the overlapping detection area, this redundancy is on the safe side and does not pose any operational issues.

3.5 Approaching determination

In terms of determining the threshold for proximity warning on platforms, while it is generally considered safe inside the braille blocks and unsafe outside (toward the platform edge), this cannot be used as a unified standard. This is because the precise installation positions of braille blocks can vary from station to station, and some stations may not have them installed at all. Therefore, instead of using the presence or absence of braille blocks as the criterion, the notification of passenger proximity is defined solely based on the distance between passengers and the train.

The following provisional criteria have been adopted:

- 100 cm or less from the vehicle (assuming a gap of 20 cm between the vehicle and the platform, and a distance of 80 cm from the platform edge to the braille blocks) is considered “danger.”
- Between 100 cm and 140 cm from the vehicle (assuming a width of 40 cm for the braille blocks with inner lines) is considered a “caution” area.
- Any distance greater than 140 cm from the vehicle is considered “safe.”

These criteria can be changed arbitrarily.

4. Passenger counting algorithm

4.1 Overall processing flow

The passenger counting algorithm using side cameras consists of three main processes, as shown in Fig. 8. Similar to the passenger

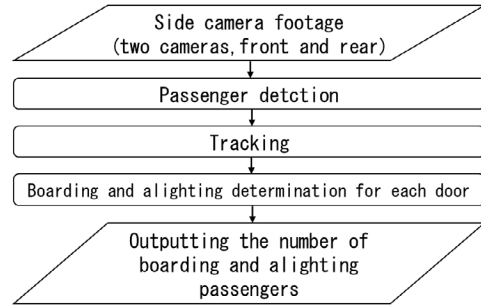


Fig. 8 Processing flow of the boarding and alighting passenger counting algorithm

detection method, target detection is performed using deep learning-based image processing, followed by tracking of the detected individuals. This allows the trajectories of the detected targets to be obtained. Next, for the detected individuals, the direction and number of passengers passing through the set door position, are determined to count the number of passengers boarding and alighting. Finally, the passenger count data are output in a format such as CSV.

In the following sections, we discuss the specific details of the processing. However, since passenger detection is the same as for the safety check support algorithm this part of the explanation is omitted.

4.2 Tracking

For the detected individuals, tracking is performed by associating detections of the same person across consecutive frames. We adopted the ByteTrack [4] algorithm for tracking. In ByteTrack, as shown in Fig. 9, even if a person previously detected with high confidence temporarily has a lower detection confidence due to occlusion or other factors, their position can be estimated by tracking based on the predictions from previous frames. This is achieved by utilizing the appearance similarity and motion consistency of the detected person across frames. Additionally, the processing time for ByteTrack is 1-3 ms per frame, enabling real-time tracking.

4.3 Boarding and alighting count

As shown in Fig. 10, a reference line (green line in Fig. 10) is set for each door to be counted. The direction and number of times this reference line is crossed are measured to count the number of passengers boarding and alighting. When counting, two points are set as tracking points, as shown by the orange and yellow points in Fig. 11. The primary tracking point for counting is the center point of the bottom edge of the head bounding box (yellow point in

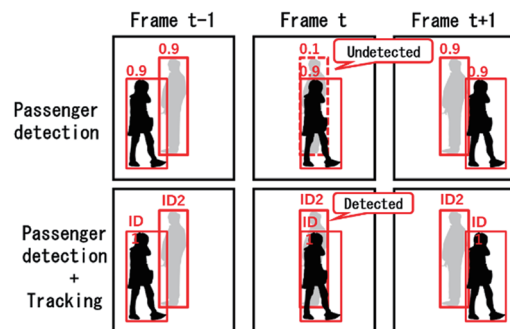


Fig. 9 Tracking using ByteTrack

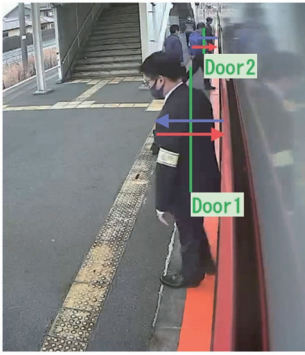


Fig. 10 Setting the doors for counting (the individuals in the image are test-related personnel)

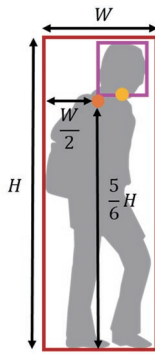


Fig. 11 Definition of tracking points

Fig. 11), as it is more likely to be visible even in crowded situations. As a backup feature in case the head is not detected, a secondary tracking point (orange point in Fig. 11) is set at a height of $5/6$ of the whole body from the reference coordinate. This height is based on the assumption that an average human body is approximately seven heads tall, taking into account the slightly shorter appearance due to the downward angle of the camera.

5. Development of onboard device

5.1 Overall device configuration

The overall configuration of the proposed equipment is shown in Fig. 12. The cameras, cables, video recording device, and display device shown in the figure are existing facilities pre-installed as part of the current side camera system. Our device, which implements the algorithms described in Chapter 3 and 4, is added to this existing equipment to introduce the new functionality.

5.2 Device design

When designing the equipment, considering that one device is

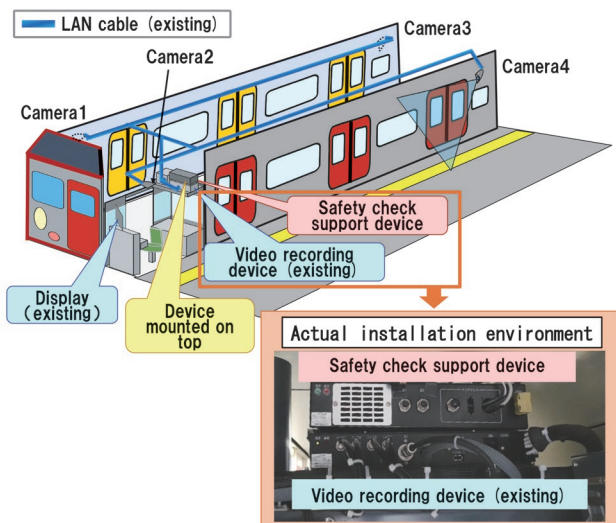


Fig. 12 Overall system configuration

to be installed in each vehicle, it is desirable to realize each unit at the lowest possible cost, as a large number of devices will be required depending on the number of vehicles. The cost hurdle in this case is the use of deep learning-based detection. This processing typically requires a large amount of parallel computing and the incorporation of expensive image processing semiconductors such as GPUs into the device.

To avoid this, we optimized the deep learning-based detection for speed, creating a model that can perform detection using only a CPU. This was achieved by applying lightweight techniques called knowledge distillation and pruning, as shown in Fig. 13, to a high-performance model that was trained normally. As a result, deep learning-based detection can be performed in about 20 ms using only one CPU, and the entire process can be completed within 100 ms.

Therefore, by using only a CPU as the processing unit of the device, it became possible to eliminate the need for a dedicated cooling fan, enabling miniaturization, low noise, improved vibration resistance (compliant with JIS E4031 “Rolling stock equipment — Vibration and shock testing methods”), and other benefits. Based on the above considerations, the appearance (Fig. 14) and specifications (Table 1) of the developed prototype safety check support device are shown. The LTE router functionality also enables the transmission of detection results and passenger count data to railway company’s headquarters.

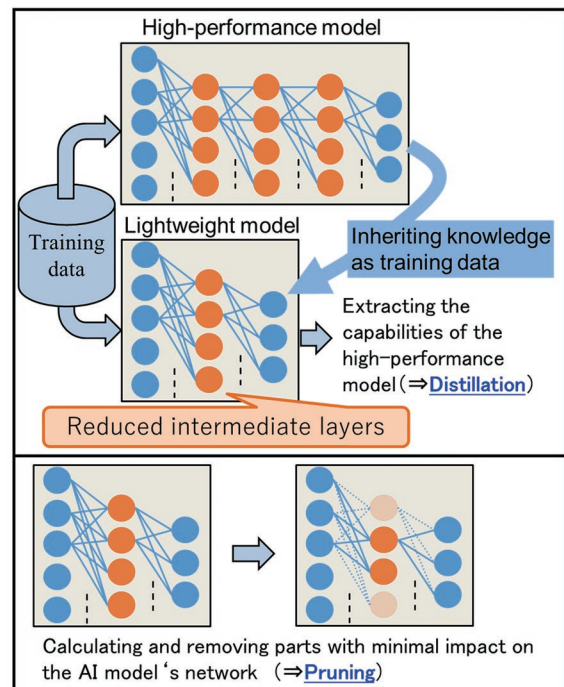


Fig. 13 Accelerating the deep learning model



Fig. 14 Appearance of the safety check support device

Table. 1 Specifications of the safety check support device

Specifications list	
Input voltage	DC100 V (+10%, -30%)
Power consumption	Max 100 W
Operating temperature	-10~50°C
Operating humidity	20%~90%
Dimensions (W×D×H)	390 mm × 260 mm × 70 mm
Design weight	5 kg or less
Onboard CPU	CPU : core i5-1185GRE CLK : 1.8 GHz Memory : 8 GB
LTE router	Closed SIM VPN

5.3 Collaboration with existing side camera system

To properly execute the proximity detection and passenger counting functions, the equipment needs to be connected and linked to the existing side camera system. The necessary collaboration includes determining the timing for activating each function and notifying the driver when necessary. Each of these aspects is explained below.

5.3.1 Activation timing

The timing of the activation of the processes is shown in Fig. 15. The vehicle status information is received from the existing system and four timing criteria are used: platform entry, door opening, door closing, and platform exit. For proximity warning notifications, during passenger boarding and alighting between door opening and closing, it is normal behavior for passengers to enter the caution or danger zones. Therefore, there is no need to issue caution or danger notifications during this timing; the timing when notification is required is when no passengers are boarding or alighting between platform entry and platform exit. Accordingly, notifications are turned off during boarding and alighting. On the other hand, for passenger counting, the processing is turned off during platform entry and platform exit, as no passengers should be boarding or alighting during these timings.

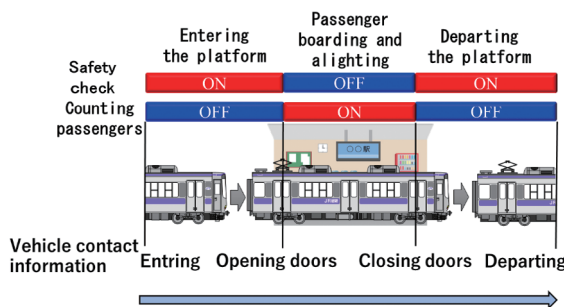


Fig. 15 Timing of processing execution

5.3.2 Notifying the driver

The proximity warning from the device is notified via existing video display such as tablet terminal. Figure 16 shows the display method created for check purposes. The frame display and audio notifications are made according to the approach status, such as “caution” or “danger.” Additionally, the type of detected target (person, wheelchair, stroller, white cane) can also be displayed (shown as white text within the screen in Fig. 16). The current display method is provisional and can be customized individually according to the operational methods and safety considerations of each operator.

6. Performance evaluation

6.1 Evaluation for proximity warning

To evaluate the performance of the proposed device, a prototype device was connected to a Series 815 train pre-equipped with a side camera system. A test run was conducted for the duration of two round trips (daytime and nighttime) covering 11 stations on the JR Kyushu Kagoshima Line (Yatsushiro - Kumamoto) using a test train (Fig. 17).

The footage of 22 station stops during the test run was analyzed, and the detection rate was evaluated. Here, the false detection rate is defined as the ratio of the number of frames where a notification was issued despite a safe situation to the total number of frames in safe situations. Similarly, the missed detection rate is defined as the ratio of the number of frames where no notification was issued despite an approach beyond the braille blocks to the total number of frames with such approaches.

The false detection rate was 0.02%, and the missed detection



Fig. 16 Example of a display screen for the driver (individuals in the image are test-related personnel)



Fig. 17 Scene from running test (individuals in the image are test-related personnel)

rate was 3.80%. The most common cases of missed detection were for white canes. However, since white canes are mostly present simultaneously with people, proximity warning can be issued as long as the person with the cane is detected. Taking this into account and excluding white canes, the false detection rate was 0.02%, and the missed detection rate was 1.75%. Furthermore, when the detection targets were limited to people, for which a larger amount of training data are available, the false detection rate was 0.00%, with no missed detections lasting more than 5 frames (0.5 seconds), and the missed detection rate was 0.36%. For wheelchairs and strollers, performance is expected to improve by increasing the amount of training data to a level similar to that for people.

6.2 Evaluation of passenger count

The performance of passenger counting was evaluated using recorded video data. Video data from 558 station stops on the Hohi Line (Kumamoto - Higoozu), where Series 815 trains are in operation, were used. The data included various conditions such as differences in timing, from the first train to the last train, differences in weather conditions (sunny, cloudy, rainy, thunderstorms), indoor and outdoor platform environments, and differences in station structures (side and island platforms). Since each vehicle of the Series 815 trains has three doors on the platform side, the front door and the middle door are designated in order of proximity to the camera (referred to as Door 1 and Door 2, respectively, in Fig. 10). Since the detection areas of the two side cameras overlap around the middle door, passengers boarding and alighting at the middle door are detected by both cameras, resulting in a double count. To compensate for this, the average or maximum of the two counts is used. In this case, the average value was adopted.

For the evaluation, the cumulative counts by visual confirmation and the device output were compared, and the accuracy (device count / visual count) was summarized for each door, as shown in Table 2.

From Table 2, excluding the middle door alighting count, the error rate was lower than 5%. On the other hand, the error rate for the middle door alighting count was 15%, which is significantly higher than the others. This is due to the influence of the ByteTrack algorithm. While ByteTrack can estimate the position by tracking even if a target that has been previously detected is temporarily occluded and its confidence decreases, it does not handle cases where the target is occluded and cannot be detected upon initial appearance. Therefore, for alighting at the middle door, there is a higher

Table 2 Accuracy of boarding and alighting passenger counting for each door

	Counting accuracy (boarding)	Counting accuracy (alighting)
Near door	95.19%	95.86%
Middle door	95.72%	84.49%

possibility of the initial appearance being occluded by people in front, leading to more missed detection cases.

The overall accuracy of the system is considered to be of practical use, considering that high frequency counts are possible by distinguishing between boarding and alighting at each station.

7. Conclusion

Aiming to further enhance safety check by utilizing side cameras, we have developed a device that detects the presence of passengers on the platform who may approach the train in real-time from camera footage using image processing technology based on deep learning, and notifies the crew member, assisting in safety check. Furthermore, this device is not only for safety check but also has the function of automatically counting the number of passengers boarding and alighting at each station. In the future, we plan to make final adjustments for practical implementation.

References

- [1] Lin, T., Maire, M., Belongie, S., Hays, J., Perona, P., Ramanan, D., Dollár, P., Zitnick, C. L., "Microsoft coco: Common objects in context," *Proceedings of the European Conference on Computer Vision*, pp. 740-755, 2014.
- [2] Yoshino, J., Nagamine, N., Mukojima, H., Goda, W., "Calculation Method of Image Transformation Parameters for Side Cameras on Rolling Stocks Using AR Markers," TER-21-067, 2021.
- [3] Forsyth, D., and Ponce, J., "Computer vision: a modern approach," Prentice hall professional technical reference, 2002.
- [4] Zhang, Y., Sun, P., Jiang, Y., Yu, Y., Yuan, Y., Luo, P., Liu, W., Wang, X., "BYTETrack, Multi-object tracking by associating every detection box," arXiv preprint arXiv:2110.06864, 2021.

Authors



Wataru GODA
 Researcher, Image Analysis Laboratory,
 Information and Communication Technology
 Division
 Research Areas: Image Processing,
 Information Technology



Nozomi NAGAMINE, Ph.D.
 Senior Chief Researcher, Head of Image
 Analysis Laboratory, Information and
 Communication Technology Division
 Research Areas: Image Processing,
 Information Technology



Hiroki MUKOJIMA
 Researcher, Image Analysis Laboratory,
 Information and Communication Technology
 Division
 Research Areas: Image Processing,
 Information Technology

Rolling Stock Scheduling Algorithm for Temporary Timetable After Natural Disaster

Satoshi KATO Taichi NAKAHIGASHI Tatsuya KOKUBO
 Transport Operation Systems Laboratory, Signalling and Operation Systems Technology Division

Jun IMAIZUMI
 Toyo University

This paper focuses on rolling stock scheduling after a large-scale natural disaster. In general, a temporary timetable is generated when sections of a line are partially disrupted by damage caused by the natural disaster. The next step is to generate a rolling stock schedule that is as close as possible to the original schedule at the time of timetable revision. We propose a two-phase rolling stock scheduling algorithm based on a mathematical programming method to cope with the temporary timetable. In addition, we confirm that the proposed algorithm can produce a practical rolling stock schedule in terms of evaluation criteria and computational time.

Key words: rolling stock scheduling, temporary timetable, disaster, duty, roster, mathematical programming

1. Introduction

In order to operate railway trains, it is necessary to prepare not only train timetables but also several related schedules. One of them is a rolling stock schedule, which determines the schedule of rolling stock to be used to realize daily train operation. It is required to propose an efficient rolling stock schedule to make effective use of limited resources [1].

When some sections of a line are partially disrupted due to damage caused by a large-scale natural disaster, it is necessary to prepare a temporary timetable and a corresponding rolling stock schedule plan. In such cases, the schedule plan needs to be prepared each time the operating section is gradually expanded according to the restoration status. This places a heavy burden on the schedule planners to prepare a tentative schedule plan due to the limited time available. In addition, it is desirable to avoid changes in the plan each time the operating section is expanded. Since the original timetable will be restored when operations have finally resumed on all sections, it is preferable for the tentative schedule at each stage to be similar to the original schedule.

In this paper, we focus on the preparation of rolling stock scheduling after a large-scale natural disaster. Then, we propose an algorithm that can automatically generate a rolling stock schedule in a short time by utilizing mathematical optimization. In addition, we show the results of case studies based on actual disrupted cases to confirm the effectiveness of the proposed algorithm.

2. Rolling stock scheduling after a large-scale natural disaster

2.1 Rolling stock schedule

A rolling stock schedule is produced by assigning rolling stock to all trains shown on a train timetable. Specifically, it consists of a “duty” which is a schedule for each working day and a “roster” which is a circulation schedule that defines the order of the duty. In the duty generation phase, it is necessary to consider the interval time between two consecutive trains. In the roster generation phase, the end station of one duty and the start station of the next duty must coincide. Otherwise, an empty run has to be inserted if necessary. In addition, the end station of the last duty of the roster should coincide

with the start station of the first duty to guarantee circularity.

An important consideration of rolling stock scheduling is to take into account the inspection cycle of the vehicles. This paper focuses on pre-departure inspections and regular inspections. The former is for functional checks with a periodicity of a few days. The latter is for detailed checks with a periodicity of several tens of days. The location and timing of each inspection should be determined so that each inspection can be carried out to satisfy the interval conditions.

In general, a roster is created for each type of rolling stock in the lowest operational cars that are not further divided. Each type generally consists of several cars, called “unit” in this paper. Even the same type of car is treated differently if the number of cars and equipment specifications are different. Here, we define “unit type” as a concept that identifies the type of car determined by the type and number of cars, and we need to create a roster for each unit type.

On some lines in Japan, splitting and combining are applied. A set of rolling stock consisting of one or more units assigned to each train is called a “composition.” Here, splitting means to split a composition into two or more separate units, and combining means to combine two or more separate units together. Splitting and combining allow flexible adjustments of traffic capacity. However, it requires additional time and work of operators at a station or a rolling stock depot, so it is desirable to reduce splitting and combining.

Figures 1 and 2 show an example of a rolling stock schedule. Figure 1 shows an example of duties on the diagram, where a circle means the start of a duty and a triangle means the end of a duty. The trains with double lines mean that the two units are operating in a combined formation. Splitting of units takes place after the operation of 102M, 105M and 57M. On the other hand, combining of units takes place before the operation of 105M, 102M and 56M. Figure 2, on the other hand, shows an example of a roster. The train number (F) means the front side of the train and (B) means the rear side of the train. The pre-departure inspections are then included in duties 3, 5, and 7. Since the units are assigned in the order of the roster, the inspection is carried out once every three days in unit type 1. Similarly, the inspection is carried out once every two days in unit types 2 and 3. The number of days in a roster means the number of units required, and in this example, each unit type requires 3 units, 2 units, and 2 units, respectively. It is therefore desirable to reduce the number of duties in terms of efficient use of railway resources.

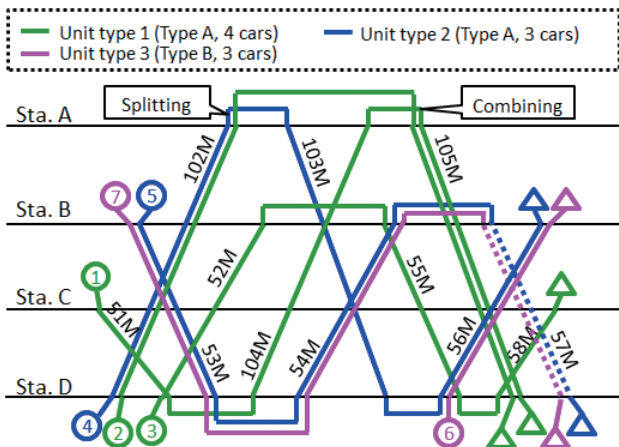


Fig. 1 Example of rolling stock duties

<Unit type 1>	
Duty	
1	C \circ 51M \rightarrow D $\xrightarrow{104M}$ A $\xrightarrow{105M(B)}$ Δ D
2	D \circ 102M(B) \rightarrow A $\xrightarrow{105M(F)}$ Δ D
3	D \circ 52M \rightarrow <Inspection> B $\xrightarrow{55M}$ D $\xrightarrow{58M}$ Δ C
<Unit type 2>	
4	D \circ 102M(F) \rightarrow A $\xrightarrow{103M}$ D $\xrightarrow{56M(F)}$ Δ B
5	B \circ 53M(B) \rightarrow D $\xrightarrow{54M(F)}$ <Inspection> B $\xrightarrow{57M(B)}$ Δ D
<Unit type 3>	
6	D \circ 56M(B) \rightarrow Δ B
7	B \circ 53M(F) \rightarrow D $\xrightarrow{54M(B)}$ <Inspection> B $\xrightarrow{57M(F)}$ Δ D

Fig. 2 Example of rolling stock rosters

2.2 Transportation planning after a large-scale natural disaster

When railway tracks and facilities at stations and rolling stock depots are damaged due to a large-scale natural disaster, operations may be suspended for a long period of time. In such a case, a schedule planner prepares a temporary train timetable and a rolling stock schedule based on the restoration plans. But in many cases, their operations resume within just a few days, so the schedule planner has to prepare a plan within a short period of time. In addition, when several sections of a line are damaged, the operating section may be expanded sequentially according to the scale of the damage and priority level of restoration. A transportation plan must be created each time the operating section is expanded, which is hard work for the schedule planner.

Figure 3 shows an example of the expansion of operating sections. In this example, the regular operating section is between stations A and H. The sections between stations C and D, and between stations F and G are suspended due to the disaster. On the first day of resumed operation, the service operates between stations A and C, and between stations D and F (the sections between stations C and D, and between stations F and H are suspended). Assuming that the rolling stock depot is adjacent to station E, the trains operating between stations A and C cannot return to the rolling stock depot, which may result in “isolated sections.” In this example, the entire

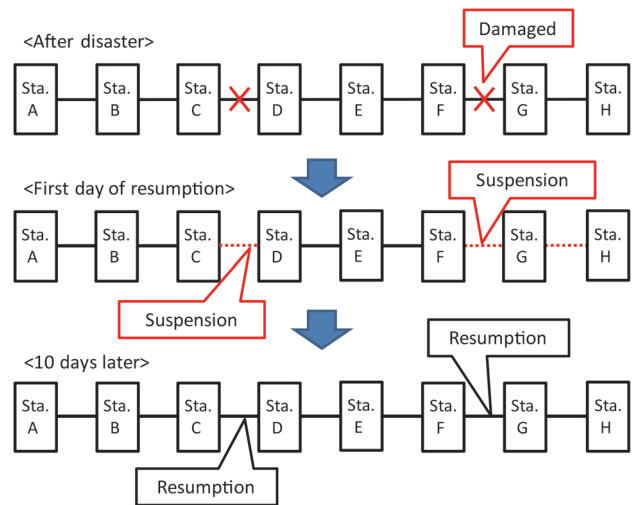


Fig. 3 Example of expansion of operating section

section resumes operation after 10 days, but the expansion of the operating section may be further subdivided.

2.3 Related work

There are many previous works of research related to rolling stock scheduling during timetable revision, for example, Alfieri et al. [2], Cacchiani et al. [3], Giacco et al. [4], etc. In recent years, there have been a few studies based on Japanese railway lines. For example, Imaizumi et al. [5] decompose the problem into creating duties and rosters, and formulate it as a mathematical optimization problem, respectively. Nishi et al. [6] propose a solution method that combines a column generation method and heuristics, considering inspection interval constraints. Kato et al. [7] model the problem as a Traveling Salesman Problem (TSP) based on Giacco et al. [4], and propose a method to reduce splitting and combining.

On the other hand, there are no studies that specifically focus on rolling stock scheduling after a disaster. Although previous studies on timetable revision can be referred to as a method for generating a rolling stock schedule, it is necessary to propose a new algorithm for a temporary timetable after a disaster.

3. Rolling stock scheduling algorithm after a large-scale disaster

3.1 Problem definition

Based on the characteristics of disaster situations described in Chapter 2, we define the problem addressed in this paper. Assumptions and constraints are as follows:

- The minimum and maximum number of cars assigned to each train are given.
- Information on whether two different trains are to be connected directly or via an empty run is given.
- Each unit type has a maximum number of available limit.
- Stations at which units can be split and combined are given.
- The possibility of combining between two unit types is given.
- For each unit type, the possible operating lines and trains that can be assigned are given.
- The pre-departure inspection and the regular inspection

shall be carried out every specified number of days. The regular inspection shall include the pre-departure inspection.

h) The possible stations where the pre-departure inspection and the regular inspection can be performed are given. For each station, there are several time periods for inspection depending on the type of inspection. In addition, there is a maximum number of units for inspection allowed for each time period.

i) The maximum number of trains to stay at each station is given. Basically, when a train arrives at a station, the number of trains staying at the station is counted as one. However, if splitting is necessary to allocate the units to other trains, this is assumed to take place at the time of arrival. In this case, if a train consisting of two units is split, the number of trains staying at the station is counted as two. On the other hand, it is assumed that combining takes place before departure.

We consider the number of duties, the number of times there are splitting and combining, and the distance of empty runs as evaluation criteria. These are also important in the rolling stock scheduling during timetable revision. In addition, we introduce an original concept called “schedule difference” to evaluate the closeness of the created schedule to the original schedule.

3.2 Concept of schedule difference

The concept of schedule difference is illustrated in Fig. 4. The left figure shows the rolling stock schedule produced at the time of the train timetable revision, which is called the “basic schedule.” The right figure shows the rolling stock schedule created after the disaster, which is called the “temporary schedule.” This is an example of a situation where train operations are resumed only between Stations B and D. In this example, we can see that although the turn-back stations are different, both the basic schedule and the temporary schedule have a turn-back of 102M-103M. Thus, if the turn-back trains are the same, there is no schedule difference even if the turn-back stations are different. On the other hand, if the turn-back trains are different, there is a schedule difference.

In this paper, we seek a rolling stock schedule with as few schedule differences as possible. Eventually, the train operation will return to the basic schedule after the operating section has been extended. Therefore, considering differences from the basic schedule in the initial stage of resumption will reduce schedule changes during the extension of the operating section and enable a smooth return to the basic schedule.

3.3 Solution approach

In this paper, we apply mathematical optimization to the production of the rolling stock schedules. There are two solution approaches: the “simultaneous method,” which simultaneously generates the set of duties and the set of rosters based on the train timetable, and the “two-phase method,” which first generates the set of duties and then uses the generated duty to generate the set of rosters.

Since the rolling stock schedule is completed by generating not only the duty but also the roster, the simultaneous method is preferable from the viewpoint of total optimization. However, because of the difficulties of the problem size, the two-phase method is also a promising option from a practical point of view. In this paper, since we assume a time-constrained situation after a disaster, we adopt the two-phase method that allows a short computational time.

The procedure of the proposed algorithm is shown below.

Step 1: Preprocessing

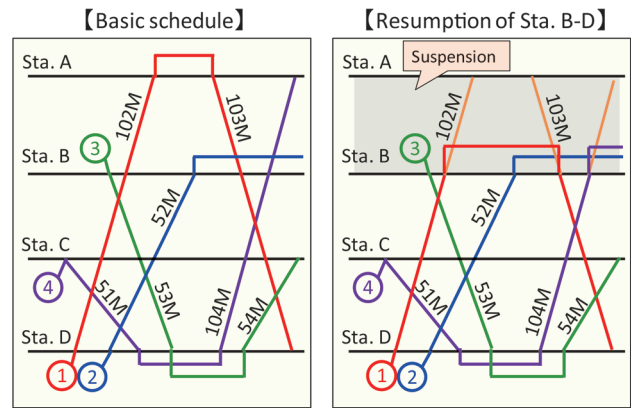


Fig. 4 Example of schedule differences

We check the train timetable if any sections have been disrupted by the disaster. If so, the problem is divided into sub-problems for each section. We then carry out the process from Step 2 for each section.

Step 2: Duty generation algorithm

We generate a set of duties for each unit type. The duty generation problem is modeled in the same way as a multi-commodity network flow problem.

Step 3: Roster generation algorithm

We generate a roster for each unit type using the set of duties obtained in Step 2. The roster generation problem is modeled in the same way as in treating a TSP.

As discussed in Section 3.1, the number of times there are splitting and combining is the evaluation criterion that should be reduced as much as possible. Splitting and combining take place during and between two duties, and the number of times there are splitting and combining is reduced with the following methods:

- The duty generation algorithm generates a set of duties to reduce splitting and combining in a duty.
- The roster generation algorithm generates a roster to reduce splitting and combining between two duties.

It is also necessary to determine the position of units such as “front” and “back” in the composition. In this paper, we consider the position as follows.

- The duty generation algorithm does not take into account the position in the composition. The algorithm detects the splitting and combining of each train and calculates the number of times splitting and combining have taken place.
- The roster generation algorithm requires the position of each unit in the composition to calculate the number of times there are splitting and combining between duties. After the duty generation algorithm, the position of each unit in the composition is determined by a rule such as reversing the position when the turn-back takes place. And these positions are used as input to the roster generation algorithm.

The time interval constraints for the pre-departure inspection and the regular inspection are taken into account in the roster generation algorithm. However, since the output of the duty generation algorithm is the input to the roster generation algorithm, if the required number of inspections is not included in the result of the duty generation algorithm, the roster generation problem will be infeasible. Therefore, the required number of pre-departure inspections and regular inspections should be included according to the number of duties to be created for each unit type in the duty generation algo-

rithm. This will ensure feasibility in the roster generation problem.

3.4 Duty generation algorithm

In this paper, we apply the multi-commodity network flow problem that is often used in rolling stock scheduling (e.g., Cacchiani et al. [3]). We can model the duty generation problem by considering commodities as unit types and flows as duties.

There are four types of nodes on the network as follows:

- (i) Departure node, which refers to the departure of each train at the starting station
- (ii) Arrival node, which refers to the arrival of each train at the ending station
- (iii) Start node, which refers to the start of the duty
- (iv) End node, which refers to the end of the duty

In addition, there are five types of arcs on the network as follows:

- (i) Train arc, which refers to a train and is drawn from the departure node to the arrival node for the train.
- (ii) Connection arc, which refers to a connection between different trains and is drawn from the arrival node to the departure node when the connection is possible (stations are coincident and the interval time is sufficient)
- (iii) Inspection arc, which refers to an inspection and is drawn from the start or arrival node to the departure node when an inspection is possible
- (iv) Start arc, which is drawn from the start node to the departure node
- (v) End arc, which is drawn from the arrival node to the end node

The cost of the train arc associated with a commercial train is set to 0; otherwise, it is set to α (this is a weight parameter). The cost of the connection arc is set to 0 if the connection is the same as the basic schedule; otherwise, it is set to β (this is also a weight parameter) taking into account the schedule difference. The cost of the start arc is set to 1. The cost of all other arcs is set to 0.

Figure 5 shows an example of a network for a multi-commodity network flow model. Several flows of each unit type move from the start node to the end node on this network. These flows ensure that each train is allocated a number of cars greater than the minimum number of cars and less than the maximum number of cars.

The following is an outline of the formulation as a mathematical optimization problem (see Ref. [8]) for details).

<Objective function>

Total cost of the arc + $\gamma \times$ the number of times there are splitting and combining during the duty (to be minimized)

Note that γ is a weight parameter.

<Constraints>

- Flow matching constraints (the number of flows entering and exiting each node is the same except at the start and end nodes)
- Upper and lower limits on the number of cars assigned to each train
- Upper limits on the number of duties for each unit type
- Inspection interval constraints of pre-departure inspection and regular inspection
- Upper limit on the number of simultaneous inspections of pre-departure inspection and regular inspection
- Logical constraints for detecting splitting or combining in a duty
- Forbidding combining between two unit types which cannot be connected

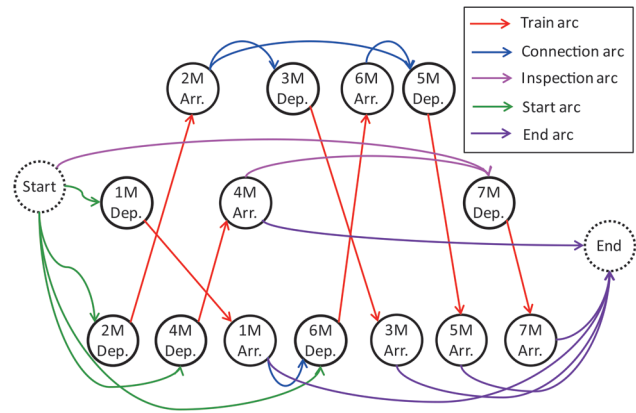


Fig. 5 Example of network for multi-commodity network flow model

- Upper limit on the number of trains that can be staying at each station
- Constraints for possible values of each variable

3.5 Roster generation algorithm

We model the roster generation problem as a TSP. A TSP can be modeled as a network in which duties are represented as nodes and connections between duties as arcs. Here, the minimization of the distance of empty runs can be achieved by taking the distance into account in the cost of the arcs.

In addition, we aim to reduce splitting and combining between two duties. In this paper, we apply the idea described in Ref. [7]. We provide information about the number of units and the position of the first and last trains of the duty corresponding to each node. Here, the position means the geographical information; for example, it is defined as 1, 2, ... from the west side of the composition. If the number of units or the position differs among the nodes to which each arc connects, we add the cost of splitting or combining to the arc. Otherwise, we use logical constraints to determine whether splitting or combining takes place. If splitting or combining is required, we add the cost of splitting or combining to the arc.

Figure 6 shows an example network of the TSP model. In this example, five duties are created in the duty generation algorithm of Step 2. The start and end times, and the start and end stations of each duty are given, so that it is possible to determine whether or not empty runs take place between two nodes. Duty 3 and 4 include a pre-departure inspection, and arcs connecting to these nodes are shown in red. We seek the least-cost cyclic path that passes through all nodes once and satisfies the inspection constraints on this network.

The following is an outline of the formulation as a mathematical optimization problem (see Ref. [8] for details).

<Objective function>

The distance of empty runs between duties + $\delta \times$ the number of times there are splitting and combining between duties (to be minimized)

Note that δ is a weight parameter.

<Constraints>

- Cyclic constraints (only one arc entering each node is selected, and only one arc exiting from each node is selected)
- Subtour elimination constraints
- Inspection interval constraints of pre-departure inspection
- Logical constraints for detecting splitting and combining

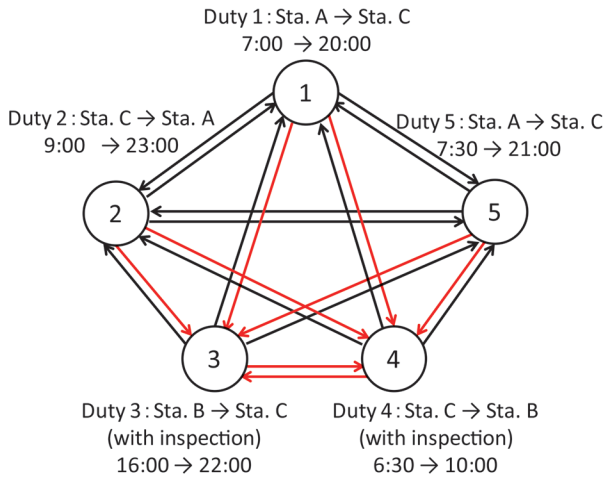


Fig. 6 Example of traveling salesman model

between duties

- Constraints on possible values of each variable

4. Case study

4.1 Lines and settings

In order to evaluate the effectiveness of the proposed method, we show the result of a case study with the restoration phase after a large-scale natural disaster that actually occurred in the past. We compare the actual rolling stock schedule and the plan created by the proposed method for the temporary timetable at that time.

In this case, the operating section has been extended over several phases. Among them, we test the proposed algorithm using three temporary timetables (called instances (a)-(c)). Instance (a) is the initial stage of the resumption of operations, instance (b) is a few days later, and instance (c) is a few days after instance (b). The number of trains and unit types are shown in Table 1 as the scale of the problem. While there is almost no change in (a) and (b), both the number of trains and the number of unit types increase in (b) and (c). The reason for this is that the operating section is extended to the station adjacent to a rolling stock depot in (c), which allows a large number of trains to operate on the line.

In order to compare the results as closely as possible with the actual schedule at that time, we set the minimum and maximum number of cars for each train, the unit types that could be assigned, etc., based on the basic schedule and the actual schedule at that time. The weight parameters of the objective function in the formulation are uniformly set to $\alpha = 0.001$, $\beta = 0.001$, $\gamma = 0.1$, $\delta = 0.01$. We use a PC with Core i7-8700K CPU and 64 GB memory for the calculations and use Gurobi Optimizer 9.5.1 [9]) to solve the mathematical optimization problem.

4.2 Results of computational experiments

Table 2 shows the results of applying the proposed algorithm to instances (a), (b), and (c). The number of duties, the number of times there are splitting and combining, the distance of empty runs, and the number of schedule differences are shown in the table as evaluation criteria. In addition, each index of the actual schedule at that time is also shown. The maximum calculation time for the duty generation is set to 3,600 seconds. We can obtain an optimal solu-

Table 1 Characteristics of each instance using case studies.

Instance	Number of trains	Number of types
(a)	394	5
(b)	402	5
(c)	572	7

tion in less than 1 second in the roster generation problem.

We can find that all evaluation criteria are almost the same or reduced compared with the actual schedule at that time in instances (a) and (b), so the result indicates that an efficient schedule has been generated. On the other hand, in instance (c), although the number of duties is the same, the number of times there are splitting and combining, and the distance of empty runs have increased compared with the actual schedule at that time, indicating that the created schedule is not efficient. In particular, the distance of empty runs has increased significantly. The reason for this is that the number of unit types is high and the number of duties for each type is relatively small in instance (c), so that the distance of empty runs increases when a roster is created from the generated duties. In addition, the GAP, which is an index for the calculation accuracy of a mathematical optimization problem, remains high even after 3,600 seconds. Therefore, we can find that the problem size of instance (c) is relatively large.

Based on the above, we try to fix the number of duties uniformly to reduce the computational load as much as possible. This reduction in the number of evaluation criteria allows for a more efficient search. As a result, a more efficient schedule can be obtained. Table 3 shows the results when the number of duties in instance (c) is fixed at 72 to 74. The maximum calculation time for the duty generation is set to 3,600 seconds, as before. We can find that the solutions can be obtained even when the number of duties is fixed at 73 and 74 duties. Although the number of times there are splitting and combining, and the distance of empty runs are the same or slightly greater than those in the schedule at that time, the number of duties is small. So, the solution with a fixed number of duties can be acceptable. Therefore, it is a very effective way to fix the number of duties and narrow the feasible region to create an efficient rolling stock schedule.

5. Conclusions

In this work, we focus on rolling stock scheduling after a large-scale disaster, and develop an automatic scheduling algorithm based on a mathematical optimization method for the temporary timetable. The proposed algorithm makes it possible to generate a rolling stock schedule that is as close as possible to the original schedule at the time of the train timetable revision.

We adopt a two-phase method in which the process is divided into generating duties and generating rosters. The duty generation problem is modeled as a multi-commodity network flow problem. Then, the roster generation problem is modeled as a Traveling Salesman Problem. In addition, we show the results of case studies using data from real lines and real disrupted cases due to a large-scale natural disaster and confirm that the proposed algorithm can generate a practical rolling stock plan in a short time. In the future, we will apply the proposed method to other lines and put it into practical use as soon as possible.

Table 2 Results of instances (a), (b) and (c)

Instance	Duties	Splitting and combining	Empty runs (km)	Schedule differences
(a)	45	16	296.1	151
(a)*	50	25	145.0	—
(b)	49	16	142.0	164
(b)*	53	34	156.3	—
(c)	72	50	461.6	220
(c)*	75	46	157.5	—

* means the actual schedule at that time.

Table 3 Results of instance (c) fixed the number of duties

Duties	Splitting and combining	Empty runs (km)	Schedule differences
72	34	932.0	212
73	46	514.7	218
74	49	345.1	199

References

- [1] Reuther, M. and Schlechte, T., "Optimization of rolling stock rotations," In Borndörfer, R., Klug, T., Lamorgese, L., Mannino, C., Reuther, M., and Schlechte, T. (Eds.), *Handbook of optimization in the railway industry*, pp. 243-264, Springer International Publishing, 2018.
- [2] Alfieri, A., Groot, R., Kroon, L., and Schrijver, A., "Efficient circulation of railway rolling stock," *Transportation Science*, Vol. 40, No. 3, pp. 378-391, 2006.
- [3] Cacchiani, V., Caprara, A., and Toth, P., "Solving a real-world train-unit assignment problem," *Mathematical Programming*, Vol. 124, pp. 207-231, 2010.
- [4] Giacco, G., Ariano, A. D., and Pacciarelli, D., "Rolling stock rostering optimization under maintenance constraints," *Journal of Intelligent Transportation Systems*, Vol. 18, No. 1, pp. 95-105, 2014.
- [5] Imaizumi, J., Yamagishi, Y., and Morito, S., "A two-phase mathematical programming approach for rolling stock circulation problem," *Transactions of the Operations Research Society of Japan*, Vol. 53, pp. 14-29, 2010 (in Japanese).
- [6] Nishi, T., Ohno, A., Inuiguchi, M., Takahashi, S., and Ueda, K., "A combined column generation and heuristics for railway short-term rolling stock planning with regular inspection constraints," *Computers and Operations Research*, Vol. 81, pp. 14-25, 2017.
- [7] Kato, S., Fukumura, N., Morito, S., Goto, K., and Nakamura, N., "A mixed integer linear programming approach to a rolling stock rostering problem with splitting and combining," presented at the *8th International Conference on Railway Operations Modelling and Analysis*, Norrköping, Sweden, June 17-20, 2019.
- [8] Kato, S., Imaizumi, J., Nakahigashi, T., and Kokubo, T., "Optimization approach to rolling stock scheduling for timetable temporarily changed due to disaster," *IEEJ Journal of Industry Applications*, Vol. 143, No. 5, pp. 405-416, 2023 (in Japanese).
- [9] Gurobi Optimizer, <https://www.gurobi.com/solutions/gurobi-optimizer/> (Reference date: June 4, 2024).

Authors



Satoshi KATO
Senior Researcher, Operation Systems Laboratory, Signalling and Operation Systems Technology Division
Research Areas: Transportation Planning, Mathematical Optimization



Taichi NAKAHIGASHI
Researcher, Operation Systems Laboratory, Signalling and Operation Systems Technology Division
Research Areas: Transportation Planning, Train Rescheduling



Jun IMAIZUMI, Dr.Eng.
Professor, Toyo University
Research Areas: Operations Research, Scheduling



Tatsuya KOKUBO
Researcher, Operation Systems Laboratory, Signalling and Operation Systems Technology Division
Research Areas: Transportation Planning, Maintenance Worker Scheduling

Cage Wear Prediction for Traction Motor Bearings of Railway Vehicles Based on Measurement of Contact Force between Rolling Element and Cage

Daisuke SUZUKI

Ken TAKAHASHI

Yoshiaki OKAMURA

Lubricating Materials Laboratory, Material Technology Division

Fumihito ITOIGAWA

Satoru MAEGAWA

Nagoya Institute of Technology, Department of Electrical and Mechanical Engineering

Traction motor bearings of railway vehicles are used at high rotational speeds and under light loads, so that their life is determined by cage wear rather than raceway flaking. In this study, the contact forces between the rolling elements and the cage were measured to predict cage wear. As a result, the magnitude, duration, and frequency of the forces were obtained. In addition, the forces were integrated with time to obtain impulses to show the relationship between impulses and cage wear.

Key words: machine element, tribology, traction motor, cylindrical roller bearing, cage wear

1. Introduction

Traction motor bearings support the rotor of traction motors of railway vehicles. Because these bearings are operated at high rotational speeds and under light loads, they are often replaced due to cage wear (wear life) rather than raceway flaking (fatigue life). Consequently, bearings must be replaced in a much shorter time than the calculated fatigue life [1]. However, there is no method for predicting cage wear under such operating conditions, making it difficult to determine the appropriate bearing life. Since cage wear occurs at the contact area between the rolling elements and the cage, it is necessary to measure and analyze the motion and the contact force between the rolling elements and the cage for predicting cage wear.

The rotational speed of the traction motor bearing varies widely depending on the acceleration and deceleration of the railway vehicles. It is known that when a bearing is used over a wide range of rotational speeds, the cage whirl motion changes with the rotational speed [2]. The cage whirl motion at low rotational speeds is in a small oscillating state. As the rotational speed increases, the cage whirl motion becomes a circular motion through a transient state. Because the contact force between the rolling element and the cage is affected by the cage whirl motion, it is necessary to observe the contact force over a wide range of rotational speeds, including the transition of the cage whirl motion. There have been several studies on measurement of the contact force between a rolling element and a cage in rolling bearings [3, 4]. However, the contact force was measured with the constraining cage whirl motion, and there have been no cases in which the contact force has been measured and analyzed under the condition of cage whirl. In this study, a measurement system capable of simultaneously measuring contact force and cage whirl motion without constraining the cage whirl motion is constructed to conduct measurements over a wide range of rotational speeds. Based on the measurement results, the volume of cage wear is discussed [5].

2. Materials and methods

2.1 Target bearing

The specifications of the target bearing are shown in Table 1.

Generally, deep groove ball bearings and cylindrical roller bearings are used in traction motor bearings, among which cylindrical roller bearings are targeted in this study. The bearing number is NU214, which is widely used in traction motor bearings. The inner ring, outer ring and rollers are made of bearing steel, and the cage is made of high-strength brass. Because the cage is guided by the rolling elements, the cage does not contact any parts other than the rollers. The target bearings are designed for traction motors, but their specifications are almost the same as those of general-purpose products. In order to eliminate the influence of the roller diameter variation on the measurement, the roller diameter difference among each other was kept below 2 μm in the bearing.

2.2 Method for measuring contact force

The contact forces between the roller and the cage were measured directly by two small load cells (LMA-A-100NM81Z050, KYOWA ELECTRONIC INSTRUMENTS CO., LTD.) attached to one of the 16 pockets as shown in Fig. 1. The curved surfaces of the cage pocket were removed by machining and load cell attachment points were provided. The load cells were bonded to these points so that they were parallel to each other and the distance between them was equal to the diameter of the cage pocket. These load cells can measure two types of forces at the front and rear of the cage pocket.

Table 1 Specifications of target bearing

Bearing type	Cylindrical roller bearing	
Inner diameter	70 mm	
Outer diameter	125 mm	
Width	24 mm	
Radial clearance	0.090-0.125 mm	
Pitch circle diameter of roller	97.5 mm	
Number of rollers	16	
Roller diameter	13 mm	
Length of roller	13 mm	
Cage guide	By rolling elements	
Material	Race rings	JIS SUJ2
	Rollers	JIS SUJ2
	Cage	JIS CAC301
Basic dynamic load rating	83,500 N	

In this paper, the force that the roller pushes the cage in the direction of cage rotation is referred to as the “force to accelerate the cage” and the force that the roller pushes the cage in the opposite direction of cage rotation is referred to as the “force to decelerate the cage.” Figure 1 shows these forces when the direction of cage rotation is forward (counterclockwise). It also shows the coordinate system and angles used to display the measurement results. The angle is defined as 0° at the center of the no-load zone (vertically above); 180° at the center of the load zone (vertically below). It should be noted that the angle increases with the direction of rotation.

2.3 Method for measuring cage whirl motion

The cage whirl motion was measured by two laser displacement meters (LK-G35A, KEYENCE CORPORATION) attached to the housing as shown in Fig. 2. One of the two laser displacement meters measured displacement in the x-direction and the other in the y-direction. The bearing housing and the outer ring were machined with the minimum necessary notches that would not interfere with the laser beams. Although the displacement that should be measured is at the center of the cage, the displacement measured with this measuring system is strictly different from the cage center displacement because the displacement is measured at the outer diameter of the cage and the displacements in the x and y directions are not independent (when the cage moves in the x-direction, the measured displacements change not only in the x-direction but also in the y-direction). However, since the outer diameter of the cage is sufficiently large compared with the diameter of the cage whirl motion, the accuracy of the cage whirl motion measurement is sufficient even if this difference is ignored. This measurement system is also

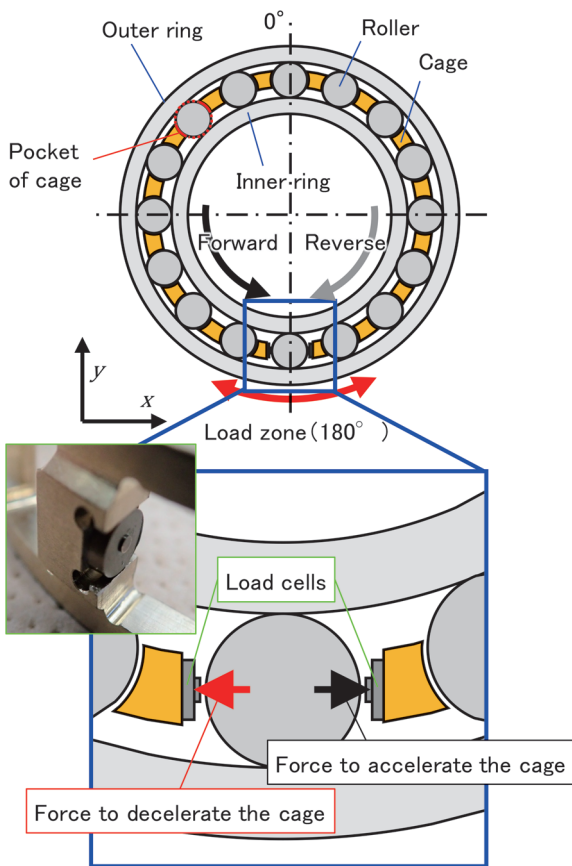


Fig. 1 Method for measuring contact force

affected by cage deformation and roundness. However, they do not affect the relative comparison of measurement results because these are sufficiently small compared to cage whirl motion and the same cage is used for all measurements.

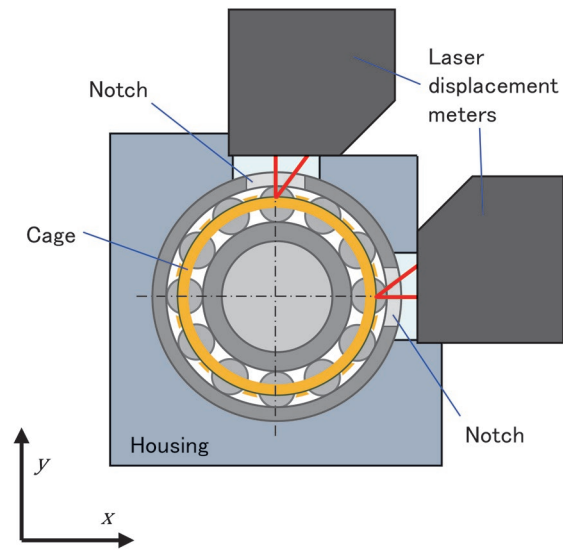


Fig. 2 Method for measuring cage whirl motion

2.4 Method for measuring contact force without constraining cage motion

Figure 3 shows a schematic diagram of a test rig capable of measuring the contact force between the roller and the cage without constraining the motion of the cage. The test rig allows the test bearing to rotate at any rotational speed and radial load within specifications. The shaft, one end of which is directly connected to the motor by a coupling, is supported by a test bearing and a support bearing (a). The rotational speed is controlled by a programmable logic controller (hereinafter referred to as PLC), and the radial load is applied by a spring through the support bearings (b) of the shaft. The radial load direction is vertically downward, and the load zone of the test bearing is also vertically downward (around 180° in Fig. 1). In order to wire the load cells attached to the rotating cage without constraining the motion of the cage, a rotor synchronized in rotation with the cage was placed in front of the cage, and the wiring was made from the load cells to this rotor. The wires are thin and light enough so that their tension does not restrict the motion of the cage. These wires are connected from the rotor to the load cell amplifier via a slip ring. Synchronization between the cage and the rotor was achieved by sending a command for the cage rotational speed, measured by the photoelectric sensor, from the PLC to the servo motor used to rotate the rotor. Both the measured contact force between the roller and the cage and the cage whirl motion are simultaneously recorded in a data logger.

2.5 Measurement conditions

Measurement conditions are listed in Table 2. The radial load was set at 970 N, which is the weight of the rotor supported by the bearings in the traction motor. This load is approximately 1.2% of the basic dynamic load rating of the test bearing (83500 N). Lithium complex soap grease was used for lubrication. A thin layer of grease was applied to the inner ring and then spread over each part of the

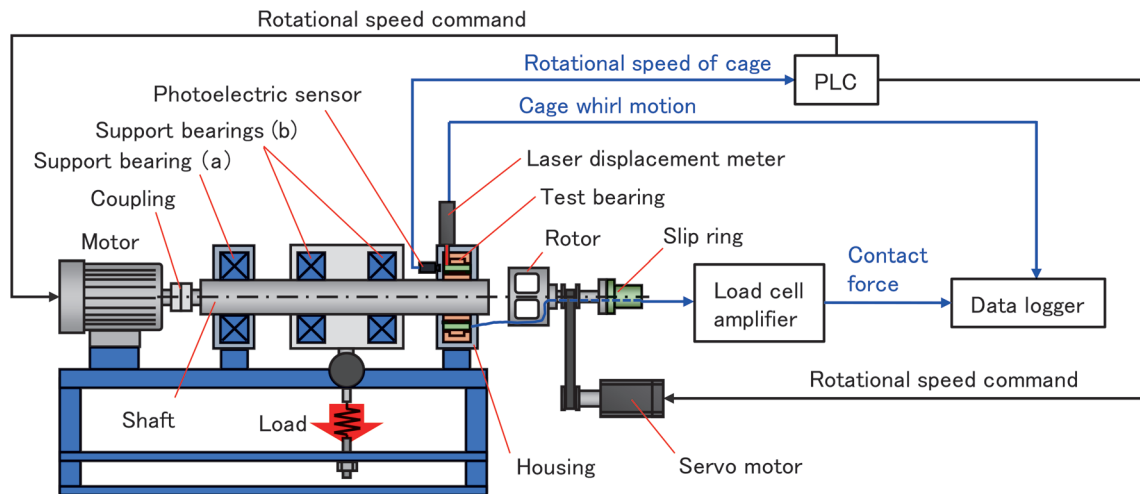


Fig. 3 Schematic diagram of test rig

bearing by rotating the bearing so that the amount of grease was the minimum required for lubrication. The direction of rotation was both forward and reverse, and the rotational speed was varied from 500, 1000, 2000, 3000 and 4000 /min to check the effect of rotational speed on the contact force between the roller and the cage. If similar data can be obtained in both directions of rotation, it can be shown that there is no bearing misalignment or load cell instrumentation error. Data were recorded at a sampling frequency of 10 kHz until the cage reached 100 rotations under each condition.

Table 2 Measurement conditions

Radial load	970 N
Lubricant	Lithium complex soap grease
Direction of rotation	Forward, Reverse
Rotational speed	500, 1000, 2000, 3000, 4000 /min

3. Results

3.1 Contact force between roller and cage

Figure 4 shows the measurement results of the contact force between the roller and the cage at rotational speeds of 1000 /min and 3000 /min. Here, the time when the pocket is positioned at 0° as shown in Fig. 1 is set to 0 s, and the measurement results until the cage completes one rotation are shown for each direction of rotation and rotational speed. Because the time required for the cage to complete one rotation is the same as the time calculated from the theoretical rotational speed of the cage, cage slip does not occur. In each graph, the black line in the top row indicates the “force to accelerate the cage” and the red line in the bottom row indicates the “force to decelerate the cage.” The area corresponding to the load zone is shaded. The graphs represent 10 rotations of the 100 rotations of the cage that were measured under each condition. The “force to accelerate the cage” tends to be generated continuously from the center to the exit of the load zone. This is because the roller is accelerated by the traction of the inner and outer rings in the load zone and contacts the front part of the cage pocket. On the other hand, the “force to decelerate the cage” tends to be generated intermittently after exiting the load zone. This is because the roller is repeatedly decelerated by the oil pressure force and accelerated by the contact with the back

part of the cage pocket. At a rotational speed of 1000 /min, the “force to accelerate the cage” is also generated from the entry to the center of the load zone. This is considered to be caused by the cage pushing the roller that is difficult to enter the load zone, but the reason why the roller is difficult to enter the load zone and the reason why this does not occur at other rotational speeds are unknown.

Next, in order to evaluate not only the contact force but also the contact time, the contact force measurement results in Fig. 4 were integrated with time to obtain the impulse. Figure 5 shows an example of the change in the impulse during one rotation of the cage when the rotational speed is 1000 /min and 3000 /min. All 100 cage rotations measured are shown. Because the trend was the same regardless of the direction of rotation, only the results for forward rotation are shown in Fig. 5. Integration was started just before each force was generated. The “force to accelerate the cage” started the integration when the roller passed through the entrance of the load zone, and the “force to decelerate the cage” started the integration when the roller passed through the exit of the load zone. The area corresponding to the load zone is also shaded. The impulse obtained from the “force to accelerate the cage” increased rapidly from the center to the exit of the load zone and then remained almost constant. In addition, during the 100 rotations of the cage, there are cases where the impulse increases significantly and other cases where it does not. These results indicate that the momentum exchange between the roller and the cage caused by the “force to accelerate the cage” is mostly generated in the load zone and is not always generated with each cage rotation. On the other hand, the impulse obtained from the “force to decelerate the cage” gradually increases from the exit of the load zone. At a rotational speed of 1000 /min, the impulse becomes constant after the roller passes through half of the no-load zone, while at a rotational speed of 3000 /min, the impulse continues to increase. In summary, the momentum exchange between the rollers and the cage due to the “force to decelerate the cage” occurs intermittently until the rollers and the cage reach the same speed or until the roller reaches the load zone, and is a highly reproducible phenomenon for each cage rotation.

Based on the above results, Fig. 6 shows the result of averaging the impulse per cage rotation for each measurement condition. The error bars in the figure indicate the standard deviations (note: negative values are not measured). The impulses per cage rotation obtained from the “force to accelerate the cage” and the “force to decelerate the cage” are close, with both decreasing up to 2000 /min

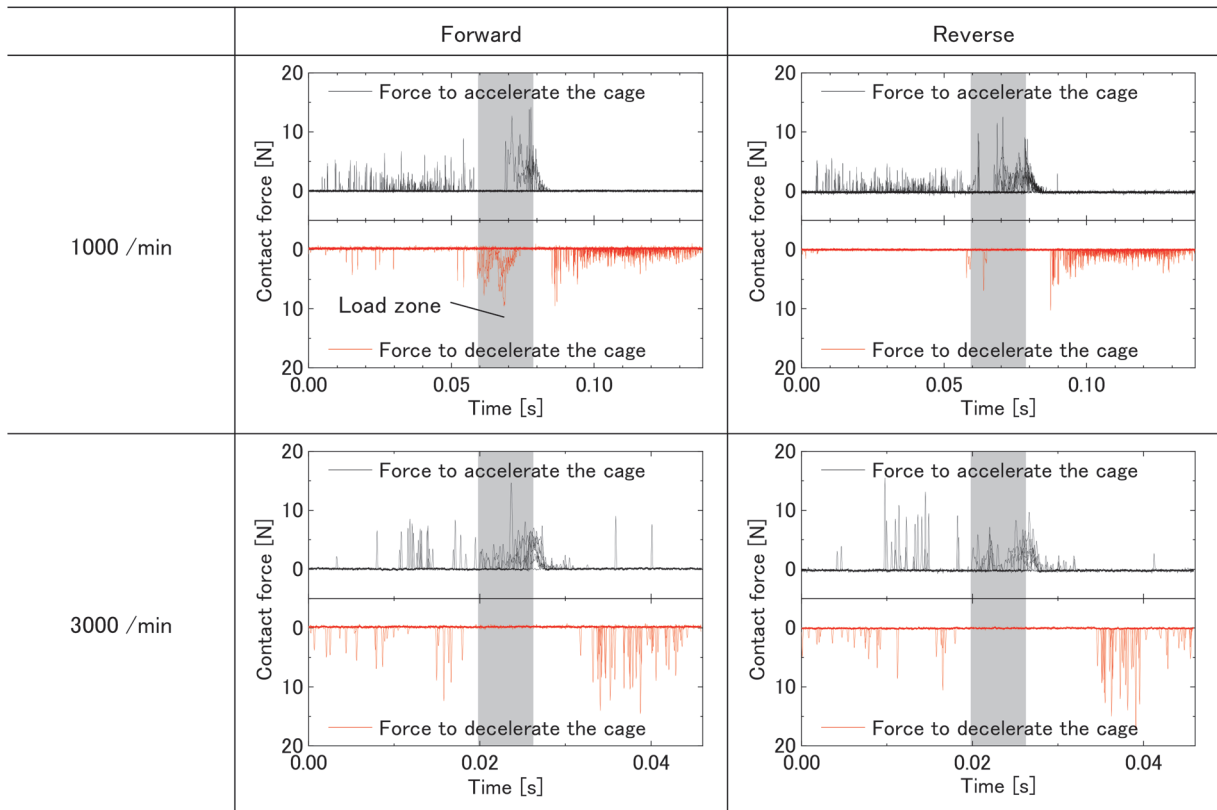


Fig. 4 Measurement result of contact force

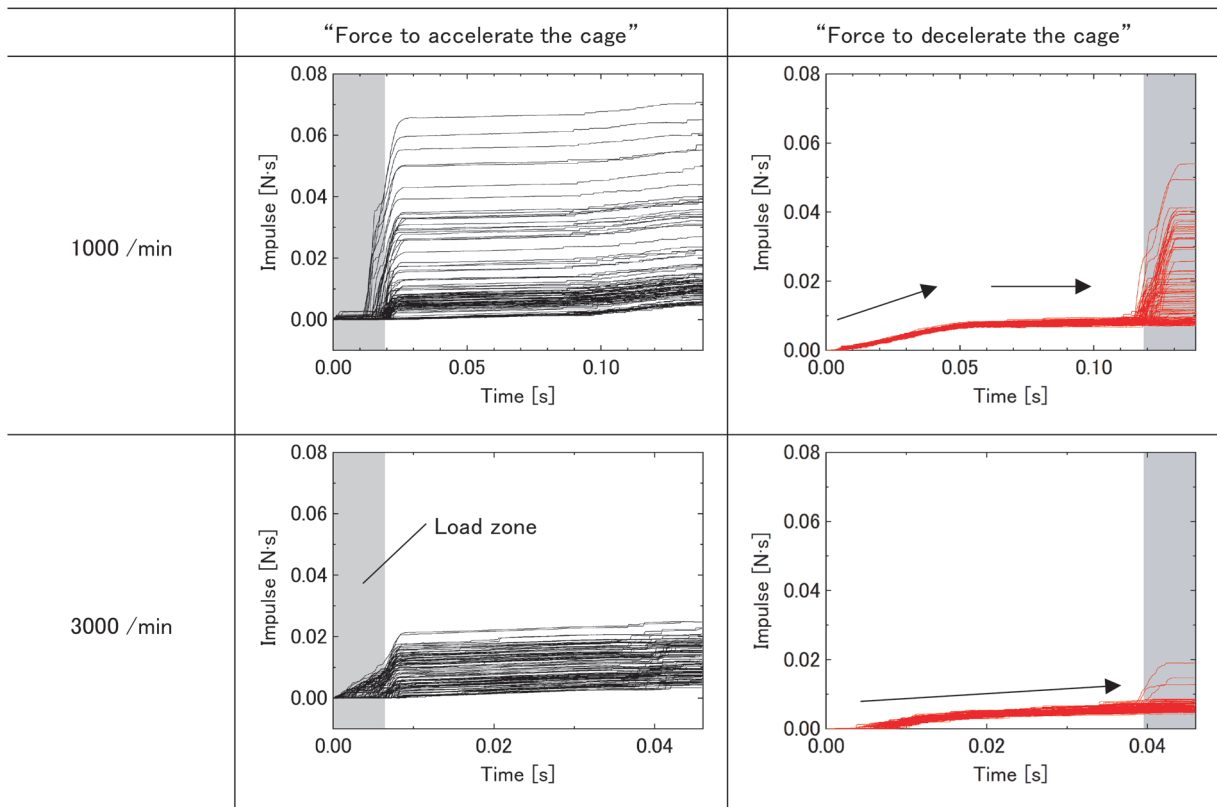


Fig. 5 Impulse obtained from contact force

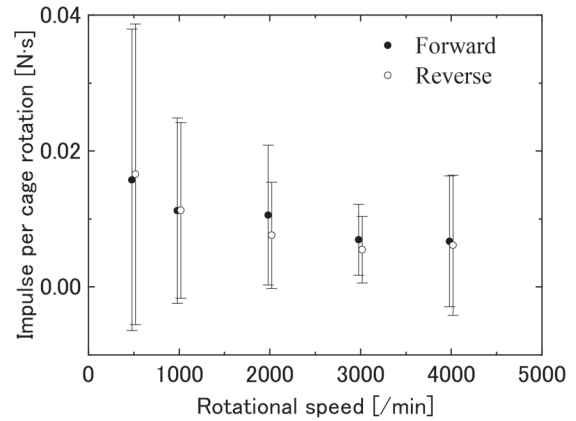
and remaining almost constant above that. Considering that the rotational speed of the cage is almost constant and that the cage is not subjected to any external force other than that from the rollers, the closeness of these values is considered reasonable. Furthermore, the standard deviation of the impulse obtained from the “force to accelerate the cage” is larger. This is because the work to accelerate the cage does not always occur in all the cage pockets, but occurs in the cage pocket located in the load zone when the cage rotational speed decreases slightly.

3.2 Cage whirl

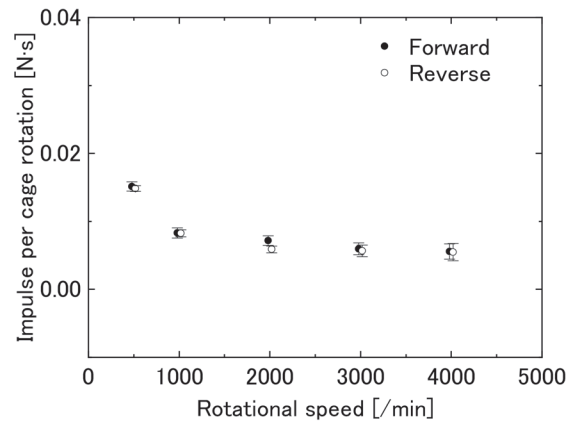
Figure 7 shows the measurement results of the cage whirl motion. This figure shows the measurement results for 10 rotations of the cage under the conditions of each rotational speed according to the coordinate system shown in Fig. 1 and Fig. 2. Note that the cage rotates counterclockwise during forward rotation and clockwise during reverse rotation. In forward and reverse rotation, the cage whirl motions show almost the same behavior in y-axis symmetry with respect to each other. The cage whirl motion oscillates mainly to the left and right in the lower part of the figure under the condition that the rotational speed is less than 1000 /min. This is because the cage hangs down with the roller at about 0° and oscillates to the left or right. As the rotational speed increases, the center of this oscillation moves in the direction of the cage rotation, and the cage whirl motion becomes circular when the rotational speed exceeds 3000 /min. At a rotational speed of 2000 /min, the cage whirl motion is in the above two transition states. As the rotational speed increases, the main force that translates the cage changes from gravity and contact force with the rollers to centrifugal force generated by the weight imbalance of the cage, which is considered to have changed the shape of the cage whirl motion. In addition, because the cage whirl motion changes with the rotational speed, it is thought that a measurement system that does not constrain the cage can be achieved.

4. Discussion

The volume of cage wear V is discussed based on the measurement results. Assuming that the wear type of the cage is adhesive wear, V follows Archard’s equation [6] shown below.



(a) Obtained from “force to accelerate the cage”



(b) Obtained from “force to decelerate the cage”

Fig. 6 Impulse per cage rotation

$$V = K \frac{WL}{H} \quad (1)$$

where K is the wear coefficient, W is the load, L is the sliding distance and H is the hardness of the softer material (in the case of this study, the hardness of the cage). Since K and H do not vary with

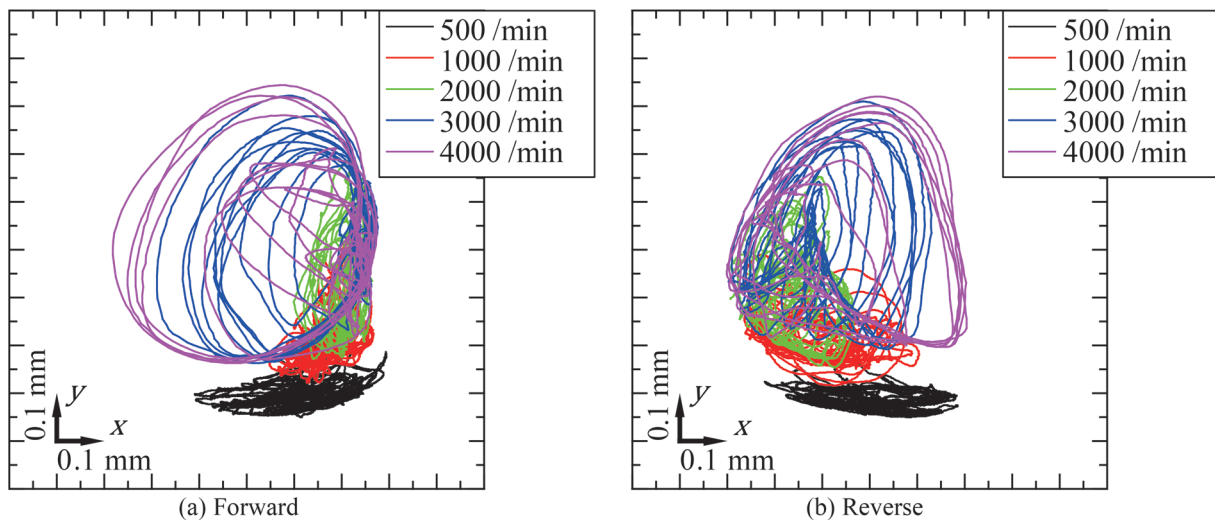
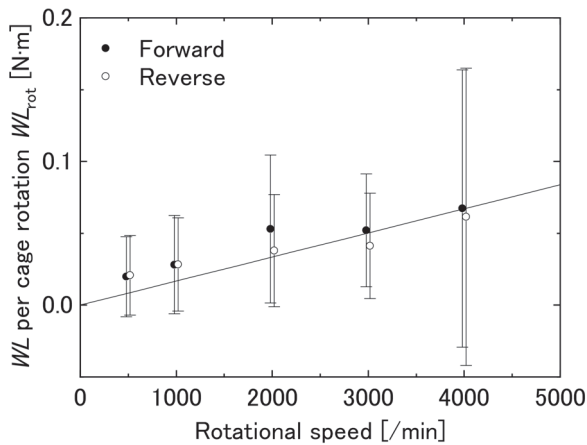


Fig. 7 Measurement result of cage whirl motion

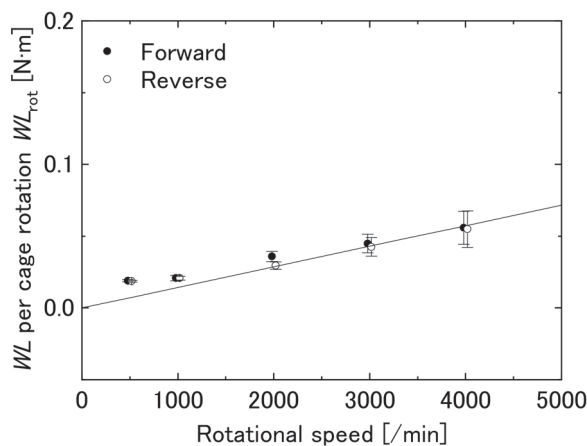
the measurement conditions, V is proportional to WL . In the case of cage wear, W is the contact force between the roller and the cage F , which varies with time and is not a constant value. Therefore, to obtain WL from the varying F , F was integrated with L . Since L is obtained by the product of the circumferential speed of the rollers $r\omega$ (where r is the roller radius and ω is the angular velocity of the roller) and time t , WL is given by the following equation.

$$WL = \int FdL = \int Fdt \cdot r\omega \quad (2)$$

From (2), WL is the product of the impulse caused by F and $r\omega$. In order to compare V per cage rotation V_{rot} between each measurement condition, WL per cage rotation WL_{rot} was obtained and is shown in Fig. 8. To obtain WL_{rot} , the impulse per cage revolution shown in Fig. 6 and the theoretically calculated $r\omega$ were used. WL_{rot} obtained from the “force to accelerate the cage” and the “force to decelerate the cage” both show a tendency to increase in proportion to the rotational speed. However, WL_{rot} at rotational speed of 500 /min and 1000 /min is above the straight line approximating the origin and the values at rotational speed of 2000 /min to 4000 /min. From the above, it can be seen that V_{rot} decreases as the rotational speed decreases, but the degree of the decrease is smaller at 500 /min and 1000 /min. This result is due to the relatively greater effect of gravity acting on the rollers at lower rotational speeds (see Ref.



(a) Obtained from “force to accelerate the cage”



(b) Obtained from “force to decelerate the cage”

Fig. 8 WL per cage rotation

[7] for details). From the above, if K is determined, V can be predicted quantitatively. Even if K is not determined, it is possible to predict how much V will change when the operating conditions are changed.

5. Conclusions

To predict cage wear in traction motor bearings, it is necessary to measure and analyze the motion and contact force between the roller and the cage. For this purpose, a measurement system was constructed to simultaneously measure the contact force and the cage whirl motion without constraining the cage motion. Using the constructed system, measurements were made over a wide range of rotational speeds. In addition to the measurement, the relationship between the contact force and the cage wear was discussed. As a result, the following findings were obtained.

- (1) As a result of the contact force measurements, the “force to accelerate the cage” occurred continuously from the center to the exit of the load zone. This is because the roller is accelerated by the traction of the inner and outer rings in the load zone and contacts the front part of the cage pocket. On the other hand, the “force to decelerate the cage” occurred intermittently after exiting the load zone. This is because the roller is repeatedly decelerated by the oil pressure force and accelerated by the contact with the back part of the cage pocket.
- (2) The result of integrating the contact force measured in (1) with time to obtain the impulse per cage revolution showed that the impulse per cage rotation obtained from the “force to accelerate the cage” and the “force to decelerate the cage” were close, both decreasing up to 2000 /min of rotational speed and almost constant above that.
- (3) The cage whirl motion oscillated mainly to the left and right in the lower part under the condition that the rotational speed is less than 1000 /min. As the rotational speed increased, the center of this oscillation moved in the direction of the cage rotation, and the cage whirl motion became circular when the rotational speed exceeded 3000 /min. At a rotational speed of 2000 /min, the cage whirl motion was in the above two transition states.
- (4) Assuming that the volume of cage wear V is proportional to the product of the contact force and the sliding distance WL , WL was derived using the impulse obtained in (2). As a result, V per cage rotation is considered to increase as the rotational speed increases.

References

- [1] International Organization for Standardization, “Rolling bearings - Dynamic load ratings and rating life,” ISO 281: 2007, 2007.
- [2] Tada, S., “Analysis of sound, vibration and motion cages during high-speed rotation,” *KOYO Engineering Journal*, No. 160E, pp. 29-36, 2002.
- [3] Kakuta, K., “The Effects of Misalignment on the Forces Acting on the Retainer of Ball Bearings,” *Journal of Basic Engineering*, Vol. 86, No. 3, pp. 449-454, 1964.
- [4] Stacke, L-E. and Fritzon, D., “Dynamic behavior of rolling bearings: simulations and experiments,” *Proceedings of the Institution of Mechanical Engineers, Part J: Journal of Engineering Tribology*, Vol. 215, No. 6, pp. 499-508, 2001.

- [5] Suzuki, D., Takahashi, K., Itoigawa, F. and Maegawa, S., "Contact forces between roller and cage pocket in cylindrical roller bearings (Consideration based on dynamic behavior between roller and cage)," *Transactions of the JSME*, Vol. 88, No. 911, DOI:10.1299/transjsme.22-00153, 2022 (in Japanese).
- [6] Archard, J.F., "Contact and Rubbing of Flat Surfaces," *Journal of Applied Physics*, Vol. 24, No. 8, p. 981, 1953.
- [7] Suzuki, D., Takahashi, K., Itoigawa, F. and Maegawa, S., "Study on Cage Wear of Railway Traction Motor Bearings Based on Analysis of Rolling Element Motion," *Machines*, Vol. 11, No. 6, p. 594, DOI:10.3390/machines11060594, 2023.

Authors



Daisuke SUZUKI, Dr.Eng.
Assistant Senior Researcher, Lubricating Materials Laboratory, Material Technology Division
Research Areas: Tribology, Machine Elements, Rolling Bearings



Fumihito ITOIGAWA, Dr.Eng.
Professor, Department of Electrical and Mechanical Engineering, Nagoya Institute of Technology
Research Areas: Manufacturing and Production Engineering, Design Engineering, Machine Elements and Tribology



Ken TAKAHASHI, Ph.D.
Senior Researcher, Lubricating Materials Laboratory, Material Technology Division
Research Areas: Tribology, Machine Elements, Rolling Bearings



Satoru MAEGAWA, Dr.Eng.
Associate Professor, Department of Electrical and Mechanical Engineering, Nagoya Institute of Technology
Research Areas: Design Engineering, Machine Elements and Tribology



Yoshiaki OKAMURA, Ph.D.
Senior Chief Researcher, Head of Lubricating Materials Laboratory, Material Technology Division
Research Areas: Tribology, Machine Elements, Rolling Bearings

Outline of Design Standard and Commentary for Railway Structures (Concrete Structures)

Ken WATANABE

Concrete Structures Laboratory, Structures Technology Division

Toshiya TADOKORO

Concrete Structures Laboratory, Structures Technology Division (Former)

Manabu IKEDA

Structural Mechanics Laboratory, Railway Dynamics Division

Masaru OKAMOTO

Steel and Hybrid Structures Laboratory, Structures Technology Division (Former)

Design Standard and Commentary for Railway Structures (Concrete Structures) was revised in January of 2023. In this revision, in addition to reorganization of the previous design standards established mainly for each type of structure and material, the introduction of the latest verification techniques has made the design standards easier to use. The application of the revised design standards to design practice will improve railway structures.

Key words: concrete structures, basic principle, structural units, parts/members

1. Introduction

A notification for “Design Standards for Railway Structures (Concrete Structures)” was issued in December 2022. This paper presents an overview of the revision of the “Design Standard for Railway Structures and its Commentary (Concrete Structures)” [1] (hereinafter referred to as “the Standard”), which was published in January 2023.

2. Background of the revision

2.1 Technical standard system for design of railway structures

The “Ministerial Ordinance to Provide Technical Standards for Railways” [2] (hereinafter referred to as “Ministerial Ordinance on Technical Standards”) was revised to the performance-based design in December 2001. The Ministerial Ordinance on Technical Standards stipulates in Article-1 that the objective of the ordinance is “to ensure safe and stable transportation, thereby contributing to the promotion of welfare of the public.” That is to say, Article-1 of this Standard requires infrastructure, rolling stock, etc. to be compatible with train operations, etc. to ensure the safety of people and facilities, while being technically and economically feasible. Article-24 of the ordinance stipulates the function of railway civil structures: that “earthworks, bridges, tunnels, and other structures shall be capable of withstanding anticipated loads; and not impede the running safety of rolling stock due to displacement of the structure caused by train loads, impacts, etc.

The Design Standard for Railway Structures and its Commentary (hereinafter referred to as the “Design Standard”) is an interpretation standard (notification). It is a non-mandatory, numerically expressed, practical interpretation of the Ordinance of the Ministry of Engineering Standards, and a commentary that summarizes the rationale for the interpretation standard and concept, etc. All Design Standards were changed to performance-based design by FY2022.

2.2 History of Revision of Design Standards for Railway Concrete Structures

Table 1 shows the evolution of the technical standards for railway concrete structures. Initially, the design and construction of concrete structures was left to the discretion of engineers. In 1914, a corpus of knowledge on reinforced concrete bridges was established, signaling the beginning of a harmonized approach. This formed the basis for the Standard Specifications for Concrete Structures of the Japan Society of Civil Engineers (JSCE). These standards were published in two volumes in 1955: the first volume on general provisions covered specifications for common themes such as loads and stresses; and the second volume on specific provisions, covered details about characteristics of specific members such as slabs, beams, and columns. In 1970, standards for conventional and Shinkansen lines were integrated. Following two further revisions, in 1992, the “Design Standards” adopted a limit state design method. The allowable stress design method, which had been used until then, is a design method that verifies that the stress acting on each section of a member is less than or equal to the allowable stress of the material constituting the member. On the other hands, the limit state design method sets limit states for each required performance and verifies that the limit values set for each limit state are satisfied. As a result of this change, safety coefficients were set for each action, material, and structural analysis method, etc. This made it easier to integrate technological advances. In addition, it made relatively easier for designers to be more clearly aware of the condition of structures from the verification results.

In response to performance requirements of the Ministerial Ordinance on Technical Standards, the Design Standards for Railway Structures and its Commentary (Concrete Structures) [3] (hereinafter referred to as the 2004 Concrete Standard), revised in 2004, introduced performance-based design. This is a design method in which the required performance of structures is specified, and the limit state design method is followed as a verification method. It is also a design method that is more flexible for the adoption and application of new materials and structures, is conducive to interna-

Table 1 Revision history of Design Standards for Railway Concrete Structures, etc.

Year Established/ Revised	Title	Remarks
1914	Corpus of knowledge about reinforced concrete bridge design	The first design and construction standards for railway structures
1955 1958	Design Criteria for Plain Concrete and Reinforced Concrete Civil Engineering Structures (Draft)	The first design and construction standards for railways structures Composed of Part 1: General Provisions, Part 2: Specific Provisions.
1961	Shinkansen Structure Design Standard (Draft)	Loads specific to Shinkansen and allowable displacement of structures
1965	Design and Construction Standard for Prestressed Concrete Railway Bridges (Draft)	The design and construction guidelines for prestressed concrete established by the Japan Society of Civil Engineers in 1961 were used as the basis for this document.
1970	Structure Design standards (reinforced and plain concrete structures, prestressed concrete railway bridges)	The design standards for both conventional and Shinkansen lines are integrated into one document. Covers the basic contents related to the design of structures.
1972	National Shinkansen Design Standards (for Joetsu, Tohoku, and Narita Shinkansen)	The guideline covers the basic contents related to the design of structures.
1974	Structure Design Standards (Reinforced and plain concrete structures, prestressed concrete railway bridges)	Revised based on the results of a committee commissioned by the Japan Society of Civil Engineers (JSCE), taking into account technological developments both within and outside Japan Railways.
1983	Building Design Standards (Reinforced and unreinforced concrete structures, prestressed concrete railway bridges)	The concept of the limit state design method was incorporated, based on the allowable stress design method.
1992	Design Standard for Railway Structures (Concrete Structures)	Introduction of limit state design method
2004	Design Standard for Railway Structures (Concrete Structures)	The performance-based design
2023	Design Standard for Railway Structures (Concrete Structures)	The performance-based design and 3-layered structure

tional harmonization, and is highly compatible in maintenance. This standard, revised in 2023, follows the performance-based design and has been revised in accordance with the issues and policies described in the following sections.

2.3 Issues surrounding railway concrete structures

The following is a list of recent issues surrounding railway concrete structures with expected responses:

- Design standards today are organized according to type of structural material, such as concrete structures, steel structures and composite structures, etc., by type of structure, such as tunnels, etc., or by actions and type of verification, such as displacement limitations and seismic design. This categorization approach complicates application of these designs in practice. In response to this complexity, it would be clearer for design standards to be grouped type of structure, and for the relationship to be clarified between structures and different parts and materials that make up the railroad system.
- There is an absence of a uniform approach to design and design related action in the current design standards [4]: this should be addressed by adopting common design concepts and referring to a common set of basic themes and topics for railway structures that constitute the railway system.
- Structural plans which establish the types, specifications, etc. of structures as a preliminary stage of verification should be included, in order to facilitate the design of practical structures which meet performance requirements.
- In order to design safe and economically viable concrete structures, the scope of application of conventional standard verification methods needs to be clarified. This would allow the latest analytical methods to be applied to complex structures and actions for which conventional verification methods are no longer suitable.
- In response to changes in the type of aggregates used on a daily basis and durability problems of concrete structures, steps should be taken to ensure the serviceable-life performance of structures by design, which takes into account local conditions, such as the characteristics of the materials at the construction site and the effects of weather during service.
- Design methods should consider questions about actual construction, and take into account conditions needed for construction and the problem of shrinking numbers of construction workers.
- Considering the damage caused by the 2011 off the Pacific coast of Tohoku Earthquake and the 2016 Kumamoto Earthquake, structure designs should be conducive to early restoration in the wake of increasingly severe natural disasters. Following the identification of these issues, a “Committee on Design Standards for Railway Concrete Structures” was established

in FY2016 and studied these issues for four years.

3. Outline of the revision

3.1 Basic policy

It is now over 18 years since the 2004 Concrete Standards were published. Therefore, it was decided they should be reviewed in the light of latest technology and other developments related to concrete structures. It was also decided that the structure of presenting these standards should change in a way which enable railway structures to function more organically as a railway system. In light of the rapid changes in social conditions and the circumstances surrounding the railway business as shown in 2.3, efforts were made to review the railway-specific technologies and supplement them with the latest technologies, referring to the research results of the Railway Technical Research Institute and the JSCE Standard Specifications for Concrete (Design) [5], etc., enacted in 2017. In addition, as a standard for interpretation, we have tried to show concrete figures and specifications. On the other hand, in cases where it is difficult to show with concrete figures and specifications, we have tried to show design methods and methods of verification, etc. [1].

3.2 Overall structure of the design standards

The railway system is composed of railway structures such as bridges, earth structures, and tunnels. Consequently, it makes sense for them to share a common set of basics such as design concepts, setting of performance requirements, and verifications. Therefore, the new standards discuss basic principles [4] for all structures and reorganize the system of design standards. Specifically, a new chapter of basic principles (Layer-1) was added to summarize the design basics for all railway structures covered by the design standard, not limited to concrete structures. The structures and structural units (Layer-2) summarizes matters related to the design of structures and structural units. This chapter creates the link between the common basic principles and the design of each structure. The section on parts and members (Layer-3) specifies materials and structures necessary for design, and summarizes matters related to the design of parts and members that constitute structural units (Fig. 1). This

Standard consists of the following four parts.

- Part I Basic Principles: specifies matters common to the design of railway structures, such as required performance and design service life. [4]
- Part II Bridge Structures: Based on Part I, the structural planning, actions, structural analysis, and verification methods for bridges (including elevated bridges) are specified. [6]
- Part III Concrete Structures: Based on Part I and Part II, the applicable requirements, response values, limit values, etc. are specified for each part and member of concrete structures. [7]
- Part IV Bearing Structures: Based on Part I and Part II, the applicable requirements, response values, limit values, etc. for bearings of concrete bridges are specified. It is assumed that the requirements will be applied to bearings for steel and composite bridge structures in the future. [8]

In principle, the verification of bridge structures is performed on the structural units of the bridge, such as bridge girders, piers, etc., in accordance with the Part II Bridge Structures. When verification is performed on structural units, the bridge mass is considered to satisfy verification by making sure that all structural units satisfy verification. However, under general design conditions, as in the past, verification may be performed on structural units such as beams, bearings, piers, footings, piles, and so on. In this case, the structural unit satisfies the verification requirements by making sure that all parts and members satisfy the verification requirements in accordance with the Part III Concrete Structures and the Part IV Bearing Structures.

Figure 2 shows how the 2004 Concrete Standard and related standards have been transferred to the various parts of this standard. Other items related to the part II, III, and IV from the related standards [9]-[14] have been transferred in the respective sections. In addition, Part I Basic Principles was based on all the design standards [9]-[18].

3.3 Basis of design

The term “railway system” is newly defined with reference to the Ordinance of the Ministry of Technical Standards. In the design of the structure, the required performance and its level shall be defined according to the purpose as a railway system and the function of the structure, and the structural plan, investigation and structural

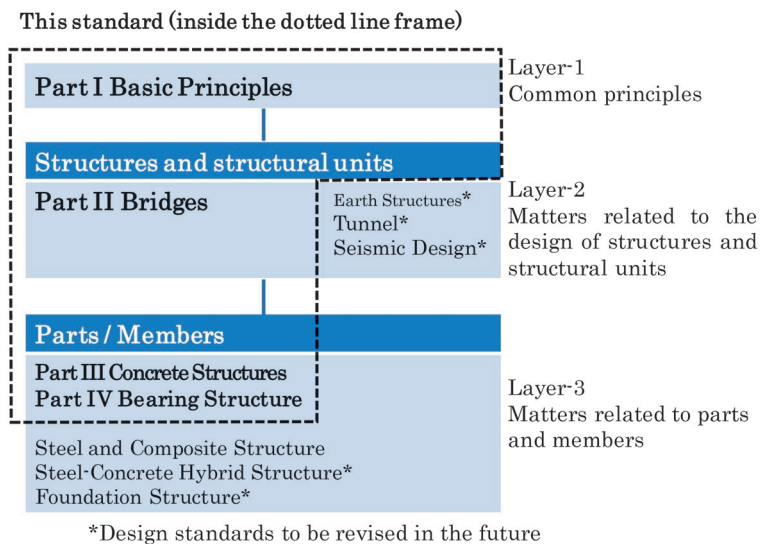


Fig. 1 System of design standards

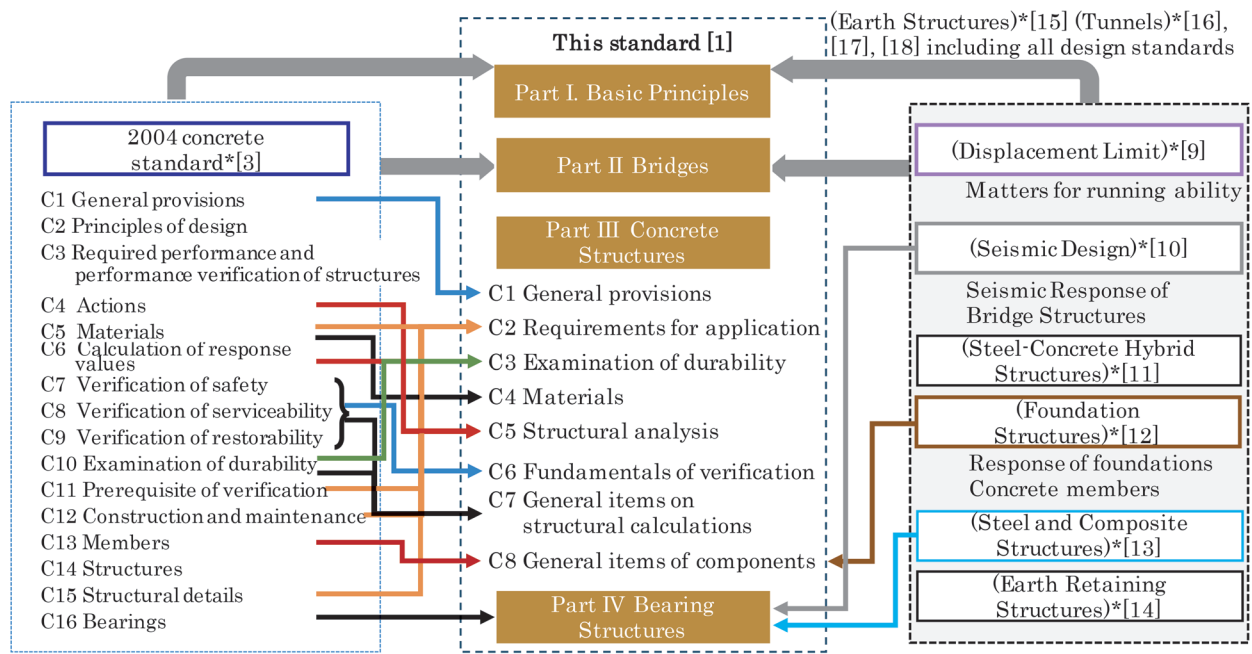


Fig. 2 Major transfers from the 2004 Concrete Standard and related standards to this standard

details shall be established and verified. Here, although the structural planning is not described in the 2004 Concrete Standard, it was added in recognition that it is important for designing better structures. From the viewpoint of realizing a sustainable society, “compatibility with society”[4] and from the viewpoint of crisis resistance to prevent catastrophic damage to structures, “redundancy and robustness” [4] shall be required in structural planning and in setting the required performance level.

3.4 Design methods for safety, etc.

In order to design safe and economically viable concrete bridges, the latest methods are described for complex structures and actions to which conventional verification methods cannot be applied.

In Part II Bridge, bridge structures are classified into structural units (girders, piers, abutments) and parts/members (beams, slabs, foundation structures, bearings, etc.), so that each verification method is presented according to each classification. Verifications focusing on bridges or each structural unit enables more rational verification for non-stationary structures such as ramen viaducts, for example, because the failure of one member does not immediately lead to the limit state of the structure.

In Part III Concrete Structures, a method [19] for calculating the design shear capacity of bar members with fixed supports at both ends, assuming members of a ramen viaduct, was introduced for shear capacity used in verifying the failure of concrete members, etc. This method allows the shear span ratio to be calculated from the shear capacity of a bar member with fixed supports at both ends. This method allows the shear reinforcement bars to have a greater effect when the shear span ratio is smaller than that of bar members under simply supported conditions with the same cross-sectional properties. Furthermore, a verification method based on nonlinear finite element analysis has been introduced and made applicable in accordance with the JSCE Standard Specifications for Concrete [Design Edition] [5] enacted in 2017. The verification methods have

been enhanced and made more sophisticated, allowing for more rational verification and more labor-saving verification for structures with a proven track record. Engineers will thus be able to use their creativity to develop flexible design solutions.

3.5 Design method considering regional specificity, aging axis, etc.

Design methods considering the time axis and the study on durability were reviewed. In the concrete structures section, a formula for calculating the shrinkage strain of concrete that can take into account the effects of rainfall conditions at the construction site and shrinkage of aggregate [20] and a new structural analysis method for predicting the long-term deformation of PC girders due to shrinkage and creep were presented. In the study on steel corrosion, the previous “study on neutralization” was changed to “study on corrosion of steel due to water penetration” [21], and the limit values of chloride ion concentration were updated to values corresponding to various cement and water binder ratios.

3.6 Design methods considering construction

In part III Concrete Structures, the introduction of technologies that contribute to reliable construction and design methods that promote such technologies are described, including optimization of reinforcement quantity in precast structures and member joints [22], use of high-strength materials [23], evaluation of initial cracking and long-term behavior of structures based on the construction process, and others.

3.7 Design methods for easily recoverable concrete structures

Based on the damage caused by the 2011 off the Pacific coast of Tohoku Earthquake and the 2016 Kumamoto Earthquake, this section presents design methods for concrete structures that can be

easily and quickly restored and whose performance can be ensured even after recovery following an earthquake.

In Part II Bridge, aspects related to recovery and restoration, such as securing access roads and work yards for restoration work and controlling damage in areas that are difficult to repair, examples of items that should be considered in the structural planning stage of bridge structures are presented. In Part IV Bearing structures, for example, it is shown that, in the case of a stopper embedded in a bearing section, damage should be controlled at a point where it is easy to repair, such as damage which occurs first to the front side of the girder seat before the loose side of the girder end, rather than damage occurring first at the loose side of the girder end, where repair work would be difficult. A more accurate calculation method for the bearing capacity of embedded stoppers has been developed [24] that takes into account the arrangement of steel bars and other factors. The method makes it possible to control damage at points that are easy to repair during earthquakes without increasing the amount of steel bars embedded in the stopper, thereby reducing restoration costs and other expenses.

4. Summary

In this revision, the previous design standards, which were established mainly for each type of structure and material, were reorganized and the latest verification techniques were introduced to enable railway structures to function more organically as a railway system. In addition, design calculation examples and design tools will be developed sequentially. Amid demands for a sustainable society, it is hoped that the application of this standard to design practice will contribute to building better railway structures unconstrained by conventional forms. It is noted that the specific contents of each item will be reported in detail in a separate paper.

Acknowledgment

This paper was discussed by the Committee on Standards for Design of Concrete Structures. The authors would like to acknowledge the efforts of the committee chairman Dr. Junichiro Niwa (then professor at Tokyo Institute of Technology), the secretary general Dr. Tadatomo Watanabe (then vice president of Hokubu Consultants), and all the committee members and secretaries for their deliberations.

References

- [1] Ministry of Land, Infrastructure, Transport and Tourism (MLIT) and Railway Technical Research Institute (ed.), *Design Standards for Railway Structures and Commentary (Concrete Structures)*, Maruzen Publishing, 2023 (in Japanese).
- [2] Ministry of Land, Infrastructure, Transport and Tourism, Railway Bureau, *Technical Standards for Railways (Civil Engineering), Fourth Edition*, 2023 (in Japanese).
- [3] Ministry of Land, Infrastructure, Transport and Tourism, and Railway Technical Research Institute, *Design Standards for Railway Structures and Commentary (Concrete Structures)*, Maruzen Publishing, 2004 (in Japanese).
- [4] Tadokoro, T., Watanabe, K., Ikeda, M. and Okamoto, M., *Design Standard and Commentary for Railway Structures (Concrete Structures) Outline of "Part I: General Principles,"*

- RTRI Report*, Vol. 37, No. 11, pp. 7-13, 2023 (in Japanese).
- [5] Japan Society of Civil Engineers, *Standard Specifications for Concrete Structures -2007 [Design]*, Maruzen Publishing, 2018 (in Japanese).
- [6] Watanabe, K., Ikeda, M. and Okamoto, M., *Design Standard and Commentary for Railway Structures (Concrete Structures) Outline of "Part II: Bridge Structures,"* RTRI Report, Vol. 37, No. 11, pp. 15-23, 2023 (in Japanese).
- [7] Watanabe, K., Nakata, Y. and Todoroki, S., *Design Standard and Commentary for Railway Structures (Concrete Structures) Outline of "Part III: Concrete Structure,"* RTRI Report, Vol. 37, No. 11, pp. 25-33, 2023 (in Japanese).
- [8] Ikeda, M., Tadokoro, T., Todoroki, S. and Toyooka, A., *Design Standard and Commentary for Railway Structures (Concrete Structures) Outline of "Part IV: Bearing Structures,"* RTRI Report, Vol. 37, No. 11, pp. 35-40, 2023 (in Japanese).
- [9] Ministry of Land, Infrastructure, Transport and Tourism (MLIT) and Railway Technical Research Institute (ed.), *Design Standards for Railway Structures and Commentary (Displacement limits)*, Maruzen Publishing, 2006 (in Japanese).
- [10] Ministry of Land, Infrastructure, Transport and Tourism (MLIT) and Railway Technical Research Institute (ed.), *Design Standards for Railway Structures and Commentary (Seismic Design)*, Maruzen Publishing, 2012.
- [11] Ministry of Land, Infrastructure, Transport and Tourism (MLIT) and Railway Technical Research Institute (ed.), *Design Standards for Railway Structures and Commentary (Steel-Concrete Hybrid Structures)*, Maruzen Publishing, 2016 (in Japanese).
- [12] Ministry of Land, Infrastructure, Transport and Tourism (MLIT) and Railway Technical Research Institute (ed.), *Design Standards for Railway Structures and Commentary (Foundation Structures)*, Maruzen Publishing, 2012 (in Japanese).
- [13] Ministry of Land, Infrastructure, Transport and Tourism (MLIT) and Railway Technical Research Institute (ed.), *Design Standards for Railway Structures and Commentary (Steel and Composite Structures)*, Maruzen Publishing, 2009 (in Japanese).
- [14] Ministry of Land, Infrastructure, Transport and Tourism (MLIT) and Railway Technical Research Institute (ed.), *Design Standards for Railway Structures and Commentary (Earth Retaining Structures)*, Maruzen Publishing, 2012 (in Japanese).
- [15] Ministry of Land, Infrastructure, Transport and Tourism (MLIT) and Railway Technical Research Institute (ed.), *Design Standards for Railway Structures and Commentary (Earth Structures)*, Maruzen Publishing, 2007 (in Japanese).
- [16] Ministry of Land, Infrastructure, Transport and Tourism (MLIT) and Railway Technical Research Institute (ed.), *Design Standards for Railway Structures and Commentary (Cut and Cover Tunnel)*, Maruzen Publishing, 2021 (in Japanese).
- [17] Ministry of Land, Infrastructure, Transport and Tourism (MLIT) and Railway Technical Research Institute (ed.), *Design Standards for Railway Structures and Commentary (Shield Tunnel)*, Maruzen Publishing, 2022 (in Japanese).
- [18] Ministry of Land, Infrastructure, Transport and Tourism (MLIT), Railway Technical Research Institute (ed.), *Design Standards for Railway Structures and Commentary (Mountain Tunnel)*, Maruzen Publishing, 2022 (in Japanese).
- [19] Nakata, Y., Watanabe, K., and Tadokoro, T., "Calculation equation of shear capacity for RC beams subjected to fix supported at both ends," *the 77th Annual Conference of JSCE*, 2022, V-621 (in Japanese).
- [20] Watanabe, K., Nakamura, M., Ishida, T. and Watanabe, T.,

- “Prediction Equation for Shrinkage Strain of Concrete Considering the Effect of Mixed Cement,” *RTRI Report*, Vol. 37, No. 1, pp. 11-19, 2023 (in Japanese).
- [21] Todoroki, S., Ishida, T., Ueda, H. and Tadokoro, T., “Design Method for Corrosion of Reinforcing Bars in Concrete Structures by Water Penetration and Carbonation Progress,” *RTRI Report*, Vol. 37, No. 10, pp. 1-8, 2023 (in Japanese).
- [22] Nakata, Y., Watanabe, K. and Tadokoro, T., “Influence of Structural Details of Beam-to-column Joint in RC Viaducts on Capacity,” *RTRI Report*, Vol. 37, No. 1, pp. 29-35, 2023 (in Japanese).
- [23] Sato, Y., Nakata, Y., Tadokoro, T. and Watanabe, K., “The damage properties and the applicability of deformation performance calculation formula of RC columns using high strength rebar,” *Proc. of the JCI*, Vol. 44, No. 2, pp. 175-180, 2022 (in Japanese).
- [24] Todoroki, S., Mori, Y., Tadokoro, T. and Watanabe, K., “Equation for Design Strength of Embedded Part of Square Steel Stopper in Railway Bridge,” *RTRI Report*, Vol. 37, No. 1, pp. 1-9, 2023 (in Japanese).

Authors



Ken WATANABE, Ph.D.
Senior Chief Researcher, Head of Concrete Structures Laboratory, Structures Technology Division
Research Areas: Design and Maintenance of Concrete Structures



Manabu IKEDA, Dr.Eng.
Senior Chief Researcher, Head of Structural Mechanics Laboratory, Railway Dynamics Division
Research Areas: Hybrid Structures, Steel Structures



Toshiya TADOKORO, Dr.Eng.
Senior Chief Researcher, Head of Concrete Structures Laboratory, Structures Technology Division (Former)
Research Areas: Design and Maintenance of Concrete Structures



Masaru OKAMOTO, Dr.Eng.
Senior Chief Researcher, Head of Steel and Hybrid Structures Laboratory, Structures Technology Division (Former)
Research Areas: Hybrid Structures, Concrete Structures

Introduction Manual for Natural Frequency Identification System of Bridge Piers by Constant Microtremor Measurement

Satoshi WATANABE Hiroki IRI Shoma FUJIWARA
Geo-hazard and risk mitigation Laboratory, Disaster Prevention Technology Division

In recent years, disasters have frequently occurred due to rapid river flooding and prolonged high water levels caused by typhoons and localized heavy rainfall. It is, therefore, necessary to establish a method for monitoring the destabilization of river piers during periods of rising water. In response to this need, we have prepared an introduction manual for a natural frequency identification system, which includes an algorithm for identifying the natural frequencies of piers from microtremor measurements, the basic specifications of acceleration sensors required to construct a microtremor measurement system, the application conditions of this system, and methods for evaluating the measurement results.

Key words: natural frequency, micro tremor, acceleration sensor, introduction manual

1. Introduction

In recent years, disasters have frequently occurred due to rapid river flooding and prolonged high water levels caused by typhoons and localized heavy rainfall. As a result, the ground around the foundations of piers located in rivers is scoured by rising water, resulting in frequent disasters such as sinking, tilting, and overturning of piers. These disasters can cause catastrophic accidents such as derailments or and overturning of trains into rivers, depending on the circumstances. It will therefore become even more important to monitor the stability of piers during periods of rising water.

The impact vibration test method [1] is used to evaluate the soundness of piers. This method identifies the natural frequency, which is an index of soundness, by directly vibrating the piers with a weight, and evaluates the soundness of the piers based on the degree of decrease in the value. However, since this method requires hitting the piers with a heavy weight, it is difficult to measure the natural frequency when the water level is rising. Therefore, we have developed a method to continuously measure the natural frequencies of piers by constantly measuring the microtremors [2, 3, 4]. As a result of this research, an algorithm was developed to identify the natural frequencies of piers by measuring microtremors at two locations at the top of the piers. The algorithm was applied to a model test and a part of a real pier in service, and the identification of the natural frequencies was confirmed to be feasible [5, 6]. A method was also developed to improve the identification accuracy when using a low-cost accelerometer as the measurement sensor [7].

In order to promote the use of the natural frequency identification system that utilizes the results of these developments, we drafted an introduction manual. The manual includes the natural frequency identification algorithm, the basic specifications of acceleration sensors required to construct the constant-microtremor measurement system, the application conditions of the above system, and the method for evaluating measurement results. This paper describes the contents of the manual in detail.

2. Organization of manual

The chapter structure of the manual is shown in Fig. 1. The manual consists of seven chapters, with Chapter 1 summarizing the

significance of the microtremor measurement and the contents of the manual, and Chapter 2 and subsequent chapters describing the specific scope of application, the natural frequency identification algorithms, and other details.

3. Scope of application of the constant microtremor measurement method

Chapter 2 of the manual describes the features of the constant microtremor measurement method as well as the foundation structures to which it is applied and points to be considered in its application. The following is an overview of the contents.

Unlike the impact vibration test, the constant microtremor mea-

Chapter 1	Significance of the microtremor measurement and contents of this manual
Chapter 2	Scope of application of the constant microtremor measurement method
2.1	Existing measurement techniques and scope of application
2.2	Structural conditions of applicable foundations
2.3	Application considerations
Chapter 3	Natural frequency identification algorithm
3.1	Overview of natural frequency identification algorithm
3.2	Overview of automatic natural frequency calculation method
3.3	Evaluation method of natural frequencies
Chapter 4	Construction of the microtremor measurement system
4.1	Basic configuration of the system for microtremor measurement
4.2	Items to be considered when constructing a measurement system
4.3	Example of measurement system configuration
Chapter 5	Selection of sensors for microtremor measurement
5.1	Velocity sensor specifications
5.2	Acceleration sensor specifications
Chapter 6	Measurement conditions
6.1	Sampling frequency and measurement time
6.2	Measurement frequency
Chapter 7	Installation method
7.1	Example of measurement system installation
7.2	Points to keep in mind when installing the system

Fig. 1 Manual Chapter Structure

surement method does not require excitation by blows. However, since this method utilizes constant microtremors, which are minute vibration phenomena, the scope of application is more limited than that of impact vibration tests. Therefore, the method is not likely to be applicable to the following piers: A: piers whose natural frequencies are difficult to identify even with impact vibration tests, B: piers with large damping constants, and excitation frequencies which are not clear, and C: piers in which the predominant frequencies of girders and ancillary structures exist near the natural frequencies.

This method is applicable to “spread foundations,” “spread foundations with wooden piles,” and “Caisson with superficial foundation.” In principle, this method does not apply to piers, rammen-type structure, abutments, and other earth-retaining structures for rivers and waterways constructed after 1976, when the Cabinet Order concerning Structural standards for River Administration Facilities was established and enforced.

If the target structure has tall piers, piers with a large degree of obliquity, piers supporting truss girders or long bridges, short piers and thick soil cover, or elevated bridges, it is recommended to confirm or obtain new impact vibration test data in advance. It is also recommended to examine whether the piers do not have the vibration characteristics of A to C above.

4. Natural frequency identification algorithm [3][8]

Chapter 3 of the manual covers details of the identification algorithm.

This method assumes that the pier vibration (response waveform) measured at the top of the piers is the sum of the ground vibration and the pier rocking vibration in response to the ground vibration. Since most of the tilting of piers due to scour occurs in the upstream direction of the river due to the restraint effect of the girders, the evaluation of natural frequencies in the perpendicular

direction to the bridge axis is used as a basis. The procedure for identifying natural frequencies using this method is as follows and the procedure is shown in Fig. 2.

I. Measure the microtremors of the horizontal and vertical components perpendicular to the bridge axis at both ends of the pier tops.

II. The position of the center of rotation of the rocking vibration is obtained from the geometric relationship between the Lissajous angle plotted as the locus of the horizontal and vertical components at each microtremor sensor and the sensor installation interval. Based on the aforementioned assumptions, the vertical component of the rocking vibration is obtained from the difference of the vertical components of the microtremors at both ends, and the horizontal component of the rocking vibration is calculated from the same geometric relationship (Fig. 3). The horizontal component of the ground vibration (input waveform) is obtained by subtracting the calculated horizontal component of the rocking vibration from the

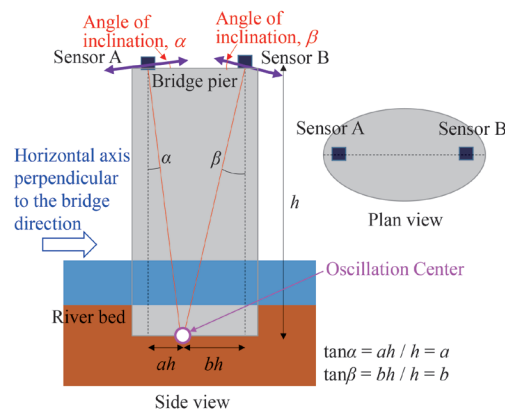


Fig. 3 Conceptual diagram of primary vibration of bridge pier [3]

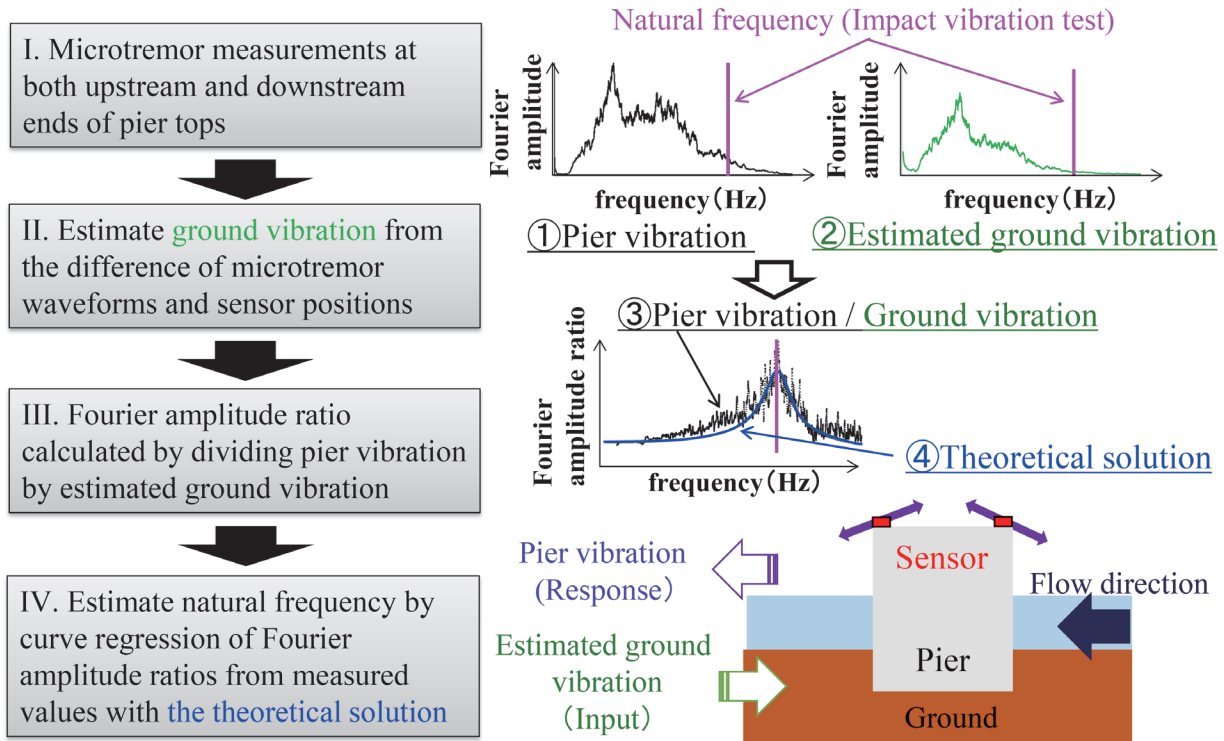


Fig. 2 The procedure of natural frequency identification algorithm

horizontal component of the microtremor measured on the pier.

III. The Fourier amplitude ratio (transfer function) is calculated by dividing the Fourier amplitude of the horizontal component of the microtremors measured on the piers by the Fourier amplitude of the horizontal component of the ground vibration estimated in II.

IV. Apply the theoretical solution of the vibration model with the damping constant expressed in (1) to the calculated Fourier amplitude ratio (transfer function). Find the frequency at which the coefficient of determination is maximum.

$$\frac{\hat{x}_a(f)}{\hat{x}_g(f)} = \frac{1 + \left(\frac{2hf}{f_0}\right)^2}{\sqrt{\left\{1 - \left(\frac{f}{f_0}\right)^2\right\}^2 + \left(\frac{2hf}{f_0}\right)^2}} \quad (1)$$

Here, $\hat{x}_a(f)$ is the Fourier amplitude of the horizontal vibration of the bridge pier, and $\hat{x}_g(f)$ is the Fourier amplitude of the vertical vibration of the bridge pier. $\hat{x}_a(f)/\hat{x}_g(f)$ is the Fourier amplitude ratio (transfer function). And where f is the frequency (Hz), f_0 is the natural frequency of the bridge pier (Hz), and h is the damping constant.

The basic principles of the identification method are as described in I to IV above, but the actual algorithm implements multiple arithmetic operations to improve the identification accuracy and automatic calculation of natural frequencies based on the processing flow. For details, please refer to Ref. [8]. The details necessary to implement these processes in the identification system are also described in detail in the manual.

The evaluation of the soundness of pier foundations based on natural frequencies in the manual is based on the evaluation of natural frequencies in impact vibration tests [9].

5. Construction of the microtremor measurement system

Chapter 4 of the manual describes the construction of a continuous microtremor measurement system.

When designing the system, it is necessary to consider the microtremor sensor, the data recording unit, and the power supply, and when installing the measurement system, it is necessary to consider the exposed environment on the bridge. Table 1 shows the items to be considered in the manual and their contents.

Table 1 Main considerations for system construction and outline of the study

Items	Outline of the study for each item
Robustness	<ul style="list-style-type: none"> Robustness considerations exposure environment Recommendation of IP67 protection class for dust and drip-proof performance.
Operating temperature	<ul style="list-style-type: none"> Confirmation of the operating temperature taking into account the installation area Waterproof performance must be maintained due to pressure changes inside the structure caused by temperature changes.
Power supply configuration	<ul style="list-style-type: none"> Determine the power supply configuration taking into account the installation conditions. Identification of each characteristic of primary and secondary batteries Necessity of power-saving design
Other	<ul style="list-style-type: none"> Ensuring electromagnetic noise resistance performance in electrified sections Ensure durability against flying objects such as ballast

6. Construction of the microtremor measurement system

6.1 Sensor specifications

Chapter 5 of the manual organizes the selection of velocity and acceleration sensors in terms of the accuracy and performance required for each sensor.

In selecting the specifications of each sensor, the characteristics of the sensor must be such that the natural frequency identification algorithm can be sufficiently applied. In the manual, the specifications of velocity sensors used in the development phase are presented as a reference. It also summarizes the specifications required for acceleration sensors, which are considered advantageous in terms of cost reduction. The specifications of the acceleration sensors considered are described below.

6.2 Synchronization accuracy

In applying the natural frequency identification algorithm, it is necessary to ensure high synchronization performance for each sensor. In addition, accelerometers with the smallest possible error between individual sensors should be selected. Specifically, the sensors should have (1) low internal noise, (2) digital output function without AD conversion or AD conversion function with low noise, and (3) output of each axis between sensors should match when installed in the same location. The manual shows the synchronization accuracy as a guideline for applicability (Fig. 4).

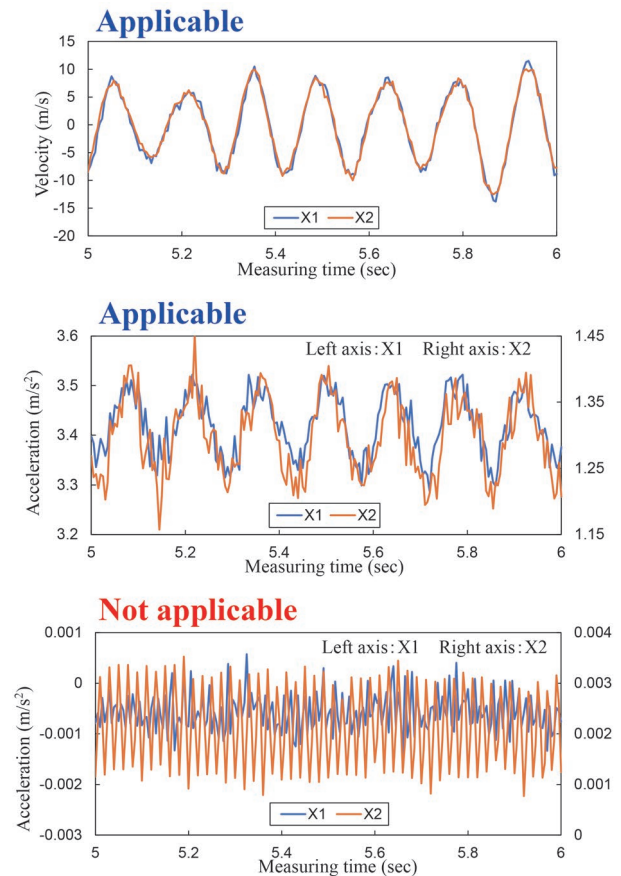


Fig. 4 Image of the degree of agreement and applicability of microtremor waveforms

6.3 External noise

Together with the specification characteristics regarding the internal noise of each accelerometer, it is necessary to eliminate the influence of external noise in the construction of the measurement system. The manual gives specific noise levels to which the identification algorithm can be applied.

6.4 Resolution

In order to investigate the effect of the minimum resolution of the accelerometer (corresponding to the minimum sensitivity of the sensor) on the accuracy of the identification, we compared the iden-

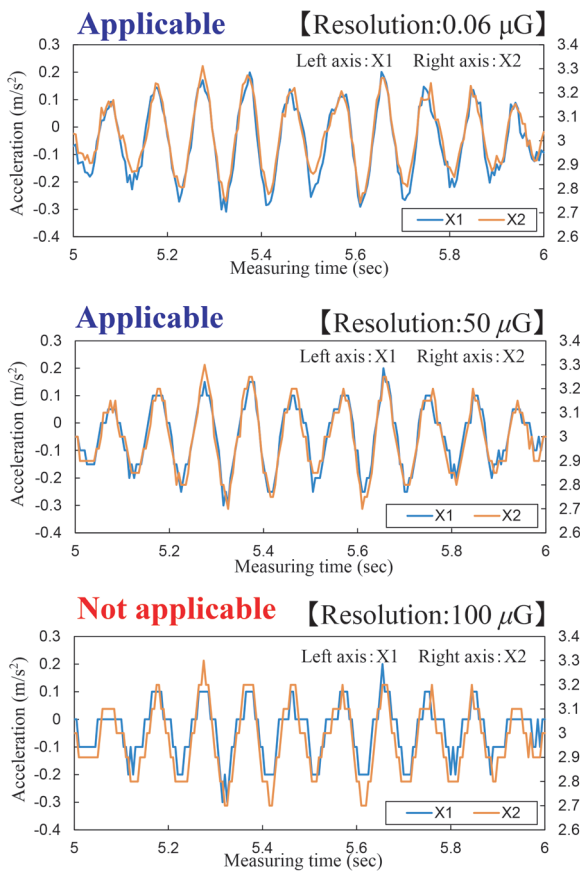


Fig. 5 Waveforms with varying resolution waveforms

tified natural frequencies and the coefficient of determination of the theoretical solution fitting by generating data with a stepwise change in the minimum resolution with respect to the original waveform. The results showed that a minimum resolution of 50 μG (approximately 3% of the amplitude RMS value of the measured waveform under all drilling conditions) is recommended (Fig. 5).

6.5 Applicability based on the shape of the transfer function

The applicability of the algorithm was verified based on the shape of the transfer function obtained by the identification algorithm. The ratio of the mean value of the total amplitude ratio area of the Fourier amplitude ratio in the transfer function to the peak value of the amplitude ratio (amplitude index) was employed as an indicator (Fig. 6). We organized the relationship between this index and the coefficient of determination during fitting with the theoretical solution.

As a result, the natural frequency can be identified in the range where the amplitude index exceeds five, and the identification accuracy improves when the amplitude index exceeds eight (Fig. 7). When applying this method, it is recommended that the applicability of the identification algorithm is determined after the waveform of the transfer function has been obtained by preliminary measurements or other means.

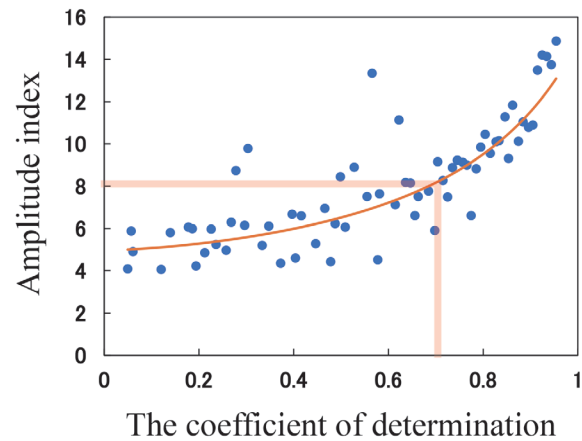


Fig. 7 Relationship between the coefficient of determination and amplitude index

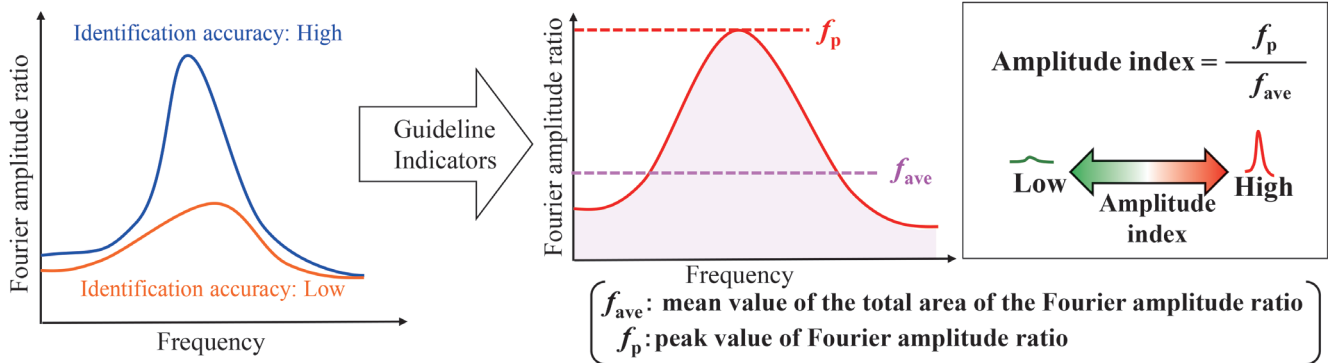


Fig. 6 Definition of amplitude index

6.6 Example of acceleration sensor specifications

As an example of accelerometer selection, Table 2 lists the main specifications of the accelerometers used in the study of the natural frequency identification algorithm.

7. Results of experiments

Chapters 6 and 7 of the manual summarize the measurement conditions and installation methods and their considerations, respectively (Fig. 8, Fig. 9). The main items described in the manual are shown in Table 3. Examples of fixing and protection of microtremor sensors are also introduced.

8. Summary

This paper describes a manual to introduce a natural frequency identification system using constant microtremor measurement. By utilizing the latest IoT-related technologies, changes in natural fre-

quencies can be confirmed easily and quickly even in remote locations. This will contribute to improving the level of social services provided by public transportation systems, such as the dissemination of operation information and the maintenance of inspection and repair systems. This manual is available from the Ministry of Land, Infrastructure, Transport and Tourism. The contents of the manual may be added to or revised in the future as new knowledge emerges.

Acknowledgment

This research was supported by the public works under Ministry of Land, Infrastructure, Transport and Tourism (JPJ002223).

Table 2 Specifications of the selected example sensor

Item	Specification
Basic Configuration	Digital 3-axis accelerometer
Sensor type	Frequency-variant type
Resolution	0.06 $\mu\text{G}/\text{LSB}$ AD Resolution 32 bit Effective resolution 28 bit
Bandwidth	DC~460 Hz
Detection range	$\pm 15 \text{ G}$
Sample rate	1,000 Sps (1 msec)
Noise density	$0.5 \mu\text{G}/\sqrt{\text{Hz}}$
Supply voltage	9~32 V
Current consumption	35 mA(Typ.) @ 12 V
Operating temperature range	$-30 \sim +70^\circ\text{C}$
Waterproof/Dustproof	IP67

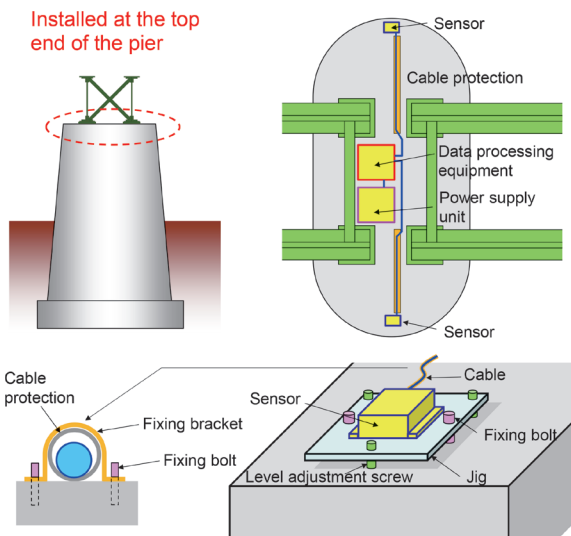


Fig. 8 Example of measurement system installation (In the case of battery-powered system)

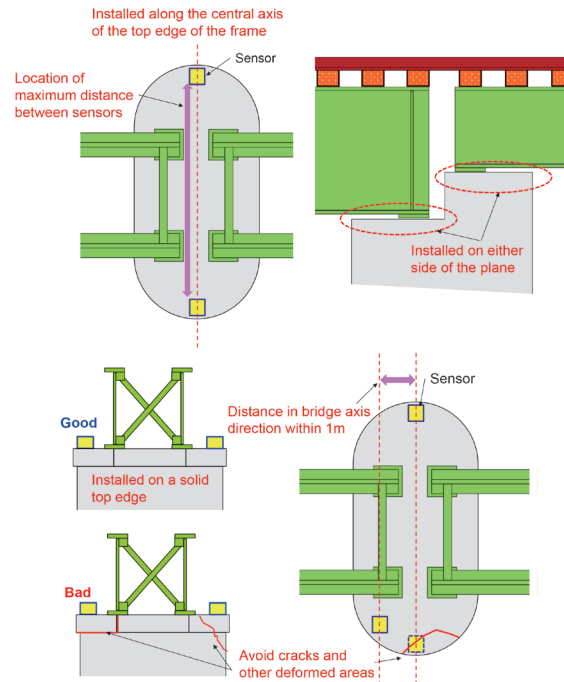


Fig. 9 Precautions for installation of microtremor sensors

Table 3 Main description of measurement conditions and installation method

Description	Contents
Sampling frequency, measurement time	<ul style="list-style-type: none"> Recommended 100Hz or higher At least 5 minutes is recommended
Measurement frequency	<ul style="list-style-type: none"> At least every 30 minutes is recommended
Installation method	<ul style="list-style-type: none"> Install along the central axis of the top end of the frame perpendicular to the bridge axis to obtain the maximum distance between the sensors. If the height of the girder seat is different at the start and end points, install the sensors on the same top edge plane. In principle, sensors should not be installed at locations with cracks or broken edges. In the case of a staggered installation, the difference in distance in the direction of the bridge axis between the microtremor sensors should be within 1 m.
Fixation of microtremor sensor	<ul style="list-style-type: none"> Rigid connection to the top of the pier Prevention of cable flapping

References

- [1] Nishimura, A. and Tanamura, S., “Study on Integrity Assessment of Railway Bridge Foundation,” *RTRI Report*, Vol. 3, No. 8, pp. 41-49, 1989 (in Japanese).
- [2] Keyaki, T., Watanabe, S., Miyashita, Y. and Ota, N., “Specification Technique of Natural Frequency Based on The Microtremor Measured at The Both Side of a Bridge Pier,” *Journal of railway engineering*, JSCE, Vol. 20, pp. 61-68, 2016 (in Japanese).
- [3] Keyaki, T., Yuasa, T., Naito, N., and Watanabe, S., “Soundness Evaluation Method of the Ground around the Pier Foundation against Scouring by Microtremor Measurements at Both Sides of the Bridge Piers,” *Japanese Geotechnical Journal*, Vol. 13, Issue 4, pp. 319-327, 2018 (in Japanese).
- [4] Watanabe, S., Naito, N., Yuasa, T., and Keyaki, T., “Applicability of a New Natural Frequency Identification Method Using Microtremors to Actual Bridges,” *Japan Society of Civil Engineers 2019 Annual Meeting*, 3-206, 2019 (in Japanese).
- [5] Watanabe, S., Naito, N., Keyaki, T., and Yuasa, T., “Verification of Identifying Method for Natural Frequencies by Model Bridge Piers with Different Cross Sections,” *The 54th Japan National Conference on Geotechnical Engineering*, pp. 1175-1176, 2019 (in Japanese).
- [6] Naito, N., Watanabe, S., Nunokawa, O., and Keyaki, T., “Influence of different ground materials on vibration characteristics of bridge pier model on spread foundation,” *The 54th Japan National Conference on Geotechnical Engineering*, pp. 1177-1178, 2019 (in Japanese).
- [7] Naito, N., Watanabe, S., Nunokawa, O., and Keyaki, T., “A Study on Improvement of Identification Accuracy of Natural Frequencies of Piers due to Microtremors,” *Japan Society of Civil Engineers 2022 Annual Meeting*, III-37, 2022 (in Japanese).
- [8] Watanabe, S., Keyaki, T., Naito, N., and Yuasa, T., “Automatic Identification Method for Natural Frequency of Bridge Piers by Microtremor Measurement at Both Sides on the Bridge Crown,” *RTRI Report*, Vol. 33, No. 9, pp. 11-16, 2019 (in Japanese).
- [9] Railway Technical Research Institute, *Maintenance Standards for Railway Structures and Commentary (Foundation and Earth Pressure Resistant Structure)*, Maruzen Publishing Co., Ltd., Tokyo, JAPAN, pp. 169-171, 2010 (in Japanese).

Authors



Satoshi WATANABE
Senior Chief Researcher, Head of Geo-hazard & Risk Mitigation Laboratory, Disaster Prevention Technology Division
Research Areas: River Disaster Prevention, Slope Disaster Prevention



Shoma FUJIWARA
Researcher of Geo-hazard & Risk Mitigation Laboratory, Disaster Prevention Technology Division
Research Areas: River Disaster Prevention, Slope Disaster Prevention



Hiroki IRI
Researcher of Geo-hazard & Risk Mitigation Laboratory, Disaster Prevention Technology Division
Research Areas: River Disaster Prevention, Slope Disaster Prevention

Summaries of Papers in RTRI REPORT (in Japanese)

Effect of Track Structure Condition on Limit Value for Uneven Displacement at Bridge Boundary

Shintaro MINOURA, Manabu IKEDA, Munemasa TOKUNAGA

(Vol.38, No.5, 1-9, 2024.5)

In the Design Standards for Railway Structure and Commentary (concrete structure) provides a guideline on the limit values for uneven displacement (angular bent / misalignment) of the track surface with regard to the recoverability of track damage at normal conditions and during earthquakes. However, in recent years, the fastening intervals and support stiffness of real railway lines have often differed from the assumptions when calculating the reference limit values in the aforementioned design standard. In addition, there is a possibility that the limit values for recoverability can be increased by selecting appropriate track structure conditions at the time of design. In this study, we sort out the track conditions that are dominant over the limit values and evaluate the influence of various parameters such as the track support stiffness and the fastening interval on the limit value of track maintenance and recoverability.

Proposal for Excitation Acceleration in Vibration Endurance Testing of Signaling Equipment

Yoshikazu OSHIMI, Shunsuke SHIOMI, Tsuyoshi KAMIYA, Ryuto ISSHIKI

(Vol.38, No.5, 11-16, 2024.5)

Signaling equipment is installed at a place where vibrations occur during the passage of trains over rails, sleepers, and roadbeds. It is therefore necessary to design signaling equipment taking into account the influence of vibration to avoid damage due to vibration. In recent years, the installation environment of signaling equipment has changed due to the speedup of trains and changes in tracks and structures. However, the details of vibration propagation to signaling equipment have not been investigated so far. In addition to current issues, this paper reports on a guideline for vibration acceleration amplitude in vibration endurance testing.

Calculation Method for Expansion and Contraction of the Spring Tension Balancer

Koki SATO, Yoshitaka YAMASHITA

(Vol.38, No.5, 17-23, 2024.5)

It has been reported that tension balancers, in some cases, may reach its movable limit. One of the causes is thought to be the creeping move of overhead contact lines. In addition, if expansion or contraction characteristics due to temperature at each of both ends of overhead contact lines are not identical, it may also cause the tension balancers to reach its movable limit. However, phenomena based on these causes have not been sufficiently investigated, so that it is required to clarify the phenomena. Therefore, we conducted numerical calculations and field tests to clarify the factors that cause the creeping move of overhead contact lines and the generation of differences in temperature expansion/contraction characteristics of tension balancers at each of both ends.

Increase of Tangential Force by Ceramic Particles on the Low Adhesion Condition

Shinya FUKAGAI, Takemasa FURUYA, Ryo TAKANO

(Vol.38, No.6, 1-6, 2024.6)

Vehicle slipping and sliding caused by fallen leaves especially in autumn is an important issue that needs to be resolved in terms of safety and on-time operation. Though the equipment which apply ceramic particles between rail and wheel of vehicle to increase the adhesion has been developed,

a complete solution has not yet reached at the peak of fallen leaves season. Therefore, the authors conducted a brake test to investigate the influence of particle amount and particle size on the tangential force. The test was conducted with paper tape attached to the rail for simulating leaves on the rail. The test results showed that the tangential force increased with the amount of particle apply. A correlation was also observed between the number of holes penetrated by particles remaining on the paper tape and the tangential force. In particular, a relatively good correlation was found between the estimated area of the holes and the tangential force. These results will contribute to design and performance evaluation of particle for improving adhesion between wheel and rail.

Fundamental Study on Contact Force Estimation Method of Pantograph/Catenary Systems using Kalman Filter

Shigeyuki KOBAYASHI, Yoshitaka YAMASHITA

(Vol.38, No.6, 7-13, 2024.6)

The contact force between overhead wires and pantographs is an important indicator for evaluating the current collection performance. This study proposes to use a Kalman filter as a model-based approach to estimate the contact force. In this paper, an external force identification method based on an augmented state-space equation is applied to solve the dynamics of pantographs. First, the validity of the proposed method is verified through by simulations based on a 2-degree-of-freedom model, in order to clarify the effect of measurement error, modeling error and variance of the contact force on the contact force estimation. A finite element model of the pantograph is then used to investigate the effect of modeling errors on the accuracy of contact force estimation.

Development of Low Strength Stabilization Method for Fouled Ballasted Tracks

Takahiro KAGEYAMA, Takahisa NAKAMURA, Masaru HOJO, Fumika TAJIMA

(Vol.38, No.6, 15-21, 2024.6)

As ballast on railway track is more crushed and grained, settlement of the track tends to occur even if after tamping, so that maintenance frequency increases. Although the basic measure to reduce the maintenance frequency is replacing the ballast with new ballast, the cost is high. Then, a low-cost method for reducing the settlement without replacing the ballast has been required. Therefore, the authors developed a low-strength stabilization method for reducing settlement without replacing the ballast. In this study, we confirmed the effectiveness of the developed method for reducing settlement through laboratory tests. In addition, we conducted field tests on a commercial line to verify the effectiveness for reducing settlement.

Survey on Railway Customers' Consciousness of Cleaning Quality in Men's Restrooms in Railway Stations

Takashi KYOTANI, Yoshiki IKEDA, Hiroshi OISHI, Tamami KAWASAKI

(Vol.38, No.6, 23-30, 2024.6)

In order to extract factors that affect customers' evaluation of men's restrooms in railway stations, we conducted surveys on railway customers' consciousness of cleaning quality in men's restrooms in railway stations. Statistical processing of the survey results revealed that two indicators, "odor satisfaction" and "urine stains on skirting boards," affect the users' evaluation of whether they would like to use the same restroom again. It also became clear that men's restrooms with dry cleaning in railway sta-

tions had statistically significantly better evaluations than men's restrooms with wet cleaning in railway stations from the viewpoint of odor.

Evaluation of Spatial and Temporal Variation of Site Effects on Superficial Subsurface Structure

Seiji TSUNO, Masahiro KORENAGA, Reo KOBAYASHI, Hiroaki YAMANAKA
(Vol.38, No.6, 31-36, 2024.6)

We investigated the spatial and temporal variation of site amplification characteristics based on observation data from high-sampling continuous borehole seismic observations and geophysical surveys, as well as using wave propagation theory, to improve the accuracy of earthquake ground motion evaluation. Furthermore, in the vicinity of the observation site at the foot of Mt. Mannichi, where bedrock is exposed, we extracted the relationship between the spatial variation in the epicenter azimuth of site amplification and the irregularly shaped underground structure.

Increased Perception of Workload and Related Cognitive Functions in Drivers with Aging

Ryo NAKAMURA, Ayanori SATO, Takayuki MASUDA, Yasuhiro KITAMURA, Munendo FUJIMICHI, Ayano SAITO
(Vol.38, No.6, 37-43, 2024.6)

With aging, the physical and cognitive functions generally tend to decline. However, taking appropriate measures, it is possible for elderly train drivers to continue their duties safely and confidently. Therefore, the first step was to obtain fundamental data for examining measures needed to enable senior drivers to continue train driving. Based on a survey result on the perceived burden of train driver's tasks, we identified the tasks that become more burdensome with aging. Furthermore, it was revealed that the increase in burden of these tasks is associated with age-related declines in visual function, attention, decision-making skill and reaction time.

Estimation of the Price Elasticity of Demand for Green-Car in Commuting Train

Ryosuke MATSUMOTO
(Vol.38, No.6, 45-51, 2024.6)

The fare of local train Green-car (higher-class car) seats will affect not only its demand, but also that of regular car of the same train. Therefore, it is important to estimate the impact of the price change on the Green-car demand, especially during weekdays' commuting time when the overcrowding is at a high level. This research focuses on a Green-car's two-stage pricing structure where the price jumps by JPY210 when travel distance exceeds 50km. Then, this research estimates the price elasticity using regression discontinuity design. The estimation results show that the elasticity is significantly larger than one, which means that the price sensitivity to demand is at a high level. Pricing decisions should be made carefully based on the estimation results of price elasticity and the current overcrowding degree of regular cars and Green-cars.

Design Method for Power Generation Systems for Diesel Vehicles Using a Permanent Magnet Synchronous Machine and a Full-Bridge Rectifier

Minoru KONDO
(Vol.38, No.7, 1-8, 2024.7)

This paper describes a design optimization method for power generation systems for diesel vehicles consisting of a permanent magnet synchronous machine, a full-bridge rectifier and phase shift capacitors inserted between them. By combining an analysis method for the proposed systems and a multi-objective optimization method, a trial design optimization was carried out with the aim of minimizing indicators related to reducing the size and weight of the system. Furthermore, the performance of the optimized design

was verified by numerical simulations, and it was confirmed that the required performance was achieved with the design while satisfying the constraints of the system.

Study on the Occurrence Conditions of Squeal Noise and High frequency Noise in a Railway Curved Section

Takeshi SUEKI, Yasuhiro SHIMIZU, Takuma NITTA, Kentarou TAKAI
(Vol.38, No.7, 9-16, 2024.7)

When a train passes through a curved track, squeal noise (below 10 kHz) and high frequency noise (above 10 kHz) are often observed. Measurements of these noises were carried out on commercial lines to understand the generation of the noises. It is found that these noises vary from wheel to wheel, having large dispersion. The analysis results showed that these noises are prominent when the outer wheel flanges contact the outer rail at specific passing velocities. In contrast to that, these noises become lower when a train is running at balancing speed in curves.

Improvement of Skeleton Curves for Nonlinear Dynamic Analysis Employing Single Degree of Freedom Model of Railway Bridges and Viaducts

Kengo NANAMI, Kimitoshi SAKAI
(Vol.38, No.7, 17-22, 2024.7)

A dynamic analysis employing the nonlinear single degree of freedom (SDOF) model is generally used to carry out the seismic design of railway bridges and viaducts. Although structures are represented with bi-linear type skeleton curve in the model, it does not necessarily reproduce the nonlinear behavior of the structure obtained from the pushover analysis. Especially, the response values calculated by the method are largely different from those obtained from the precise model for small and medium earthquakes. In this study, a new skeleton curve employing the ellipse function was proposed to improve the precision of dynamic response in regions at around yielding. It was confirmed that the non-linear response estimated by the SDOF model with proposed curve showed good agreement with that from precise dynamic analysis.

Estimation Method of Melting Volume of Current Collecting Materials at Contact Loss Point by using ϕ - θ Theory

Chikara YAMASHITA, Koki NEMOTO, Takuya OHARA
(Vol.38, No.7, 23-28, 2024.7)

In order to control electric wear of current collecting materials such as contact wire and contact strip in electric railways, it is necessary to understand the relationship between current and melting volume at a contact loss point. In this paper, we propose a method for estimating melting volume of contact wire whose film resistance is taken into account, based on the ϕ - θ theory. To verify the proposed method, we carried out wear tests under two current conditions to measure melting depth, melting radius, and melting volume. The wear test results showed that experimental values of melting volume of the contact wire were in the range where contact boundary factor α was estimated from 0.90 to 0.94.

A Study on Parameter Setting for Deformation Characteristics for Dynamic Grand Response Analysis

Keigo TSUKIOKA, Yasutomo YAMAUCHI, Masanori YAMAMOTO, Tomoya ONODERA, Jun IZAWA
(Vol.38, No.7, 29-35, 2024.7)

A dynamic ground response analysis has been used in practice as a recommended method for seismic design of railway structures in Japan. The GHE-S model, which can precisely reproduce the deformation characteristics of soils from small to large shear strain levels, is applied to the analyses.

The parameters of the GHE-S model are usually set by designers according to the deformation characteristics obtained from laboratory tests. Therefore, the accuracy of the analysis is greatly dependent on how the parameters are set and how the deformation characteristics are obtained. Consequently, this paper examines how to set up the deformation characteristics of soils in a ground response analysis.

Editorial Board

Chairperson: Kimitoshi ASHIYA

Co-Chairperson: Hisayo DOI

Editors: Ryohei IKEDA, Fumiko MORIMOTO, Nozomi NAGAMINE, Daisuke SUZUKI, Erimitsu SUZUKI, Kenichiro AIDA, Munemasa TOKUNAGA, Fumihiko URAKAWA, Kazuhide YASHIRO

QUARTERLY REPORT of RTRI

第 65 卷 第 3 号

Vol. 65, No. 3

2024 年 8 月 1 日 発行

Published date: 1 August 2024

監修・発行所：公益財団法人鉄道総合技術研究所

Supervision/Publisher: Railway Technical Research Institute

〒 185-8540 東京都国分寺市光町 2-8-38

Address: 2-8-38 Hikari-cho, Kokubunji-shi, Tokyo 185-8540, Japan

発行人：芦谷公稔

Issuer: Dr. Kimitoshi ASHIYA

問い合わせ：鉄道総研広報

Contact us: Public Relations, Railway Technical Research Institute

Mail Address: rtripr@rtri.or.jp

QUARTERLY
REPORT of
RTRI